universität wien

MASTERARBEIT | MASTER'S THESIS

Titel | Title

Refining and Extending our Knowledge of the Chromosome Configuration of Oral Cavity Symbionts

verfasst von | submitted by

Éanna Will Peter Joseph O'Shea

angestrebter akademischer Grad | in partial fulfilment of the requirements for the degree of

Master of Science (MSc)

Wien | Vienna, 2025

Studienkennzahl lt. Studienblatt | Degree programme code as it appears on the student record sheet:	UA 066 830
Studienrichtung lt. Studienblatt | Degree programme as it appears on the student record sheet:	Masterstudium Molecular Microbiology, Microbial Ecology and Immunobiology
Betreut von | Supervisor:	Assoz. Prof. Dr. Silvia Bulgheresi Privatdoz.

Table of Contents

Figures, Tables & Equations

Acknowledgments

I would like to thank my supervisor, Silvia Bulgheresi, for warmly welcoming me into her group. Her advice, support, and encouragement throughout this project were invaluable in helping me overcome challenges and celebrate the successes along the way.

I would especially like to express my gratitude to Nicole Krause for her patience, generosity, and consistent guidance. Her willingness to share her knowledge, answer my endless questions, and provide thoughtful feedback have been instrumental in my professional and scientific development.

I'm would also like to thank the rest of the ECB group for their kindness and support. Finally, I would like to extend my thanks to the rest of the Archaea Biology and Ecogenomics Division fostering such a collaborative and positive environment, where curiosity and teamwork were always encouraged.

Abstract

Despite the importance of microbial symbiosis for environmental and host wellbeing, the specialised cell biology of symbionts remains largely underexplored. The *Neisseriaceae* bacteria *Alysiella filiformis, Simonsiella muelleri*, and *Conchiformibius kuhniae* are common symbionts in the oral cavities of various mammals, including humans. These bacteria attach to the host squamous epithelium, where they grow as multicellular filaments. *A. filiformis* exhibits a stable longitudinal chromosome configuration, with the origin of replication (*ori*) localised at the cell pole. In this work, we revealed that the left and right chromosomal arms are also stable, primarily localising to midcell. Building on the previously observed subpolar *ori* location in *S. muelleri*, we discovered a potentially unique chromosome arrangement featuring – not the *ori* – but a cluster of five *parS* sites about 500 Kb away tethering each of the two chromosomes to one cell pole. Finally, we found that *C. kuhniae* populations contain both monoploid and diploid cells, marking, to our knowledge, the first known example of bistable ploidy in a prokaryote. These findings provide new insights into the extraordinary chromosome configuration of these pervasive oral symbionts.

German Abstract

Trotz der Bedeutung mikrobieller Symbiose für die Umwelt und das Wohlbefinden des Wirtes ist die spezialisierte Zellbiologie von Symbionten weitgehend unerforscht. Die *Neisseriaceae*-Bakterien *Alysiella filiformis, Simonsiella muelleri* und *Conchiformibius kuhniae* sind häufige Symbionten in der Mundhöhle verschiedener Säugetiere, einschließlich des Menschen. Diese Bakterien heften sich an das Plattenepithel des Wirtes und wachsen dort als mehrzellige Filamente. *A. filiformis* weist eine stabile longitudinale Chromosomenkonfiguration auf, wobei der Replikationsursprung (*ori*) am Zellpol (*ori-ter*) lokalisiert ist. In dieser Arbeit zeigten wir, dass die linken und rechten Chromosomenarme ebenfalls stabil sind und sich hauptsächlich in der Zellmitte befinden. Aufbauend auf der zuvor beobachteten subpolaren *ori*-Lage bei *S. muelleri* entdeckten wir eine potenziell einzigartige Chromosomenanordnung, die – nicht den *ori* – sondern einen Cluster von fünf *parS*-Stellen etwa 500 kb entfernt aufweist und jedes der beiden Chromosomen an einen Zellpol bindet. Schließlich stellten wir fest, dass *C. kuhniae*-Populationen sowohl monoploide als auch diploide Zellen enthalten. Dies stellt unseres Wissens nach das erste bekannte Beispiel für bistabile Ploidie bei einem Prokaryoten dar. Diese Erkenntnisse liefern neue Einblicke in die außergewöhnliche Chromosomenkonfiguration dieser weit verbreiteten oralen Symbionten.

Introduction

Microbial Symbiosis

Symbiosis, as first described by H. A. de Bary in his 1878 presentation to the meeting of German Natural Scientists and Physicians, is the "living together of unlike organisms" (Oulhen et al., 2016). Symbiotic relationships are ubiquitous across all ecosystems and form an essential part of many biological systems. They are often responsible for development of complex or unique cell biology (Dethlefsen et al., 2007). Evidence even suggests that eukaryotic cells as we know them today emerged from protoeukaryotes engulfing their bacterial symbionts. These eventually became cellular organelles and enabled the development of more complex multicellular life forms (Zachar & Boza, 2020). These multicellular organisms often form new symbiotic relationships with microorganisms which can have an impact on host or environmental wellbeing (S. Egan et al., 2020).

The diversity and complexity of symbiotic interactions necessitates classification, based on several specific characteristics or criteria. One common classification method is by the physical location the interaction occurs. Microbial symbionts found living on the host surface are known as ectosymbionts, while microbes that are integrated into the host are referred to as endosymbionts (Douglas, 2009). Another classification considers how the relationship effects the parties involved: mutualism (both benefit), commensalism (one benefits other is unaffected) and parasitism (one benefits, one is harmed) (Parmentier & Michel, 2013). Symbiotic relationships can also be classified by the degree of reliance between the two parties. Obligate symbiotic relationships are essential for the survival of one or both organisms, whereas facultative symbiotic relationships are beneficial but not essential (Frank, 1997). Finally, relationships can be classified by the mode of transmission or acquisition of the microbial symbiont. Symbionts acquired from the environment are transferred horizontally, while symbionts transferred from parent to offspring (usually via the female germ line) are transferred vertically. Vertical transmission allows for uninterrupted contact with their symbiotic partner and generally seen in organisms that cannot survive independently (i.e. obligate symbionts) (Bright & Bulgheresi, 2010).

One notable example of symbiotic interactions between microbes and more complex forms of life is the relationship between sap feeding aphids and the bacterium *Buchnera aphidicola*. These bacterial endosymbionts dwell within specialised aphid cells called bacteriocytes. Here, they synthesise essential amino acids that are absent from the aphids limited diet (Baumann & Baumann, 1998; Kaltenpoth et al., 2025). The bacteria, in return, receives a safe, secluded environment and other nutrients from its host (mutualism). This relationship is essential to the survival of both species (obligate) and the bacteria are transmitted directly (vertically) from the mother during embryonic development (Baumann & Baumann, 1998; Bright & Bulgheresi, 2010). A completely

contrasting relationship occurs between the *Armillaria* fungus and several plant species. This fungus can live independently on decaying wood and other plant matter but can also colonise the roots and bark of living trees (Heinzelmann et al., 2019). This can lead to wood rot and eventual tree decline – a perfect example of a facultative, parasitic ectosymbiont (Heinzelmann et al., 2019). Many examples of symbiotic relationships which benefit or harm their hosts to various degrees have been described. There are also cases of microbes that maintain close contact with their host where the relationship defies classification or cannot be conclusively determined. These relationships are still deemed symbiotic, even when the nature of the interaction (i.e. mutualism, commensalism or parasitism) is undefined.

In previous decades, research into microbial symbiosis has often heavily focused on pathogenic organisms. More recently the scientific focus has begun to shift (Moran, 2006). There is now greater appreciation for the crucial role microbes play in ecosystem integrity (e.g. nutrient cycling) and host wellbeing (e.g. enhancing the immune system) (Dethlefsen et al., 2007).

Human Microbiome

The human microbiome is a complex and dynamic symbiotic network comprised of trillions of microorganisms. Diverse microbial communities are found almost everywhere in the human body, inhabiting the skin, mouth, gut, urogenital tract, to name just a few examples (Lloyd-Price et al., 2016). In these environments, they form mutualistic relationships with each other and their host, playing important roles in health and wellness (Ogunrinola et al., 2020).

Of these micro-ecosystems, the microbiome of the gastrointestinal tract is the most well researched. Home to upwards of 3000 individual bacterial species, it is the largest and most diverse microbial community in the human body (Dethlefsen et al., 2007; Rosenberg, 2024). The gut microbiome is essential for human health and wellbeing, with many bacterial species playing important roles in nutrient metabolism and pathogen defence (Dethlefsen et al., 2007). For example, *Bacteroides thetaiotaomicron* enhances nutrient absorption and energy extraction by assisting in the breakdown of complex carbohydrates (Porter et al., 2018). *Faecalibacterium prausnitzii* supports gut barrier integrity by producing the short chain fatty acid butyrate (Ferreira-Halder et al., 2017). The gut microbiome has also been linked to various pathologies, including inflammatory bowel disease, diabetes, autism, and cancer (Lloyd-Price et al., 2016). The largest organ in the human body, the skin, assisted by its microbiome acts as the first line of protection from the outside world. *Staphylococcus epiderrodis* produces antimicrobial peptides and *Cutibacterium acnes* maintains the skins acidic pH preventing the colonisation of pathogenic microorganisms (Chiu et al., 2017; Glatthardt et al., 2024; Zheng et al., 2020).

Interestingly, despite the role microbiomes play in human health, there is no defined 'healthy microbiome', every individual is unique with substantial differences observed between microbial community composition (Lloyd-Price et al., 2016). This variation is attributable to several factors – including age, geography, lifestyle, occupation, diet and even method of delivery at birth (Hollister et al., 2014; Lloyd-Price et al., 2016). The development of an individual's microbiome begins when a baby moves from the sterile womb and is first exposed to the outside environment. Colonisation begins during birth; babies delivered vaginally are first exposed to the maternal vaginal microbiome, followed by microorganisms from the surrounding environment. When babies are delivered by caesarean section, the first contact is instead made with skin microbiome (Neu & Rushing, 2011). The microbiome continues to develop, with further colonisation occurring with the introduction of food, first milk (breast or formula) and later with solid foods, continuing until approximately 3 years of age. Microbiome composition often fluctuates during periods of hormonal change, such as sexual maturation or pregnancy. After adolescence, however, it typically stabilises and remains relatively consistent throughout adult life (Kundu et al., 2017; Lloyd-Price et al., 2016).

After the gastrointestinal tract, the oral microbiome is considered the second most diverse environment in the human body. Owing to the relative ease of sample collection, it is also, to date, one of the most well-researched (Deo & Deshmukh, 2019; Lu et al., 2019). There are multiple distinct niches in the human mouth, including the teeth, tonsils, cheeks, tongue and hard and soft palates. These allow for the colonisation of over 700 unique bacterial species (Arweiler & Netuschil, 2016; Perera et al., 2016). These bacteria belong to almost 200 genera and 12 phyla such as *Firmicutes, Proteobacteria, Actinobacteria, Spirochetes*, and *Chlamydiae*, to name a few (Deo & Deshmukh, 2019). Only 280 of these species have been cultivated and named, with the rest only identified using 16S rRNA gene-based sequencing studies (Arweiler & Netuschil, 2016; Deo & Deshmukh, 2019). The establishment of the oral microbiome begins shortly after birth. The genera *Streptococcus, Lactobacillus, Actinomyces, Neisseria and Veillonella* tend to be the initial colonisers on the soft surfaces, such as the cheek, tongue and gums (Deo & Deshmukh, 2019). Microbiome diversity increases rapidly with the emergence of teeth and colonisation occurs on these non-shedding surfaces (Deo & Deshmukh, 2019). The balance can be disturbed by certain lifestyle choices (e.g. diet) or during diseased states (e.g. tooth decay). The composition otherwise remains relatively stable after the establishment of adult teeth, with a reduction of diversity observed in older age when teeth are lost (Deo & Deshmukh, 2019; Patil et al., 2013; Rajasekaran et al., 2024).

The oral microbiome plays roles in digestion, immune modulation, and pathogen defence, and is essential to human health, wellbeing, and development (Dewhirst et al., 2010). An early coloniser of the oral mucosa, *Streptococcus salivarius*, produces enzymes that work alongside human saliva contributing to the pre-digestion of complex

carbohydrates (Chiu et al., 2017; Shimizu et al., 2025). This organism, *Streptococcus mitis* and *Rothia mucilaginosa* among others produce antimicrobial compounds that prevent the colonisation of pathogenic bacteria like *Streptococcus pneumoniae* (Chiu et al., 2017; Marsh, 2000). Disruptions (or dysbiosis) of the oral microbiome can lead to tonsillitis, gingivitis, tooth decay and even oral cancer (Dewhirst et al., 2010; Lu et al., 2019; Zhao et al., 2017). The oral cavity of humans is a major gate way into the rest of the human body. It takes in both food and air as they pass through to the stomach and gastrointestinal tract or trachea and lungs (Deo & Deshmukh, 2019). The continuous connecting epithelial surfaces allow for the spread of bacteria colonising the oral cavity to the neighbouring sites (Dewhirst et al., 2010). The oral microbiota has therefore been linked to systemic pathologies such as cardiovascular disease, diabetes, stroke and arthritis to name a few (Dewhirst et al., 2010; Genco et al., 2005; Han & Wang, 2013; Joshipura et al., 1996, 2003; Li et al., 2000).

Multicellular Bacteria

One of the most important evolutionary innovations is the emergence of multicellular life. The occurrence of multicellular bacteria in diverse ecosystems and unrelated species serves as a fascinating example of convergent evolution (Lyons & Kolter, 2015). According to Lyons et al., bacteria can only be classed as multicellular if they meet two specific criteria. Firstly, cells of the same species must adhere to each other to form a single evolutionary unit. Secondly, these adhered cells must engage in intercellular communication that coordinates their activity (Lyons & Kolter, 2015). Multicellular bacteria can be broadly classified into various groups based on their structure and behaviour, with aggregative and filamentous forms being the most common. Aggregative multicellular bacteria can often live as single cells but come together in times of high stress to form swarms or biofilms, held together by an extracellular matrix. Biofilm forming bacteria have been particularly well described due to their prevalence in natural environments and their role in disease (Lyons & Kolter, 2015). Filamentous bacteria form long, organised chains that join end-to-end or side-by-side, and individual cells often share a periplasm or even cytoplasm. These can be simple straight filaments, or form more complex branching filaments (Lyons & Kolter, 2015).

The commonality of multicellular organisms indicates this lifestyle must offer some selective advantages. Living in close cooperation with other bacterial cells often grants increased resistance to physical and chemical stress. Individual cells are protected from predation and the enhanced ability to collect and store essential nutrients allows for the colonisation of new environments (Bonner, 1998; D. Kaiser, 2001). Multicellular life can, however, also be detrimental. Adhesion and communication with other cells can deplete energy resources and the combined larger size can reduce overall mobility (Bonner, 1998; D. Kaiser, 2001). Moreover, individual cells within multicellular

structures are not necessarily uniform and can exhibit different characteristics, including variations in size or gene expression (Bonner, 1998; D. Kaiser, 2001).

Phenotypic Heterogeneity

Phenotypic heterogeneity, or functional diversity in a population of genetically identical bacterial cells, can arise even in a uniform environment (Ruiz et al., 2020). Cells or groups of cells within a population can exhibit variations in growth rate, metabolism, stress response or gene expression (Weigel & Dersch, 2018). In natural ecosystems bacteria must compete against other organisms for survival in a harsh, rapidly changing environment (Ruiz et al., 2020). The emergence of unique cell types is a form of non-genetic variation that can increase overall fitness of a bacterial population. It allows for the adaption to fluctuating environmental signals and competition against cohabiting organisms of different species (Weigel & Dersch, 2018). These variant cells can perform specialised functions as part of a division of labour, cooperating to benefit the bacterial community as a whole (Ruiz et al., 2020). Phenotypic heterogeneity can alternatively be a "bet-hedging" strategy. This is where multiple unique cell types are produced that are resistant to various environmental stresses. It allows for the continued survival of the population at the expense of individual cells lacking a specific phenotype (Ruiz et al., 2020).

Pseudomonas aeruginosa is an opportunistic human pathogen that can cause serious chronic respiratory infections. Phenotypic heterogeneity is considered a prominent virulence factor essential for host colonisation and formation of biofilms, with some studies reporting upwards of 400 distinct cell variants (Workentine & Surette, 2011). Cells living in a structured community like a biofilm are protected against environmental stresses such as antibiotic treatment (Weigel & Dersch, 2018). Biofilm maintenance is undertaken by specific cell types. Some cells are responsible for the initiation of biofilm formation and production of the extracellular matrix, while others allow for biofilm expansion via surface motility. These specialised cells are supported by the rest of the biofilm through the provision of essential nutrients (Ruiz et al., 2020). The burden of synthesising various toxins and metabolites is shared across the whole community, therefore increasing the fitness of an individual cell (Weigel & Dersch, 2018).

Caulobacter crescentus is a motile gram-negative bacterium commonly found in nutrient-poor aquatic environment such as freshwater lakes and streams (Govers & Jacobs-Wagner, 2020). To survive in this hostile environment *Caulobacter* has two distinctive morphologies that it shifts between during its life cycle. These two cell types are genetically identical but functionally different: the sessile 'stalked' cell and the motile 'swarmer' cell (Woldemeskel & Goley, 2017). The stalked cells are equipped with a tubular cell envelope extension at one pole. This is tipped with a 'holdfast' material that allows for adhesion to environmental surfaces (Govers & Jacobs-Wagner, 2020;

Woldemeskel & Goley, 2017). During cell reproduction, the stalked cell elongates and replicates its DNA. This is followed by the sprouting of flagellum from the free (i.e. unattached cell pole). Finally, division occurs, producing the morphologically distinct swarmer daughter cell (Woldemeskel & Goley, 2017). The stalked cell can immediately continue propagation of more daughter cells. The swarmer cells are motile and can relocate in search of resources but are unable to enter the cell cycle or initiate DNA replication (Govers & Jacobs-Wagner, 2020; Toro et al., 2008). The swarmer must release its flagellum, retract its pili and finish its differentiation by producing a stalk before it can divide and produce daughter cells (Toro et al., 2008; Woldemeskel & Goley, 2017). These two distinct phenotypes make *Caulobacter* an important organism for the study of cellular differentiation and asymmetric cell division (Govers & Jacobs-Wagner, 2020; Toro et al., 2008; Woldemeskel & Goley, 2017).

Bacterial Cell Reproduction

To maintain cell shape and ensure faithful transmission of genetic material to daughter cells, bacterial reproduction must be tightly regulated. This requires a high level of organisation and coordination in the creation of new cells (cell division) as well as in the duplication and distribution of genetic material (chromosome replication and segregation, respectively) (Angert, 2005; Egan & Vollmer, 2013; Reyes-Lamothe & Sherratt, 2019). In model rod-shaped organisms like *Escherichia coli* and *Bacillus subtilis* the regulation and molecular mechanisms of bacterial cell reproduction has been studied extensively (Angert, 2005; Reyes-Lamothe & Sherratt, 2019). Bacterial cell reproduction typically occurs in a sequence of overlapping events known as binary fission. First, chromosome replication is initiated, followed closely by or overlapping with chromosome segregation. The cell then grows to accommodate the duplicated chromosomes and finally divide to create two distinct daughter cells (Reyes-Lamothe & Sherratt, 2019).

Chromosome Replication

Reliable duplication of genetic material is a vital step in cellular reproduction in every organism. In bacteria, replication can be broken down to three stages: initiation, elongation, and termination (Reyes-Lamothe et al., 2008; Reyes-Lamothe & Sherratt, 2019; Wang et al., 2013).

Initiation begins at the origin of replication (*ori*), where DnaA, aided by bacterial histone- like proteins (HU), unwinds DNA to form an open complex for replisome assembly (Konieczny & Helinski, 1997; Speck & Messer, 2001). DnaB helicase is loaded into the open complex by DnaC and further unwinds the DNA. SSBs (single strand binding proteins) stabilise the unwound strands and gyrase relieves topological stress (Soultanas, 2005). Primase synthesises RNA primers for DNA polymerase III to begin elongation (Soultanas, 2005).

During elongation, helicase continues DNA unwinding. DNA polymerase III extends the RNA primers at bidirectional forks that move in opposite directions away from the *ori* (Reyes-Lamothe & Sherratt, 2019). The leading strand is synthesized continuously while the lagging strand is extended in short fragments (Okazaki fragments) which are later processed by polymerase I and ligase to create a complete strand (Reyes-Lamothe & Sherratt, 2019; Yao & O'Donnell, 2009).

Termination of DNA replication occurs at *ter* sites, where forks meet and are blocked by terminator proteins in a replication fork trap (Duggin et al., 2008; Duggin & Bell, 2009). Replisomes are disassembled, topoisomerase IV resolves interlinked chromosomes for cell division and finally the XerCD recombinase system recognises the *diff* site and catalyses site-specific recombination to resolve the dimer into two monomeric chromosomes (Dewar & Walter, 2017). The acronym ter will hence forth refer to the region of the chromosome containing the dif site, the site at which the XerCD system performs site-specific recombination.

Chromosome Segregation

The segregation of bacterial chromosomes is strictly regulated to ensure even distribution of genetic material and prevent the creation of anucleated daughter cells (Wang et al., 2013). The replication and segregation steps overlap significantly, with segregation beginning prior to replication termination (Wang et al., 2013).

The tri-component ParABS system is the most common active segregation mechanism, conserved in up to two-thirds of bacterial species studied (Jalal & Le, 2020). This system comprises three components: the ParA ATPase, the DNA-binding protein and CTPase ParB and its DNA-binding site *parS* (Jalal & Le, 2020). Following the formation of the initiation complex at *ori,* ParB binds to the *parS* sites located near the *ori*, forming a nucleoprotein complex (figure 1 A) (Wang et al., 2013). This binding stimulates the recruitment of additional ParB molecules that bind the DNA, creating a network of protein-DNA complexes (Wang et al., 2013). These complexes stimulate the ParA which, through cycles of ATP binding and hydrolysis drives the movement of the ParB-*parS* complex. As a result, the newly duplicated *ori* is directed towards the opposite pole (Jalal & Le, 2020). SMC (structural maintenance of chromosome) complex is also recruited to the bound ParB. This complex assists with chromosome segregation by reducing DNA entanglement (Wang et al., 2013).

The best studied bacterium, *E. coli*, interestingly lacks a ParABS system (Wang & Rudner, 2014). It is believed that the chromosome is instead driven primarily by passive self-organisation mechanisms. During chromosome replication the two replisomes progress bi-directionally and the duplicated *ori* regions are pushed towards opposite poles (Gogou et al., 2021). This movement is likely made possible by physical properties of the nucleoid, including supercoiling, entropic forces, and transcriptional activity

(Gogou et al., 2021; Harju & Broedersz, 2024). The SMC analogue MukBEF aids in the compaction of the newly synthesised DNA (Harju & Broedersz, 2024).

Cell Division

The creation of two distinct daughter cells begins after the initiation of chromosome replication and segregation. Two major protein complexes coordinate cell growth and division in rod-shaped bacteria: the elongasome and divisome. The precise spatial and temporal regulation of these complexes ensures balanced growth and division, preserving the characteristic rod morphology of the organism (Egan & Vollmer, 2013; Reyes-Lamothe & Sherratt, 2019).

Bacterial cell division has been extensively studied in transversally dividing, model, rod-shaped bacteria, like *E. coli*. The elongasome, directs cell wall synthesis during elongation. Guided by the actin-like protein MreB, new peptidoglycan is inserted along the lateral cell walls causing the cell to lengthen (figure 1 B) (Egan & Vollmer, 2013). Following cell elongation, the second multiprotein complex, the divisome, assembles at midcell. The tubulin-like protein FtsZ forms a contractile ring at mid-point spanning the width of the cell, known as the Z-ring (figure 1 B) (Egan & Vollmer, 2013; Reyes-Lamothe & Sherratt, 2019). As the divisome matures, the complex recruits' enzymes and downstream cell division proteins (Egan & Vollmer, 2013; Reyes-Lamothe & Sherratt, 2019). After chromosome replication and segregation are completed, the membrane tethered Z-ring begins to constrict. New peptidoglycan is synthesised and inserted to form the cell poles (Egan & Vollmer, 2013; Reyes-Lamothe & Sherratt, 2019). The elongated cell divides transversally (across the short axis of the cell) creating two new symmetrical daughter cells. (figure 1 B) (Reyes-Lamothe & Sherratt, 2019).

Cell elongation and transverse division is not universal to all rod-shaped bacteria. True appreciation for the full complexity and diversity of bacterial cell division can only be reached by looking past model organisms. Several rod-shaped bacteria have been observed expanding, increasing in width instead of length. The Z-ring in these organisms follows the long axis, stretching between cell poles. Upon constriction, the cell divides longitudinally, producing daughter cells side-by-side instead of end-to-end (figure X C) (Leisch et al., 2012).

The ectosymbionts *Candidatus* Thiosymbion oneisti, and *Candidatus* Thiosymbion hypermnestrae live attached by a single cell pole to their marine nematode partners (*Laxus oneistus* and *Robbea hypermnestrae,* respectively) (figure 1 C) (Ott et al., 2014; Polz et al., 1994). When live cells were incubated with peptidoglycan precursors it was discovered that the insertion of new cell wall began at the pole and proceeded inwards. FtsZ was found to localise similarly along the length of the cell. Z-ring constriction followed, separating longitudinally thus producing daughter cells side by side (Leisch et al., 2012; Pende et al., 2018). Longitudinal division has also previously been observed in other animal associated symbionts namely insects and dolphins (Dudek et al., 2023;

Ramond et al., 2016). The recurrence of this division mode across diverse host-associated suggests it may confer specific adaptive advantages, such as continued contact with the host surface during division and minimal exposure to the host immune system (Weber et al., 2019).

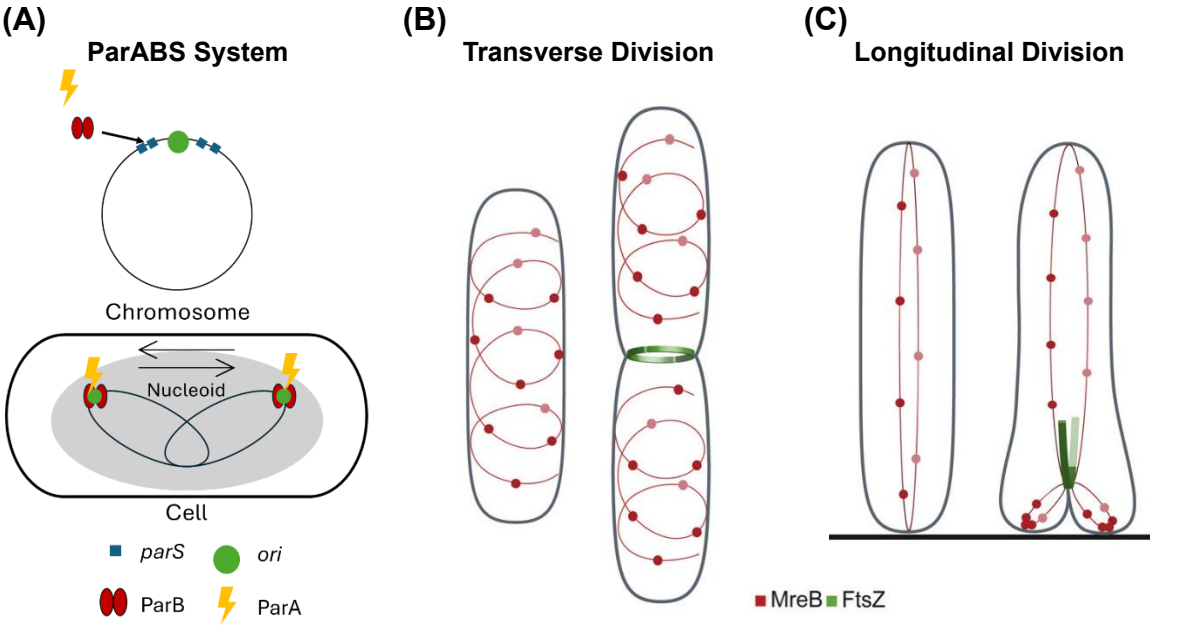

Figure 1: Bacterial Chromosome Segregation and Cell Division. (A) After chromosome replication begins, the protein ParB binds to the *parS* sites flanking the newly replicated origin (*ori*). ParA then drives the ParB-*parS* complexes to the cell poles causing segregation of the new daughter chromosomes. **(B)** & **(C)** The localisation of MreB directs the elongation or widening of a dividing rod-shaped bacterial cell. FtsZ monomers polymerize into a Z-ring that constricts to produce daughter cells. ((A) modelled on Rampelotto & Woldringh, 2024, (B)& (C) adapted from Pende et al., 2018)

Bacterial Genome Organisation

Bacterial genomes are compact highly organised structures that reflects the evolutionary drive for efficiency and adaptability. Usually smaller than eukaryotes they range from 130 Kbp to over 14 Mbp, with *E. coli* genome measuring approximately 4600 Kbp in length (Niki et al., 2000; Niki & Hiraga, 1998; Reyes-Lamothe et al., 2008). They are generally composed of a single, circular double-stranded DNA molecule (chromosome) although there have been recent reports of multiple circular or even linear chromosomes in some species (Galperin, 2007; Soppa, 2014). Some bacteria will also contain small, double stranded, circular DNA molecules called plasmids. Typically containing non-essential genes (e.g. antibiotic resistance or virulence factors) they can be transferred between bacteria and are a key component in bacterial evolution and adaption (Rodríguez-Beltrán et al., 2021). To understand the fundamentals of bacterial cell physiology, cell division, and gene regulation, it is crucial to first build a foundational knowledge of how bacteria organise and package their DNA. This can be achieved by examining ploidy, chromosome configuration and chromatin compaction (explored below).

Ploidy

The majority of known bacteria are monoploid, containing a singular circular chromosome housing all essential genes (Soppa, 2014). Recent investigations have discovered the existence of prokaryotic organisms containing two (diploid) or more (polyploid) copies of their chromosomes (Soppa, 2014). Diploidy and polyploidy has evolved independently in both bacteria and archaea from diverse phylogenetic groups, indicating it provides some selective evolutionary advantages (Soppa, 2014).

The bacteria *Deinococcus radiodurans* contains between 4 and 10 genome copies depending on growth stage and is highly resistant to damage by ionising radiation and desiccation (Cox & Battista, 2005; Hansen, 1978). It is proposed that this high level of genetic redundancy coupled with an extremely efficient recombination system is responsible for increased resistance to DNA damage (Cox & Battista, 2005; Hansen, 1978).

There have also been reported examples of polyploid induced by interactions with a symbiotic partner. *Ensifer meliloti* is a free living monoploid bacteria that can form a symbiotic relationship with several species of legumes. Upon entering the root nodules of the host plant, where it fixes nitrogen, the bacterium undergoes terminal differentiation (Penterman et al., 2014). During this process, the bacterial DNA content increase 5- to 10-fold and the bacteria loses its ability to survive independently (Farkas et al., 2014; Penterman et al., 2014). Peptides produced by the legume appear to inhibit the polymerisation of FtsZ, preventing cell septation, while other peptides have been found to inhibit bacterial protein translation (Farkas et al., 2014). This allows the plant to strictly govern the size, morphology and metabolism of the bacterial symbiont and thus maximise the returns (Kondorosi et al., 2013). The advantages to *E. meliloti,* however, are unclear and the association may even be harmful (Kondorosi et al., 2013).

Chromosome Configuration

Chromosome configuration refers to the positioning of key regions of the chromosome such as the beginning and end of replication (the origin, *ori* and terminus, *ter* respectively) (Wang & Rudner, 2014). In model rod-shaped bacteria that are not dividing, chromosomes are found in one of two major configurations: transverse or longitudinal (figure 2 A). In the transverse configuration (also referred to as "left–*ori*–right"), the origin and terminus are positioned at midcell, with the left and right arms of the chromosome extending into opposite halves of the cell (Wang & Rudner, 2014). In contrast, the longitudinal configuration (also known as "*ori–ter*") features the *ori* and *ter* located at opposite cell poles and the chromosome arms aligned along the long axis of the cell (Wang & Rudner, 2014).

In several free-living rod-shaped bacteria, the chromosome configuration is dynamic and can transition between transverse and longitudinal states (Wang & Rudner, 2014).

These transitions often correlate with stages of the cell cycle or environmental conditions (e.g. nutrient stress) (figure 2 B) (Wang & Rudner, 2014). This flexibility may reflect a need to optimise chromosome positioning for replication efficiency, segregation accuracy, and proper cell division (Wang & Rudner, 2014). Maintaining a stable chromosome configuration may also be beneficial to some organisms in specific conditions (Weber et al., 2019).

The model rod-shaped organism *E. coli* displays both transverse and longitudinal configurations depending on the growth rate. The reproduction of cells grown in minimal media is stalled and the chromosome configuration is transverse (Wang & Rudner, 2014). In contrast, when cells are grown in rich media, multiple rounds of replication occur simultaneously. The origins duplicate early and quickly move to localise at the cell poles, adopting an *ori-ter* configuration (Wang & Rudner, 2014). Chromosome configuration in *B. subtilis* also alternates between transverse and longitudinal at different stages in the cell cycle. Prior to replication the chromosome is transversely configured. During replication the new *ori* moves to the pole but migrates back to midcell once chromosome segregation is completed. This alternating pattern was observed regardless of the rate of cell growth (Wang & Rudner, 2014).

The dynamic chromosome configuration described in transversally dividing, free-living, rod-shaped bacteria is not universal. Some bacteria may adopt a configuration that is not affected by nutrient availability or cell cycle stage. Examples include the previously described longitudinally dividing nematode symbionts *Ca*. T. oneisti (Weber et al., 2019) and *Ca*. T. hypermnestrae (Viehboeck et al., 2024).

Ca. T. oneisti maintains a “semi-stable configuration”, with the *ori* consistently localising to midcell regardless of cell cycle and across generations (Weber et al., 2019). Prior to the commencement of cell division, the *ter* also localise to the midcell, creating a transverse configuration (Weber et al., 2019). However, as the cell cycle progresses the *ter* migrates to the cell poles, before eventually returning to its original position when cell division is complete (figure 2 C) (Weber et al., 2019). Additionally, the ParB protein localise with the *ori*, indicating its likely involvement in chromosome segregation (Weber et al., 2019).

These initial observations of a semi-stable chromosome configuration in *Ca. T. oneisti* inspired further investigations into the chromosome configuration of *Ca. T. hypermnestrae*. In this organism, the *ori* and *ter* localise to the opposite poles. The *ori* is found at the host attached proximal pole and the *ter* at the free distal pole. This stable longitudinal configuration is maintained regardless of stage in cell cycle or environmental conditions (figure 2 C) (Viehboeck et al., 2024). It is suggested that this chromosome configuration may support a symbiotic lifestyle. It may ensure the consistent positioning of genetic loci mediating host interactions to the proximal pole of the cell (Viehboeck et al., 2024).

Chromatin Compaction

Unlike eukaryotes, bacterial DNA is not enclosed in a nucleus. The chromosome, which is usually significantly longer than the length of the cell, is condensed into is condensed into a region called the nucleoid, occupying just 15-25% of the total cell volume (Joyeux, 2015). This compaction is governed by several highly organised but dynamic structural and molecular mechanisms. These allow for reorganisation during various stages in the cell cycle and are essential for faithful chromosome replication and segregation (Kisner & Kuwada, 2020). These mechanisms include supercoiling, (nucleoid-associated proteins), macromolecular crowding and condensin-like complexes (e.g. SMC – structural maintenance of chromosome) (Joyeux, 2015; Shen & Landick, 2019).

Supercoiling is the winding of the DNA double helix beyond its relaxed state, which reduces the effective volume of the chromosome. This is achieved with the assistance of the enzymes DNA gyrase and topoisomerase I / IV (Reyes-Lamothe & Sherratt, 2019; Wang et al., 2013). Supercoiling is not only critical for DNA compaction but also for the organisation of DNA into topological domains (or loops). They not only condense the genetic material further but also act as a dynamic regulator of gene expression, responsive to environmental and metabolic changes (Reyes-Lamothe & Sherratt, 2019; Wang et al., 2013)

The stability of these DNA loops is maintained by interaction with proteins such as NAPs. These proteins (e.g. HU, Fis and IHF) bind to DNA, inducing bends and creating bridges between different DNA regions. This leads to the formation of loops and other secondary structures (Dillon & Dorman, 2010). The histone-like protein HU is the most highly conserved NAP, abundantly found in many bacterial species during growth (Dillon & Dorman, 2010). It binds non-specifically to the supercoiled DNA, not only playing a role in topological reshaping of the wound DNA, in the formation of RNA-DNA complexes (Dillon & Dorman, 2010).

The dense environment of the bacterial cytoplasm also contributes to chromosome compaction via macromolecular crowding that physically restricts the space the chromosome can occupy (Dillon & Dorman, 2010; Harju & Broedersz, 2024). Finally, SMC complexes like MuKBEF found in *E. coli,* further maintains DNA compaction and are especially important during chromosome replication, segregation, and cell division (Dillon & Dorman, 2010; Harju & Broedersz, 2024).

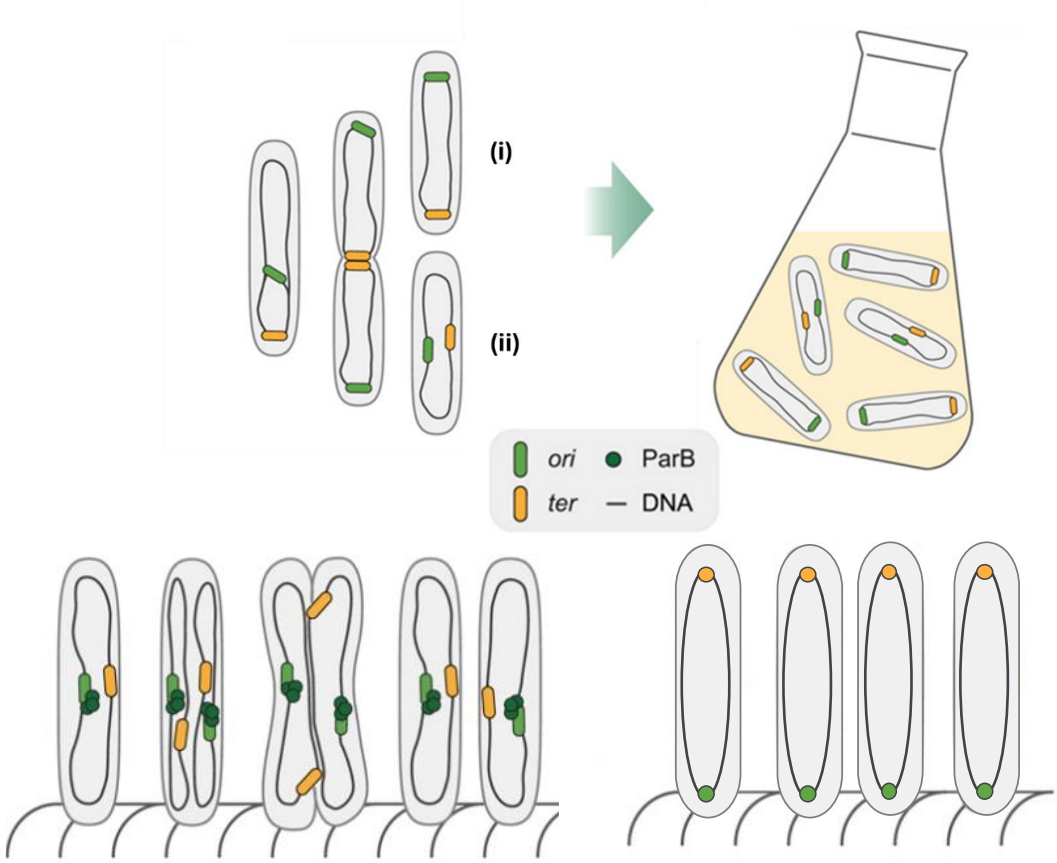

Figure 2: Dynamic Chromosome Configuration in Model Rods & Stable Chromosome Configuration in Bacterial Symbionts. The origin (*ori*, green) marks the start of bi-directional DNA replication, while the terminus (*ter*, orange) is where replication forks meet. (top) There are two configurations in model rods: (i) longitudinal with the *ori* and *ter* at the cell poles, or (ii) transverse with the *ori* and *ter* located at midcell. (Bottom left) Transverse chromosome configuration in the nematode- attached symbiont *Ca*. T. oneisti and (bottom right) longitudinal chromosome configuration in the nematode-attached symbiont *Ca*. T. hypermnestraes. (Image adapted from Viehboeck et al., 2024; Weber et al., 2019)

Multicellular longitudinally dividing *Neisseriaceae*

The *subject* of this study will be the gram-negative, Gammaproteobacteria *Alysiella filiformis, Simonsiella muelleri, Conchiformibius steedae* and *Conchiformibius kuhniae* (Hedlund & Kuhn, 2006; Hedlund & Tønjum, 2015, 2015; Nyby et al., 1977; Steed, 1963). They have thus far been exclusively found living as symbionts of the oral cavity of warm-blooded vertebrates such as dogs, sheep, chickens and humans (Nyby et al., 1977; Steed, 1963). Growing in long multicellular filaments, they are most commonly found living attached to mucosal squamous epithelium cells of the hosts hard pallet. They have also been found colonising other areas of the mouth, such as the tongue, cheeks and throat (Hedlund & Kuhn, 2006). Despite belonging to the *Neisseriaceae* family with *N. meningitidis* and *N. gonorrhoeae,* these symbionts are non-pathogenic, although their exact role in human health (if any) remains unclear.

The rod-shaped, monoploid *A. filiformis* forms ribbon like filaments that attach to the host surface by a single pole (figure 3 A). In contrast, the diploid organism *S. muelleri* forms shorter filaments comprised of longer thinner, crescent-shaped cells with both poles attached to the host epithelium (figure 3 B). *C. steedae* is similarly diploid and crescent-shaped with bipolar host attachment, but filaments are comprised of cells longer than those in *S. muelleri* (figure 3 C). All three organisms possess host-proximal fimbriae. The fimbriae are found at the host attached pole of *A. filiformis,* and on the concave ventral side of the curved *S. muelleri* and *C. steedae* (G. E. Kaiser & Starzyk, 1973; Nyby et al., 1977; Nyongesa et al., 2022; Viehboeck et al., 2024). Until this study, little was known about *C. kuhniae,* and it is hypothesised to have similar ploidy and morphology as its close relative the aforementioned *C. steedae*.

Longitudinal Division of Multicellular Oral Symbionts

Longitudinal cell division has been observed in several obligate bacterial symbionts such as nematodes, dolphins and insects (Dudek et al., 2023; Leisch et al., 2012; Pende et al., 2018; Ramond et al., 2016), and more recently in *A. filiformis*, *S. muelleri*, and *C. steedae* (Nyongesa et al., 2022). In *A. filiformis* division begins at the host attached, fimbriated (proximal – P) pole moving towards the free (distal – D) pole (Nyongesa et al., 2022). In *S. muelleri* and *C. steedae* – which are crescent-shaped and attached to the host surface by both poles – separation begins simultaneously at both poles moving towards each other and meeting at midcell (Nyongesa et al., 2022).

Chromosome Configuration of Oral Symbionts

Using DNA-FISH (Fluorescence in-situ hybridization) the chromosome of the monoploid *A. filiformis* were found in a longitudinal configuration. They maintain a similarly stable host polarised *ori* localisation as seen in *Ca*. T. hypermnestrae with the *ter* in the distal (free) pole (figure 3 A) (Viehboeck et al., 2024). A longitudinal stable chromosome configuration is also found in the diploid *C. steedae*. Here, the two *ori* are each positioned at one of the host-attached poles and the two *ter* at the midcell (figure 3 C) (Viehboeck et al., 2024).

DNA-FISH experiments were performed on the diploid *S. muelleri*. As seen in *C. steedae*, both *ter* localised to the midcell. Interestingly however, the *ori* was subpolar (figure 3 B) (Viehboeck et al., 2024). This was initially attributed to the curve of the crescent-shaped cell distorting the localisation when observed in only two dimensions. However, when using 3D-SIM (Structured illumination microscopy) the *ori* was still sub-polar (supplemental figure 1, N. Krause, unpublished). This stable subpolar *ori* may be unique to S. *muelleri* but raised speculation about which chromosomal region, if not the *ori*, is located at the cell pole.

Moreover, chromosome conformation capture (3C) was used to probe the interactions between the right and left chromosomal arms of *A. filiformis, S. muelleri,* and C.

steedae (Viehboeck et al., 2024). The genetic contact maps of *S. muelleri* and C. *steedae* display a secondary diagonal, indicative of interarm DNA contacts. In contrast, a secondary diagonal was barely detected in the *A. filiformis* genetic contact map (Viehboeck et al., 2024). Although the chromosome configuration in all three organisms appears stable, these results suggest that interarm interactions occur at much lower frequencies in *A. filiformis* (Viehboeck et al., 2024). One possible explanation is that the two chromosome arms in the monoploid *A. filiformis* are laying longitudinally but are simply positioned further apart than in the thinner, longer and apparently diploid *C. steedae* and *S. muelleri* (Viehboeck et al., 2024). Alternatively, despite the stable polar localisation of the *ori* and *ter*, the chromosome arms in *A. filiformis* may remain dynamic and move freely. Finally, the lack of interarm interactions may also reflect the absence of SMC-based *ori-ter* oriented loop extrusion mechanism (Wang et al., 2017).

Conchiformibius kuhniae & New Genetic Tools

Unfortunately, the in-depth study of the mechanisms that maintain the stable chromosome configuration has been hampered by the inability to perform targeted genetic modifications. Recently, the previously unexplored organism *Conchiformibius kuhniae* has become genetically tractable, opening new avenues for investigation (supplemental figure 2, Krause & Veyrier, unpublished). The chromosome segregation system ParABS system as well as the genes encoding for the SMC complex are present in the genomes of *A. filiformis, S. muelleri, C. steedae,* and *C. kuhniae*. They may play a role in the maintenance of the stable chromosome configuration and/or segregation. By unlocking the ability to genetically manipulate *C. kuhniae* this hypothesis can now be tested. ParB knockouts of *C. kuhniae* can now be created and the chromosome configuration of these mutants can be compared to the wild type. However, prior to this study, there was no information on the chromosome configuration of the wild type *C. kuhniae*. It is hypothesised to be diploid and have longitudinal stable chromosome configuration based on observations of the related *C. steedae* (Viehboeck et al., 2024).

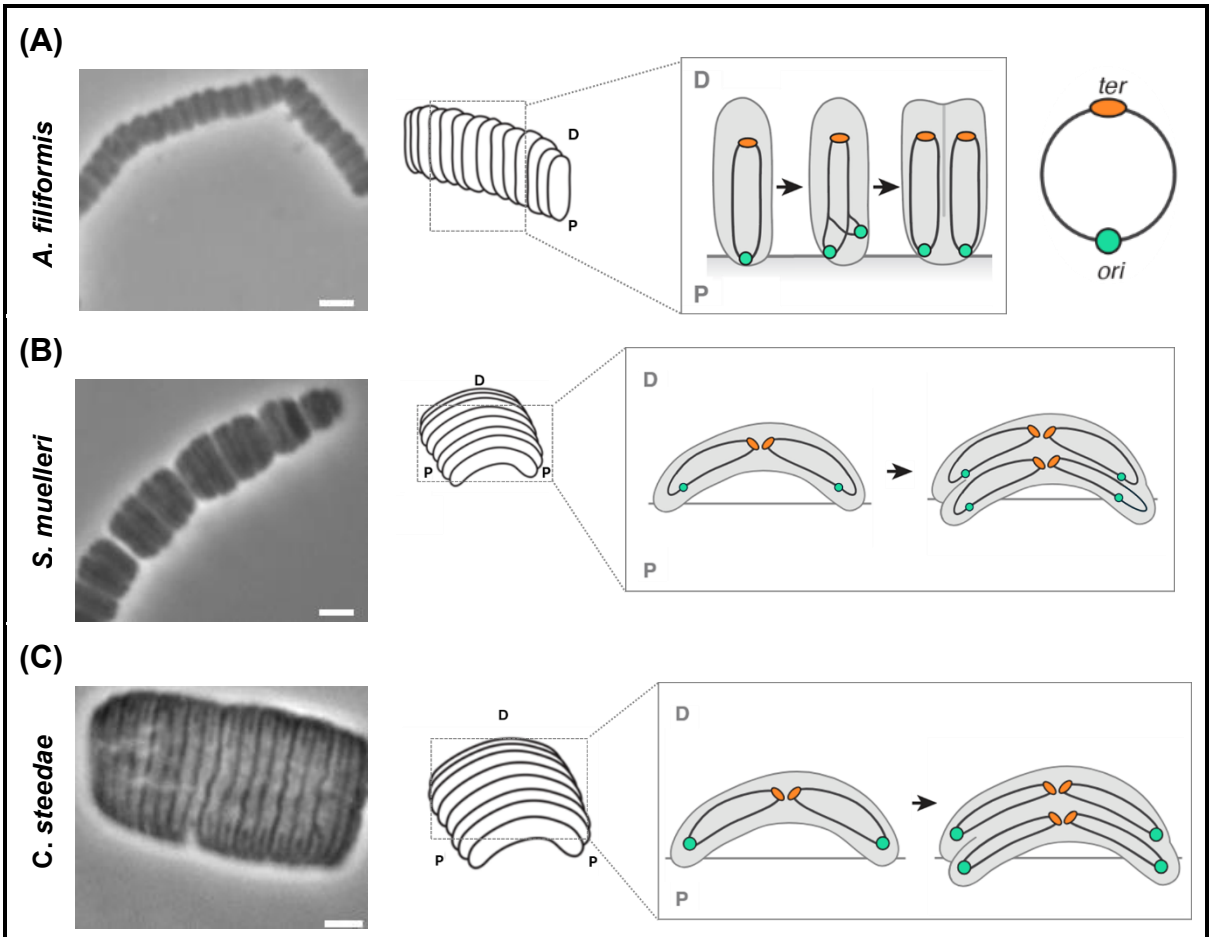

Figure 3: Representative Images, Sketches & Schematic Representations of Chromosome Configuration of *A. filiformis* (A), *S. muelleri* (B) & *C. steedae* (C). Left Panels: Phase contrast microscope images. Top down view. Scale bar is 2 µm. Middle Panels: Sketches of filaments (lateral view). **(A)** *A. filiformis* is rod-shaped, **(B)** *S. muelleri* and **(C)** *C. steedae* are crescent-shaped as displayed in the filament sketches in the middle panels. Right panels: Schematic representations of chromosome configurations of (A) *A. filiformis*, (B) *S. muelleri* and (C) *C. steedae*. The origin of DNA replication (*ori*) is green, and the terminus (*ter*) is orange. P: Host-attached pole (proximal). D: distal (free, unattached pole). (Adapted from Viehboeck et al., 2024)

Research Questions & Aims

Research in bacterial cell biology, especially chromosome configuration and segregation, has in the past primarily focused on free-living, model, rod-shaped organisms such as *Escherichia coli* and *Bacillus subtilis*. This has limited our understanding of the true diversity that exists, particularly among symbiotic bacteria. Preliminary results have demonstrated that chromosome configuration of several longitudinally dividing oral symbionts is stable (Viehboeck et al., 2024). The mechanism that leads to this stable chromosome configuration is unknown but may involve the chromosome segregation system ParABS. The consistent localisation of the *ori* at the host-attached pole may play a role in its symbiotic nature. This study aimed to further explore the stable chromosome configuration of *A. filiformis* and *S. muelleri,* in addition to determining the chromosome configuration of *C. kuhniae* for the first time. The questions outlined below were addressed.

1. Are the centres of the *left* & *right* chromosomal arms of *A. filiformis* stably localised at midcell?

As outlined previously, despite *A. filiformis*, *S. muelleri,* and *C. steedae* all sharing a stable chromosome configuration, 3C-seq predicted that *A. filiformis* has a lower frequency of interarm contacts than that observed in *S. muelleri* and C. *steedae* (Viehboeck et al., 2024). This may indicate instability of the right and left chromosome arms in *A. filiformis*. Therefore, the first aim of this project was to establish if the centre of the left and right arms are stably at midcell. This was achieved using direct gene FISH on a central region of either the right or the left arm.

2. Are there *parS* Sites Localised at the Cell Poles, in *S. muelleri*?

Experiments using direct gene FISH demonstrated that unlike the related *A. filiformis* and *C. steedae,* the *ori* of *S. muelleri*, which is flanked by three *parS* sites, was sub-polarly localised (Viehboeck et al., 2024). This stable subpolar *ori* localisation may be unique to *S. muelleri* but raises the question whether other *parS* sites are polar. Based on the chromosome map of *S. muelleri*, a cluster of five *parS* (hence forth referred to as the 5X-*parS* cluster), is found at position 1,447,496 bp, 206,519 bp away from the *ori* (figure 4 B). It is therefore reasonable to suggest that this 5X-*parS* cluster rather than the *ori* might be polar in *S. muelleri*. The binding of ParB to this 5X-*parS* cluster may contribute to the maintenance of stable chromosome configuration and/or lateral chromosome segregation. The second aim of this project was therefore to determine if the 5X-*parS* cluster localise to the poles of S. *muelleri*. This was again accomplished using direct gene FISH to specifically target this region.

3. Does *C. kuhniae* also have a stable longitudinal chromosome configuration?

The newly acquired ability to genetically modify a longitudinally dividing oral symbiont, *C. kuhniae*, (Krause, unpublished) has opened up several avenues for further investigation. Although, little is known about its cell biology, based on the morphologically similar and phylogenetically related *C. steedae,* it is hypothesised to be diploid and have a similarly stable longitudinal chromosome configuration (Viehboeck et al., 2024). The final aim of this Master thesis was to perform direct gene FISH on *C. kuhniae* to localise the *ori* and *ter*. Crucially, determination of the chromosome configuration in the first genetically tractable multicellular *Neisseriaceae* paves the way to the discovery of the underlying molecular mechanisms.

Methods

A. filiformis, S. muelleri, C. steedae & *C. kuhniae* Strains & Cultivation

Bacterial strains were ordered from the "Leibniz Institute DSMZ-German Collection of Microorganisms and Cell Cultures" (*A. filiformis* - DSM No.: 16848, *S. muelleri* - DSM No.: 2579, *C. steedae* DSM No.: 2580 & *C. kuhniae* DSM No.: 17694).

15% glycerol stock solutions of each bacterial strain were created and stored at -80°C until required. All media was prepared in advance. To prepare media powdered components were dissolved in Milli-Q H_2O, autoclaved and stored at 4°C (tables 1-7). Prior to inoculation media was warmed to 37°C. All glassware used for bacterial culture (e.g. baffled or Erlenmeyer flasks) were thoroughly rinsed with RO (reverse osmosis) purified water and then autoclaved. All inoculations and later sampling were carried out in a UV sterilised laminar flow cabinet to minimise contamination.

A. filiformis

Glycerol stocks of *A. filiformis* were added to a baffled flask containing PY media (table 1) in the dilution ratio of 1:1000 (e.g. 50 µl glycerol stock in 50 ml PY media). These were incubated for approximately 16-18 hours overnight at 120 rpm at 37°C. Overnight cultures were used to inoculate an Erlenmeyer flask containing B media (table 2) (1:1000 dilution ratio), which were incubated at 120 rpm at 37°C.

S. muelleri

100 µl of *S. muelleri* glycerol stocks were inoculated onto BSTSY agar plates, (table 3) spread, and incubated at 37°C for 18-24 hours. Colonies from these plates were inoculated into an Erlenmeyer flask containing 100 ml of BSTSY media (table 3) and grown overnight at 120 rpm at 37°C. BSTSY media could alternatively be inoculated directly using glycerol stocks in a 1:1000 dilution and grown overnight at 120 rpm at 37°C.

C. steedae

Similarly to *S. muelleri* described above, *C. steedae* could be first grown on BSTSY plates (table 3) followed by inoculation into BSTSY media (table 3). Alternately, glycerol stocks could be directly inoculated into BSTSY media. All cultures were incubated at 37°C and liquid cultures were shook at 120 rpm.

C. kuhniae

100 µl of *C. kuhniae* glycerol stocks were inoculated onto GCB plates (table 4) and incubated at 37°C overnight. Colonies from these plates were transferred into liquid GCB media (table 5) and incubated in a 37°C incubator shaking at 120 rpm. Glycerol stocks could also be added directly to GCB liquid media in a 1:1000 dilution and incubated at 120rpm 37°C overnight.

Table 1: PY Medium	
Ingredient	**Percentage (% wt/vol)**
Peptone from meat	1.5
Yeast Extract	0.3
NaCl	0.5
K_2HPO_4	0.25
Agar*	1.2*
Post autoclaving 12.5% glucose solution was added for a final concentration of 0.025% (%vol/vol). * Only added when creating plates.	

Table 2: B Medium	
Ingredient	**Percentage (% wt/vol)**
Peptone from meat	1.5
Yeast Extract	0.3
NaCl	0.5
K_2HPO_4	0.1
Agar*	1.2*
Post autoclaving 12.5% glucose solution was added for a final concentration of 0.025% (%vol/vol). * Only added when creating plates.	

Table 3: BSTSY Medium	
Ingredient	**Percentage (wt/vol %)**
Tryptone soja bouillon without dextrose	2.75
Yeast Extract	0.4
Agar*	1.5
Post autoclaving Foetal Bovine Serum was added for a final concentration of 10% (%vol/vol). * Only added when creating plates	

Table 4: GCB Medium	
Ingredient	**Percentage (wt/vol %)**
Proteose Peptone	1.5
K_2HPO_4	0.4
KH_2PO_4	0.1
NaCl	0.5
Prior to autoclaving pH was adjusted to 7.2 using NaOH. Post autoclaving Kellogg's supplement 1 & 2 (tables 6 & 7) were added to the ratios of 1:100 & 1:1000.	

Table 5: GCB Agar	
Ingredient	**Percentage (wt/vol %)**
GC Agar Base (Oxide CM0367)	3.8
Post autoclaving Kellogg's supplement 1 & 2 (tables 6 & 7) were added to the ratios of 1:100 & 1:1000.	

Table 6: Kellogg's Supplement 1	
Ingredient	**Percentage (wt/vol %)**
$C_6H_{12}O_6$ – Glucose	40
$C_5H_{10}N_2O_3$- L-glutamine	1
$C_{12}H_{19}ClN_4O_7P_2S$- Thiamine Pyrophosphate	0.002
Components dissolved in Milli-Q at 37°C followed by sterile filtration using a 0.22µm membrane, aliquoted and stored at -20°C	

Table 7: Kellogg's Supplement 2	
Ingredient	**Percentage (wt./vol %)**
FeN_3O_9-$9H_20$	0.5
Components dissolved in Milli-Q at 37°C followed by sterile filtration using a 0.22µm membrane, aliquoted and stored at -20°C	

Sample Collection, Bacterial Cell Fixation & DNA Extraction

Post inoculation into liquid media, bacterial growth was monitored at regular intervals. 1 ml samples of culture were transferred to cuvettes, and a spectrophotometer was used to measure the optical density at a wavelength of 600 (OD_{600}). Growth curves constructed on these organisms in the past have established that they reach exponential phase at approximately 0.2-0.3 OD_{600} and enter stationary phase at approximately 0.9 OD_{600}. Unless otherwise stated, all cells from liquid culture were fixed at in mid-exponential phase (≈ 0.5 OD_{600}).

Bacterial Cell Fixation

When liquid cultures had reached the desired OD_{600}, 1ml samples were taken. These samples were mixed with 37% paraformaldehyde for a final concentration of 4% and incubated for 1 hour at room temperature (or 4°C overnight). The samples were then centrifuged for 5 minutes at 5000xg. The supernatant was carefully discarded, and the pellet was resuspended in 500µl of 1X PBS to remove any residual paraformaldehyde and then again centrifuged. This wash step was repeated, and the resulting cell pellet was resuspended in a small volume (5-100µl based on pellet size) of 1X PBS. Fixed cells were stored for up to a week at 4°C.

When fixing cells grown from solid agar media, 10µl disposable inoculation loops were used to pick colonies which were then resuspended in 1ml of 1X PBS. Fixation then continued as described above.

DNA Extraction

Genomic DNA was extracted using a phenol-chloroform based protocol. Bacterial cultures were grown until exponential phase and pelleted, then stored at -20C until required for DNA extraction. While cell pellets were left to thaw on ice (approximately 5 minutes) TLB was freshly prepared (table 8). 450 µl was used to resuspend the thawed pellets and they were vortexed thoroughly.

RNA was removed from the sample via the addition of 10 mg/ml RNase A (final concentration 2mg/ml). Lysozyme solution with the final concentration of 100 mg/ml was prepared (table 14) and added to the cell suspension for a final concentration of 2mg/ml. The samples were vortexed and then incubated at 37°C 350 rpm for 30 minutes. This was followed by the addition of 20 mg/ml of Proteinase K (final concentration 1mg/ml) and a further 30-minute incubation at 50°C, 350 rpm.

500 µl of Phenol: chloroform: isoamyl alcohol solution (25:24:1, 1X volume) was added and the sample was vortexed for 1 minute. This was followed by a 5-minute max speed centrifugation at 4°C. This causes the solution to separate into distinct phases, and the upper phase was transferred to a fresh 1.5 ml Eppendorf tube. This was then combined with 500 µl of chloroform: isoamyl alcohol (24:1, 1X volume), vortexed and centrifuged as described above. The resulting upper phase was again transferred into a fresh Eppendorf tube.

This second upper phase was mixed with 7.5M NH_4OAc and 5mg/ml glycogen (final concentration 2.5M and 5µg/ml, respectively) and vortexed. Sample was combined with precooled 100% EtOH in a ratio of 1:2, vortexed, and incubated for 30 minutes at -20°C. The sample was centrifuged at 4°C for 30 minutes at max speed and the supernatant carefully decanted and discarded. The resulting pellet was washed with 80% precooled EtOH. This was followed by 15-minute max speed centrifugation at 4°C. The supernatant was removed, and the tube was spun and air dried to allow for the

evaporation of residual EtOH. 30 µl of DEPC-H_2O was added and the sample was shaken at 37°C 300rpm for 1 hour. The sample was quickly spun down and the nanodrop was used to measure the DNA concentration. The final DNA extraction was then stored at -20°C until required.

Table 8: TLB

	Stock Concentration	Final Concentration
NaCl	5M	100mM
Tris-HCl (pH = 8.0)	1M	10mM
EDTA (pH =8.0)	0.5M	25mM
SDS (20%)	20%	0.5% (v/v)
Components were combined with 0.1% DEPC (diethyl pyrocarbonate) treated water for a final volume of 1 ml.		

Fluorescence in-situ hybridization (FISH)

Direct-gene FISH protocol was modified from (Barrero-Canosa et al., 2017; Moraru & Barrero-Canosa, 2021) and was successfully performed on multicellular oral symbionts previously (Viehboeck et al., 2024).

Design of Gene Probes

The areas of interest that would be targeted by specially designed DNA probes were first identified on the bacterial genome. The origin (*ori*) and terminus (*ter*) sites of *A. filiformis* (targets in previous FISH experiments) were predicted using the bioinformatics tool Genskew (https://genskew.csb.univie.ac.at/). It calculates skew values (typically GC or AT skew) across sliding windows in the genome using the formula $(nucleotide_1 - nucleotide_2) / (nucleotide_1 + nucleotide_2)$. The cumulative skew plot reveals patterns where the global minimum often indicates the origin of replication, and the global maximum marks the terminus. These predictions align with known genomic features and can be validated with sequencing coverage and replication-associated motifs. The centre of the regions connecting the predicted *ori* and *ter* in *A. filiformis* on the left and right side were selected as the target for DNA FISH (figure 4 A). The left arm typically has a negative gene skew while the right is positive. The clusters of 5X-*parS sites* were found near the predicted *ori* of *S. muelleri* (figure 4 B). The *ori* and *ter* of *C. kuhniae* were similarly predicted using Geneskew (figure 4 C).

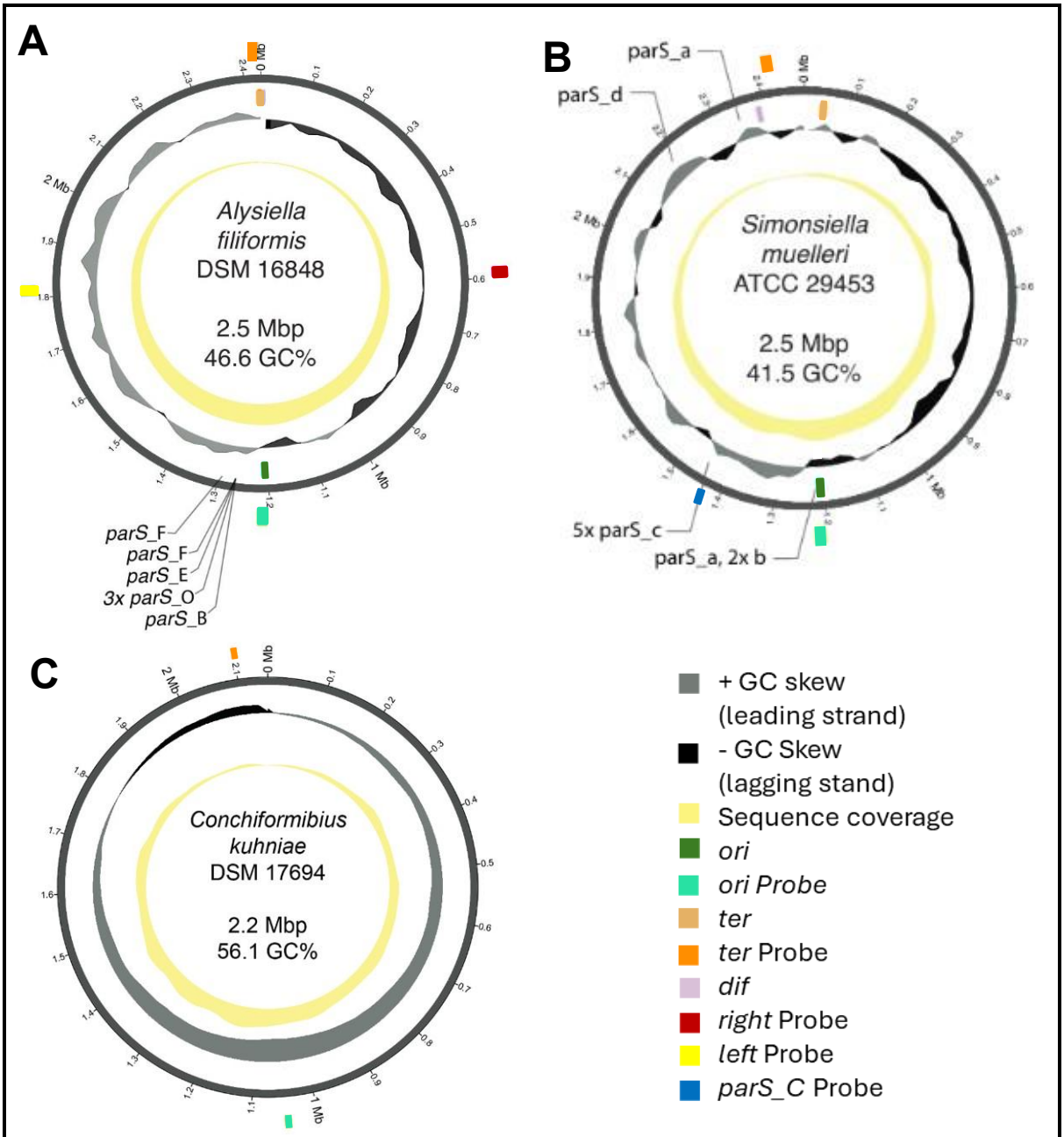

Figure 4: Chromosome Maps of (A) *A. filiformis*, (B) *S. muelleri* & (C) *C. kuhniae*. The dark grey outer circle is the position in Megabase of the genome. The middle circle represents the GC skew: grey is positive (leading strand) and black is negative (lagging strand). The yellow inner circle represents the sequencing coverage. Positions of the *ori* (dark green), *ter* (tan), *dif* (purple) can be seen between the outer and middle rings. The locations of *parS* on the genome are labelled. The specific targets of DNA FISH probes are represented by boxes on the outer ring: *ori* probe (light green), *ter* (orange), left (yellow), right (red) and 5X-*parS* (blue). (Figures A-B adapted from Viehboeck et al., 2024 & C from Krause, unpublished).

Following identification, the Software Gene-Prober (Moraru & Barrero-Canosa, 2021) was used to design a specific set of polynucleotides for the right and left arms of *A. filiformis* and the 5X-*parS* sites of *S. muelleri*. For *A. filiformis,* fragments approximately 10,000 bp long that covered the centre of the right chromosomal arm were input into the software, along with the whole genome sequence. The software was configured using specific parameters (e.g. polynucleotide length of 300bp, GC content of 40-60%)

and the protocol was allowed to run. The software produced multiple candidate probes (and corresponding primer pairs) that target the region of interest. Of these, 10 probes were chosen based on proximity to each other. This was repeated for the left chromosomal arm of *A. filiformis* (table 10). A similar approach was initially taken for the production of probes to target the 5X-*parS* sites of *S. muelleri*. However, the presence of multiple sequence repeats in this region made this challenging and 10 unique probes could not be produced. The region of interest was therefore expanded to include sections flanking either side of the *parS* site cluster repeats to give a total region of 10,000 bps. This yielded 9 unique probes and corresponding primer pairs (table 9).

Server issues prevented Gene-Prober from being used to design the probes for the *ori* and *ter* of *C. kuhniae*. These probes were instead designed manually using the application Primer3plus (https://www.primer3plus.com/index.html). The *ori* was divided into 10 sections (numbered 1-10) of approximately 850 bp in length. An additional 500 bp at the start and end of the *ori* were also selected and numbered 0 and 11 respectively. Each section was individually uploaded to Primer3plus which returned a list of 10 forward and reverse primers. Primer pairs were verified and the most appropriate were chosen (table 11). This was then repeated for the *ter* region of *C. kuhniae*.

All primers designed using either Gene-Prober or Primer3plus were produced by Microsynth (https://www.microsynth.com/home-ch.html) (tables 9-11). The dried primer stocks were then reconstituted with DEPC water as directed to produce a solution of 100µM in concentration. Working primer of 10µM concentration stocks were created.

Table 9: *S. muelleri* Polynucleotides used for FISH probes

Target	Probe No.	Primer	Sequence (5'-3')	Product (nt)
S. muelleri 5x *parS* (9335 bp)	1	Sm_ParS_1F	AATACCCATCCTACGTCTGA	300
		Sm_ParS_1R	CTCTTGTTGGCGTTCTAAAATC	
	2	Sm_ParS_2F	TTATGCACGTGAGATTGAC	300
		Sm_ParS_2R	GCATTACGCAACAAGTCAT	
	3	Sm_ParS_3F	CAACATCACAAAGTACCAGTAC	300
		Sm_ParS_3R	CTACGGCTGTAGGTGATAAT	
	4	Sm_ParS_4F	TGGATATTCCTGTGGTACCA	300
		Sm_ParS_4R	CTGGGTCATAAGTGTAATTCAC	
	5	Sm_ParS_5F	GTAAAGCTAAAGACCACACAG	300
		Sm_ParS_5R	GTACACCTGTAACAGTTGT	
	6	Sm_ParS_6F	AGGCAATGTAACGACAGAAG	300
		Sm_ParS_6R	GTAACTGTGTAAACCGCCTTA	
	7	Sm_ParS_7F	GGTAATACCAAAGGCACAAATC	300
		Sm_ParS_7R	CGGTTCTAATTGCAACGTC	
	8	Sm_ParS_8F	AGTTCTGGCGTGACTTTATT	300
		Sm_ParS_8R	AACTTTACCAGTCGTGTAAC	
	9	Sm_ParS_9F	TACTGATAGTTTACCAGTAGCG	300
		Sm_ParS_9R	AATTTTGCTGTTGAGGTATCG	

Table 10: *A. filiformis* Polynucleotides used for FISH probes				
Target	**Probe No.**	**Primer**	**Sequence (5'-3')**	**Product (nt)**
A. filiformis Centre of Right Chromosome Arm (7846 bp)	1	Af_rightarm1F	ACGATAAACCTTGATGTTGC	300
		Af_rightarm1R	TTGATGATGCGCTTGAAAC	
	2	Af_rightarm2F	AAAATCGGTCAAAATAGCCC	300
		Af_rightarm2R	CAAACGCATTATCCCAATCTC	
	3	Af_rightarm3F	GCAGCCTGAAAATTATTCG	300
		Af_rightarm3R	TTGCAAAACGTGGACATC	
	4	Af_rightarm4F	CAAACGTGGCAAATTTCG	300
		Af_rightarm4R	CGCAAACAAAATCAAGGCTA	317 (new)
		Af_Rightarm_4R_New	GGCACCAAATAGCGTACC	
	5	Af_rightarm5F	AATGTCGCTGATTGGTTTG	300
		Af_rightarm5R	GCCAAACTCAATGCAAACA	
	6	Af_rightarm6F	GCAGGCGAATTTGGTTTT	300
		Af_rightarm6R	GTGGTTGTCAATCACGGTA	
	7	Af_rightarm7F	CTGAAACGGCTTTTTAGGTG	300
		Af_rightarm7R	CAGCCGACTTAACCCAAG	
	8	Af_rightarm8F	GTGTGATTTGTTCGCGTG	300
		Af_rightarm8R	ATGAACACAATTTGCCCG	283 (new)
		Af_Rightarm_8F_New	GAATAAACGCAGGGTACG	
	9	Af_rightarm9F	GCGGTTACTTTGGCTTTG	300
		Af_rightarm9R	ACACCACAAACAAAATCACG	280 (new)
		Af_Rightarm_9F_New	TTTGCCAAAATCGGGCG	
		Af_Rightarm_9R_New	CAAACAAAATCACGCCAAAT	
	10	Af_rightarm10F	CAAACATTTGCTTGTTGCC	300
		Af_rightarm10R	AATTCTTGCGCCATTTCC	286 (new)
		Af_Rightarm_10F_New	ACGGCTTTGAATGCTTTG	
		Af_Rightarm_10R_New	GCGTATTGCCAAAATCCAC	
A. filiformis Centre of Left Chromosome Arm (6718 bp)	1	Af_leftarm1F	TGCAGGTTTAGGAACATCTAC	300
		Af_leftarm1R	GCTGAAATTCCGGGTTTG	
	2	Af_leftarm2F	GATGGCAACCAAGTCTTTATC	300
		Af_leftarm2R	ATGGTGTTGTGTATCTGCA	
	3	Af_leftarm3F	AACCTGTATTGGGAATGGAAC	300
		Af_leftarm3R	AAGCCCTGATTATTGAGTCG	
	4	Af_leftarm4F	GACTCCACAAACTCTTGTAAAC	300
		Af_leftarm4R	AAACGTTATCGGACTAGACATC	303 (new)
		Af_Leftarm_4F_New	CACTCGGCTCACTTCCG	
		Af_Leftarm_4R_New	CTAGACATCAGCCCCAGC	
	5	Af_leftarm5F	TTTATTCTTCTGATGGCGTG	300
		Af_leftarm5R	CAATTTTGTAGGCAAGCAAG	282 (new)
		Af_Leftarm_5R_New	AGGCTTCATTGAATTTGCG	
	6	Af_leftarm6F	CACTTTGACCAAAGACCAAA	300
		Af_leftarm6R	CGTTCGTAAATCAATTCGGC	
	7	Af_leftarm7F	GCGCAATTTTCCATCAAAAG	300
		Af_leftarm7R	TGGGTAACATAAGGACGGT	
	8	Af_leftarm8F	GGCTACGATTTCCACAGTAA	300
		Af_leftarm8R	GAAACCAAAACGTTGCACA	
	9	Af_leftarm9F	GCAACTTAACGATGCCAG	300
		Af_leftarm9R	TTGCCCACATAATCTTGTG	314 (new)
		Af_Leftarm_9F_New	GCGCTGGAAAAATTGCAA	
	10	Af_leftarm10F	CGGTTATGCGTCATTGGA	300
		Af_leftarm10R	TTTTTCTTGCGCGTGATG	316 (new)
		Af_Leftarm_10F_New	TCAAATCCACATCGCGC	

Table 11: *C. kuhniae* Polynucleotides used for FISH probes				
Target	**Probe No.**	**Primer**	**Sequence (5'-3')**	**Product (nt)**
C. kuhniae ori Region (8960 bp)	0	Ck_Ori_0F	CGGAACACGTTGATGTTG	456
		Ck_Ori_0R	CCATCTGATGTTGAGAACC	
	1	Ck_Ori_1F	GCTTGTTCTGTTGGAAGG	367
		Ck_Ori_1R	GATGAATTGCCAAGACGG	
	2	Ck_Ori_2F	GCATTCGTTACATCGTCC	348
		Ck_Ori_2R	GAATACGGTATCGAGGTG	
	3	Ck_Ori_3F	GAAGCCTTCCAAGAACTG	358
		Ck_Ori_3R	CTTTGGCAAGGTAGGAAG	
	4	Ck_Ori_4F	GAGTGGGTTTCGAATACC	398
		Ck_Ori_4R	GATGTTGTTCAGGTAGGC	
	5	Ck_Ori_5F	GGACAACACTATCCCATC	448
		Ck_Ori_5R	TCTGTTCGGACATGAGAG	
	6	Ck_Ori_6F	GCCTTTGCCTTCTACAAG	313
		Ck_Ori_6R	GCTTGGGAGCTTATCATC	
	7	Ck_Ori_7F	CTTATACGCTGATGCACC	347
		Ck_Ori_7R	GTCAAGCAGGGTACTTTC	
	8	Ck_Ori_8F	GAACAATATTGGGCAGTG	336
		Ck_Ori_8R	CGCCCTAAATAATGTGCC	
	9	Ck_Ori_9F	GGACAAGATGGTGATGTC	430
		Ck_Ori_9R	CTCATCGCCTACGTTTAAG	
	10	Ck_Ori_10F	GGTGAGAAAACGGTTCAC	338
		Ck_Ori_10R	CACGCCCATAAAGTGAAAC	
	11	Ck_Ori_11F	CAAGGCGTGTTTCCCATG	243
		Ck_Ori_11R	CAGCACAAAAGGTATGAGC	
C. kuhniae ter Region (8853 bp)	0	Ck_Ter_0F	GCATTATTCATACGGCTC	314
		Ck_Ter_0R	GGAAAACAGATGCCACTG	
	1	Ck_Ter_1F	GTATCTTGGTATTGGTACGG	370
		Ck_Ter_1R	GTCATGATGTCGGTTCTG	
	2	Ck_Ter_2F	CGATTACCGAGTTTGACG	380
		Ck_Ter_2R	GACATCTGTTTCATTCGG	
	3	Ck_Ter_3F	AATGATACTGCCCTACCC	350
		Ck_Ter_3R	CAGTAAGCCAAAATCGGG	
	4	Ck_Ter_4F	CGTTCCGACTATTCTGTC	347
		Ck_Ter_4R	GTATTGAAGACCTTGACCC	
	5	Ck_Ter_5F	GTTGTTCGGGGGTAATTG	301
		Ck_Ter_5R	GGGGACATCATTATTTTCC	
	6	Ck_Ter_6F	GTATGTGGACATCGTTACC	377
		Ck_Ter_6R	CCGTGAACGACACTTTAG	
	7	Ck_Ter_7F	GAATTGGGTGGCTTTCAG	328
		Ck_Ter_7R	CACAATCATCAGTCCGAC	
	8	Ck_Ter_8F	GCCTACGACTACATCATC	317
		Ck_Ter_8R	CAGTGGTCAAAGTCCAAG	
	9	Ck_Ter_9F	GAACAAACCCCTGATTGG	307
		Ck_Ter_9R	CTCTTCCCAATCCTGTTC	
	10	Ck_Ter_10F	GGCAGTTACAAGACAATC	309
		Ck_Ter_10R	GGTTGTTTCAGATGGGTG	
	11	Ck_Ter_11F	GTAAACCGCACCGTATTC	303
		Ck_Ter_11R	GCCGAAAAACAGCAAGTC	

Gene Probe Synthesis

Touch-down PCR was used to generate the polynucleotide probes. PCR master mix was created as outlined (table 12 & 13). To confirm successful amplification, gel electrophoresis was performed using a 1% agarose gel. A 100bp ladder was used as a marker to check if band was at expected height for the product.

If PCR reactions using GoTaq polymerase failed, it was substituted for Phusion polymerase. The same master mix was created (table 12) with the exception of $MgCl_2$ which was replaced with additional DEPC-H_2O. Following PCR reactions, 1µl of DNA loading dye was mixed with 5µl reaction sample which was then loaded onto 1% agarose gel and run as normal.

After function of primer pairs was confirmed the number of individual PCR reactions per probe was increased. The resulting products where pooled and purified using the NEB Monarch® PCR and DNA Cleanup Kit (NEB, T1030). This was repeated until at least 100 ng/µl PCR product for each probe was obtained. A sample of each probe was then sent for sequence confirmation by Eurofins genomics.

Table 12: PCR Master Mix

	Stock Concentration	**Final Concentration**
GoTaq Buffer	5X	1X
$MgCl_2$	25mM	1.5mM
Forward Primer	10µM	0.2µM
Reverse Primer	10µM	0.2µM
dNTPs	10mM	0.2mM
GoTaq Polymerase	5u/µl	1.25u

Combined with DEPC-H_2O for a final volume of 24µl per reaction required. Master mix was then aliquoted into PCR tubes and 1µl of genomic DNA was then added to act as template. These were then transferred to a thermocycler and the reaction carried out in table 13 was carried out

Table 13: PCR conditions for probe synthesis

98°C	98°C	63°C* [Δ-0.3°C]	72°C	4°C
5 min.	30 Sec	30 Sec	30Sec **	Pause
	30-35 cycles			

Example of thermocycler settings used for the creation of Probes. *Starting temperature adjusted with the melting temperatures of primers ** Extension time dependent on template length and polymerase. 30 Sec per 1KB for Phusion and 1 min per 1KB for GoTaq

Labelling

ULYSIS Alexa Fluor 594 nucleic acid labelling kit (Thermo Fisher, U21654) was used to fluorescently label the prepared DNA probes. The PCR products were combined with labelling buffer to a final concentration of 1µg DNA in 10µl. 100 ng/µl of all 10 *A. filiformis* right probes were combined and the volume was then adjusted to 10µl with labelling buffer.

This DNA solution was first denatured by heating to 95°C for 5 minutes in a thermocycler and then quickly placed on ice to cool. 15µl of labelling reagent was added and the reaction was incubated for 30 minutes at 80°C in the thermocycler. The tube was moved to ice to quench the reaction and then centrifuged.

The excess labelling reagent was removed using a gel filtration–based spin column. The column was prepared by first inverting several times to resuspend the gel and then centrifuged at 1000xg for 2 minutes to remove the storage buffer. 25µl of labelling buffer was added and the column was again centrifuged to wash any residual storage buffer. Measuring the volume of flowthrough post centrifugation also served to confirm column integrity. The fluorescently labelled probe was then added to the column and centrifuged for 4 minutes at 1000xg. The DNA concentration and fluorescent signal was measured using a nanodrop and the labelled probe was aliquoted and stored at -20°C until required.

Cell Immobilisation & Permeabilization

10 well epoxy microscope slides were thoroughly cleaned with 100% ethanol and allowed to air dry. To facilitate adherence of cells, 30µl of poly-l-lysine was added to each well and allowed to stand for 10 minutes. The solution was knocked off and the slide was placed in the oven at 37°C to dry. Small volumes (1-2µl) of previously fixed cells (described above) were added to each well and the slide was returned to the incubator for the cells to dry down. The cells were then further dehydrated by 1 minute submersion in 3 increasing concentrations of EtOH (50%, 80%, & 100%) and the slide was air dried at room temperature.

To allow for the full penetration of the high molecular weight gene probes the bacterial cell wall must first be made permeable *via* lysozyme treatment. Powdered lysozyme was added to lysozyme buffer (table 14) and fresh lysozyme solution was created with a final concentration of 0.5mg/ml and kept on ice. Slides were placed in a tissue lined, sealable glass incubation chamber, and 30µl of lysozyme solution was added to each well. Any remaining solution was poured onto the tissue lining and the chamber was placed in a 37°C incubator for 1 hour. To remove the excess lysozyme buffer, the slides were then transferred to Milli-Q H_2O for 1 minute then 100% EtOH for 1 minute and allowed to air dry.

Table 14: Lysozyme buffer

	Stock Concentration	**Final Concentration**
PBS	10X	1X
Tris-HCl	1M	100 mM
EDTA	0.5 M	50 mM
Solutes were combined with Milli-Q H_2O for a minimum volume of 50ml, prepared in advance for the creation of fresh lysozyme solution. (Barrero-Canosa et al., 2017)		

Denaturation & Hybridization:

The specificity and efficiency of probe binding depends on probe GC content, incubation temperature, and hybridization/wash buffer composition. Hybridization occurs below the probe's melting temperature (T_m), where half of the DNA is double-stranded. Guanine-cytosine (GC) are connected with 3 hydrogen bonds that only denature at high temperatures. Therefore, probe T_m increases with higher GC content. Sodium ions (Na^+) stabilise the DNA double helix thus increasing the Probe T_m and increasing the hybridisation efficiency. Formamide conversely, decrease the T_m and increase the hybridization efficiency by destabilising the DNA double helix. These changes to T_m are proportional to the concentration of Na^+ and formamide in the hybridization and wash buffers. The optimal hybridisation occurs at high salt concentrations (e.g. 0.9M Na^+) which leads to an extremely high T_m and thus high hybridisation temperatures. Optimal hybridization occurs at 46°C, requiring buffer conditions (Na^+ and formamide levels) that ensure this temperature is 20–30°C below the probe's T_m. A formula (equation 1) can estimate T_m based on buffer composition, but optimal formamide concentration should be experimentally confirmed using gene FISH and detection efficiency testing (Barrero-Canosa et al., 2017; Moraru & Barrero-Canosa, 2021).

Hybridization buffer with the optimum formamide concentration for the GC content of the probe was prepared in advance (table 15) (usually 35-45%). The hybridization mixture was created by the addition of labelled probe to the hybridisation buffer for a final concentration of 100-400 pg/µl and vortexed thoroughly. Probe concentration used was selected based on labelled probe concentration specificity, this could be adjusted in future experiments to optimise fluorescence signal obtained.

A humidity chamber was created by lining an airtight glass box with tissue paper and placing an empty tip rack on top. The tissue paper was soaked in a formamide-water solution with equal formamide concentration to the hybridisation buffer. The slides with the immobilised cells were placed on the tip rack and 30µl of hybridization mixture was added to each well. The chamber was sealed and placed in an oven prewarmed to 85°C for 40 minutes to denature the target DNA and the labelled dsDNA probe. This denaturation step was by a followed a 2-hour incubation at 46°C to allow the denatured probes to hybridize to the target region.

During this incubation, the wash buffer was prepared in two 50ml falcon tubes and placed in a water bath to heat to 48°C. The composition of the wash buffer can also affect the specificity of the polynucleotide probes. The concentration of NaCl was adjusted based on the formamide concentration of the hybridization buffer (table 16). A low salt concentration was used to remove any short, unspecific oligonucleotide-hybrids. The buffer was heated to a temperature below the melting point of the newly formed target-probe hybrids. Following hybridization, the slides were removed from the

humidity chamber and quickly dipped in one falcon tube of warmed wash buffer to remove residual hybridisation buffer. They were transferred to the other falcon and placed back in the water bath for 15 minutes with the temperature maintained at 48°C. The slides were subsequently placed in a 50ml falcon tube containing 1X PBS and incubated in the dark for 10 minutes at room temperature and then air dried.

Equation 1:

$$T_m = 81.5 + 16.6\ \log 10\left(\frac{Na^+}{1 + 0.7Na^+}\right) + 0.41(\%GC) - \frac{500}{N} - 0.63F$$

Dependency of the DNA:DNA hybrids Melting temperature (T_m) on different factors. Molar concentration of Na+ ions (Na^+), GC content (*%GC*), Polynucleotide length (*N*), & Formamide concentration (*F*) (Barrero-Canosa et al., 2017; Moraru & Barrero-Canosa, 2021)

Table 15: Hybridization Buffer

	Stock Concentration	**Final concentration**
Dextran Sulphate (DS)	-	20% (wt/vol)
Formamide (FM)	100%	35-45%*
SCC	20X	5X
EDTA	5M (pH 8)	20mM
Nucleic acid blocking reagent (BR)	10%	1%
Sheared Salmon Sperm DNA (SSS)	10 mg/ml	0.25 mg/mL
Yeast RNA (YR)	10 mg/ml	0.25 mg/mL
SDS	20%	0.1%

DS, SSC, EDTA and Milli-Q H_2O were combined in a falcon tube, vortexed and then heated in a water bath to 48°C to allow for DS to dissolve fully. The solution was then cooled to room temperature and BR, SSS, YR, FM, & SDS were added. The solution was vortexed, 0.22µm sterile filtered, aliquoted and stored at -20°C. * percentage of formamide varied and was balanced with the volume of Milli-Q used when dissolving DS.

Table 16: Wash Buffer

	Stock Concentration	**Final Concentration**	**NaCl Concentration (formamide %) ***		
			45%	**40%**	**35%**
NaCl	5M	-	30mM	46mM	70mM
Tris-HCl	1M	20mM	-		
EDTA	0.5M	5mM	-		
SDS	20%	0.01% (wt/vol)	-		

Combined with Milli-Q for a minimum volume of 250ml. * NaCl concentration. varies with the percentage of formamide used in the hybridisation buffer and chamber and was adjusted with the use of additional Milli-Q.

Counterstaining & Mounting

Hoechst 33342 was diluted in 1X PBS for a final concentration of 0.5mg/ml and 30µl was added to each well to counterstain the DNA. The counterstaining solution was allowed to sit on the slide for 10 minutes in the dark at room temperature. Slides were then washed for 1 minute in 1X PBS and 1 minute in Milli-Q H_2O.

The slide was allowed to fully air dry and then 1µl of the fluorescence preserving mounting media Vectashield was spotted onto each well. The wells were carefully covered with a coverslip; the edges were sealed with nail varnish, and the slide was air dried. Imaging was carried out as detailed below (methods section e).

Translation Blocking in *S. muelleri* & *C. steedae* Using Antibiotics

Bacterial strains were inoculated into 100ml of their preferred media, and the growth was monitored regularly until it reached an OD_{600} of approximately 0.5. The cultures were split into two falcon tubes, and the antibiotic chloramphenicol was added to a final concentration of 25 µg/ml. These treated cultures were then incubated at 37°C shaking for 30 minutes. 1ml was taken from each treated culture and fixed as described above in Methods b. (i). Coverslips were coated in poly-L lysine and incubated at room temperature for 10 minutes, rinsed with water and allowed to air dry. Small volumes of fixed cells were added to the coverslips, spotted in a circular shape and then dried down at 37°C. The DNA was stained with Hoechst 33342 diluted in PBS (final concentration 0.5mg/ml) and incubated in the dark for 10 minutes. This was followed by 1 minute wash in 1X PBS and then 1 minute in Milli-Q H_2O. 2µl of Vectashield was added to a slide and the coverslip was carefully placed (cell side down) on top. The coverslip was then secured with nail varnish and allowed to dry. Imaging was carried out as detailed below (methods section e).

Microscopy & Data Analysis

Microscopy

Imaging for all fluorescence microscopy experiments were carried out using a Nikon Eclipse NI microscope, the attached camera MFCool (Jenoptik) with its compatible software ProgRes Capture Pro 2.8.8 software (Jenoptik).

Image Analysis

ImageJ (1.54g) and the plugin ObjectJ (Nyongesa et al., 2022) were used to analyse microscope images. This plugin automatically added filament axes, box shaped cell outlines (width) and pole points (cell length). These were fairly accurate and reliable for *A. filiformis* but required significant manual adjustments for *S. muelleri*, *C. steedae* and *C. kuhniae*. ObjectJ than localised the fluorescent signal within the cell width and length. Overlay fluorescent images were also created using ImageJ.

Statistical Analysis

Construction of statistical figures was performed using the RStudio (2024.04.2+764) with the following plugins: ggplot2, ggExtra, dplyr, plyr, gridExtra, grid, extrafont, readxl, viridis, and ggpointdensity.

Morphometric measurements

Images obtained and analysed (with Fil-tracer tool and ObjectJ plugin) during the *ori* FISH experiments were used to determine the morphometric measurements of *C. kuhniae*. The filament axis (filament length), cell boxes (width), and pole points (cell length) were added automatically and then manually adjusted. The average cell size and filament length for all filaments was compared to the averages for each phenotype.

Results

The Centre of left & right Arms of *A. filiformis* are Located at Midcell & Segregate Laterally

To investigate the localisation and lateral segregation of genetic loci in the chromosomal arms of *A. filiformis,* specific probes were designed for use in DNA FISH (fluorescence in situ hybridisation). These 20,000 bp-long probes targeted the centre of the left or right chromosomal arms starting at positions 1,814,049 bp and 598,016 bp respectively, hence forth referred to as probe L or R (figures 4 A and 5 A). Using probe L, 95.5% (n=355) of the cells contained only one focus and 4.5% (n=17) contained two foci (figure 5 B). In DNA FISH experiments using probe R, one focus was present in 81% of cells (n=420) and two focus in 17% of cells (n=84) (figure 5 B). The large proportion of cells containing a single focus L or R focus (95.2% and 80.9%, respectively) confirms *A. filiformis* is monoploid.

In cells where a single focus was present, probe L predominantly localised to the middle of the long axis, i.e. in the central third of the cell (0.3-0.6; figure 5 C & D). Probe R displays a similar localisation pattern (figure 5 F & G), but foci are more spread across the cell (see the flattened (plateau-like) distribution of foci along the normalized cell length and normalized width overlying or flanking panels D & G, respectively, of figure 5). Population analysis found that both probes L and R clustered at centre of the short axis (between -0.3 and 0.3) in cells containing one focus (figure 5 D G). In cells containing two or more foci, both probes L and R likewise localised primarily to the central third of the long axis (0.3-0.6; figure 5 E & H). However, probes L and R appeared spread across the short axis of the cell (laterally) resulting in heat maps displaying two to three clusters of foci side by side (see distributions along the normalized cell width overlying panels E & H of figure 5).

These DNA FISH results demonstrated that: 1) in the monoploid *A. filiformis,* irrespective of the number of foci present in the cell, the centre of both left and right chromosomal arms primarily localised to the midcell. 2) The R signal was more spread, especially along the long axis than the L signal. 3) In cells containing two or more foci, these tended to be excluded from the centre of the short axis indicating lateral chromosome segregation.

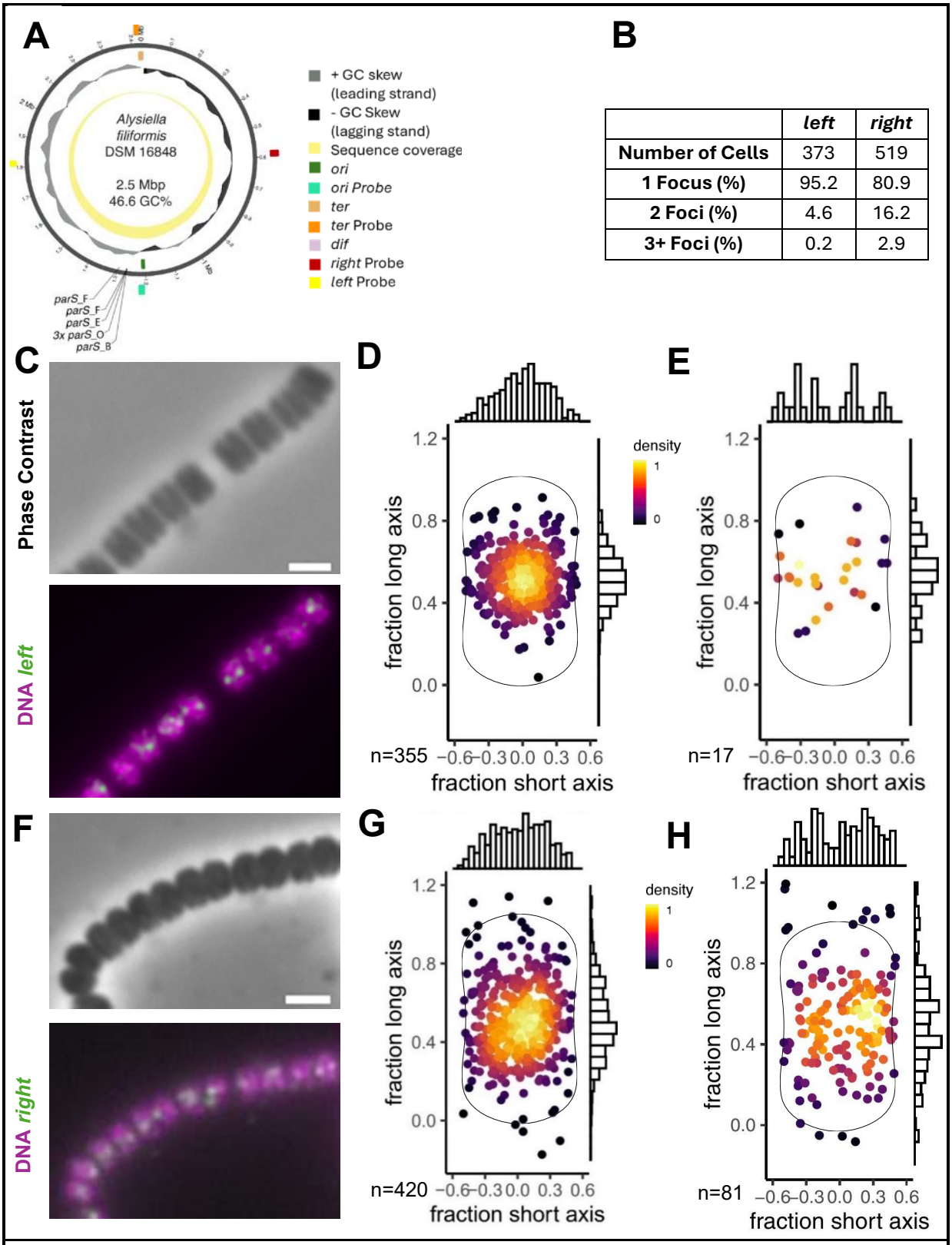

Figure 5: DNA FISH Targeting the *right & left* Arms of *A. filiformis*. **(A)** GC Skew map of *A. filiformis* genome with *ori, ter, right & left* probes marked. **(B)** Total number of cells & percentage containing 1, 2 & 3+ foci. **(C)** Representative images of cells with *left* arm probe and **(F)** *right* arm probe. Upper panels are phase contrast images. Lower panels are overlay of the DNA (Hoechst 33342) signal (magenta) and the DNA FISH signal (green). Scale bar is 2 µm. **(D)** Heat maps representing the location of *left* arm in cells with 1 focus and **(E)** in cells with 2 foci. **(G)** Heat maps representing the location of *right* arm in cells with 1 focus and **(H)** in cells with 2 foci. Each focus is mapped based on its relative position along the normalised length and width of the corresponding cell.

Cluster of Five *parS* Sites Localise at the Cell Poles of *S. muelleri*

To determine if the cluster of 5X-*parS* sites localises to the cell poles, specific DNA FISH probes were designed targeting a 2,000 bp long region, starting at 1,447,496 bp. This was located 206,519 bp away from the origin of DNA replication (*ori*) of *S. muelleri* (figures 4 B and 6 A). The majority of cells contained two foci 57% (n = 189), with one focus observed in only 20% (n=66) of cells and 3 or more foci found in 23% (n= 76) (figure 6 B). The fact that 80% of the cells contain two foci or more confirms *S. muelleri* is diploid.

When 189 cells containing two foci were analysed, two clusters of 5X-*parS* foci appeared one in the upper and one in the lower third of the long axis (0.8 µm-1.2 µm and 0 – 0.4 µm, respectively; see bimodal distribution of foci along the normalized cell length flanking panel D of figure 6) (figure 6 D). These clusters spread evenly across the normalised cell width between -0.5 and 0.5 (figure 6). When we analysed 76 cells containing three or more foci, two of clusters 5X-*parS* foci were again observed, localising to the top and bottom third of the long axis (see bimodal distribution along the length flanking panel E of figure 6) and spread across the short axis. (see foci distribution along the width overlying panel E of figure 6).

All in all, DNA FISH revealed that the 5X-*parS* cluster of each of the two chromosomes is primarily polar (figure 6 C).

Image analysis for this experiment was conducted by N. Krause.

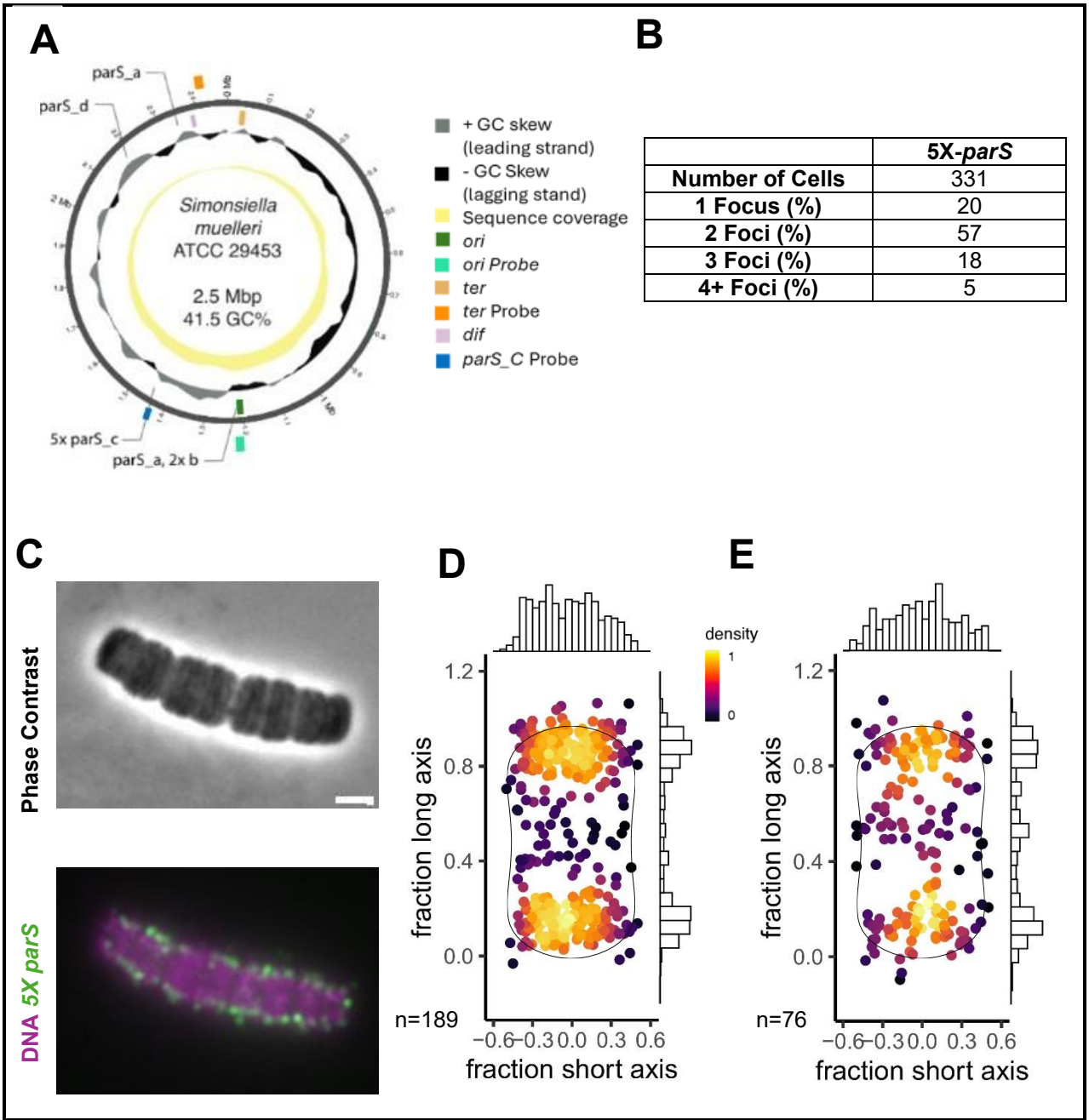

Figure 6: DNA FISH Targeting the 5X-*parS* Cluster of *S. muelleri*. **(A)** GC Skew map of *S. muelleri* genome with *ori, ter* & *parS* probes marked. **(B)** Total number of cells & percentage containing 1, 2, 3 & 4+ foci. **(C)** Representative images of a filament subjected to DNA FISH 5X-*parS* probe. Upper panel is phase contrast image. The lower panel is an overlay of the DNA (Hoechst 33342) signal (magenta) and the DNA FISH signal (green). Scale bar is 2 µm. **(D)** Heat map representing the location of the *parS* cluster foci in cells with 2 foci. **(E)** Heat map representing the location of the 5X-*parS* cluster foci in cells with 3 or more foci. Each focus is mapped based on its relative position along the normalised length and width of the corresponding cell. (Figures A, D & E courtesy of N Krause)

DNA Excluded from Midcell in Translationally Halted *S. muelleri* & *C. steedae*

The DNA of control (untreated) and chloramphenicol treated *S. muelleri* was stained with Hoechst 33342. In the untreated control cells, the DNA was evenly distributed across the long axis of the cell (figure 7 B, green), and no gaps were observed in the representative images (figure 7 A upper). In contrast, in the chloramphenicol treated cells, the fluorescent signal dropped significantly (~ 50%) in the central third of the cell (figure 7 B, magenta). A gap can be seen in the stained DNA in the representative images, indicating exclusion of DNA from midcell (figure 7 A lower).

Translational blocking was also performed on *C. steedae* which displays a slight bi-focal distribution of the DNA (magenta) in untreated cells (figure 7 C, upper middle and right panels and total fluorescence in figure 7 D, green). Chloramphenicol treatment induced a reduction of approximately 33% in DNA signal (purple) in the central third of the cell (when compared to the control) (figure 7 D). Disruption to DNA distribution can be seen in the further exclusion of DNA from the midcell (figure 7 C, bottom middle and right panels), compared to untreated cells (figure 7 C, upper middle and right panels). Surprisingly, chloramphenicol treatment also altered the morphology of *C. steedae*, with cells and filaments bent or curled inwards (figure 7 C, bottom panels). Morphological defects were not observed in chloramphenicol-treated *S. muelleri* filaments.

Image analysis for these experiments was conducted by N. Krause.

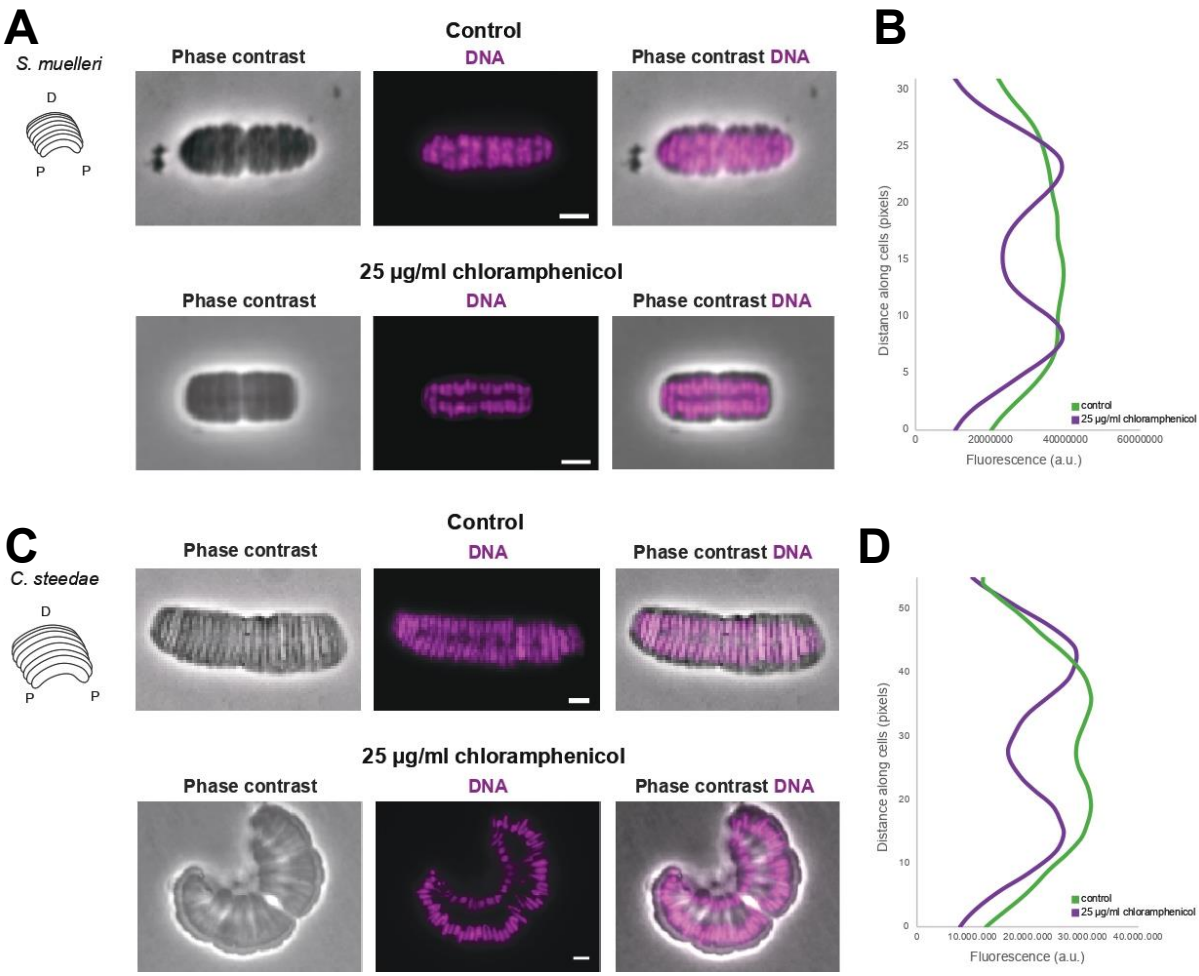

Figure 7: DNA Localisation in Untreated & Translationally Halted *S. muelleri* & *C. steedae*. (A) Sketch of a *S. muelleri* filament (left). Phase contrast and fluorescence microscopy images displaying the distribution of DNA (Hoechst 33343) signal in untreated (top) and chloramphenicol treated *S. muelleri* cells (bottom). **(B)** DNA fluorescence signal emitted by 107 untreated (control) cells (green) and 87 chloramphenicol-treated cells (purple) plotted against the normalised cell long axis. **(C)** Sketch of a *C. steedae* filament (left). Phase contrast and fluorescent microscopy images displaying the distribution of DNA (Hoechst 33343) signal in untreated (top) and chloramphenicol treated *C. steedae* cells (bottom). **(D)** DNA fluorescence signal emitted by 96 untreated (control) cells (green) and 87 chloramphenicol-treated cells (purple) plotted against the normalised cell long axis. All scale bars are 2 µm. (Figures produced by N. Krause, Unpublished).

C. kuhniae is Dimorphic with Rod & Crescent-shaped Cells

Early experiments conducted on *C. kuhniae* grown in liquid media revealed two distinct morphologies in a single culture (figure 8 A i ii). These initial observations were supported by scanning electron micrographs produced by the Veyrier lab (unpublished). These images additionally revealed that the shorter cells were rod-shaped (figure 8 B, D i) and longer cells were crescent-shaped (figure 8 C, D ii).

Morphometric measurements of cells visualised at the light microscope revealed that the crescent-shaped cells were ~1 µm longer than rod-shaped cells with a mean length of 3.048 µm and 2.069 µm, respectively (figure 8 E & supplemental table 1). Crescent-shaped cells had greater length variability, indicated by a larger IQR (Interquartile range) and higher standard deviation (0.618 µm) (figure 8 E & supplemental table 1). Rod cells are more uniform with a smaller IQR and standard deviation (0.28 µm) but include some shorter outliers (figure 8 E & supplemental table 1). A two-tailed Mann-Whitney U test confirmed a statistically significant difference in length ($U = 1{,}152{,}138.5$, $Z = 33.84$, $p < 0.001$). The common language effect size of 0.94 means there is 94% chance that a randomly chosen crescent-shaped cell is longer than a randomly chosen rod-shaped cell.

Crescent and rod-shaped cells were both approximately 1 µm in width with close means and medians (figure 8 F & supplemental table 1). Both have relatively high but comparable standard deviations (~0.42), with some wider crescent-shaped outliers (figure 8 F & supplemental table 1. High standard deviation in cell width (rather than in length) is consistent with cells widening rather than lengthening. Statistical testing found no significant difference in width between rod-shaped and crescent-shaped cells ($U= 635{,}865.5$, $Z= 1.415$, $p= 0.157$).

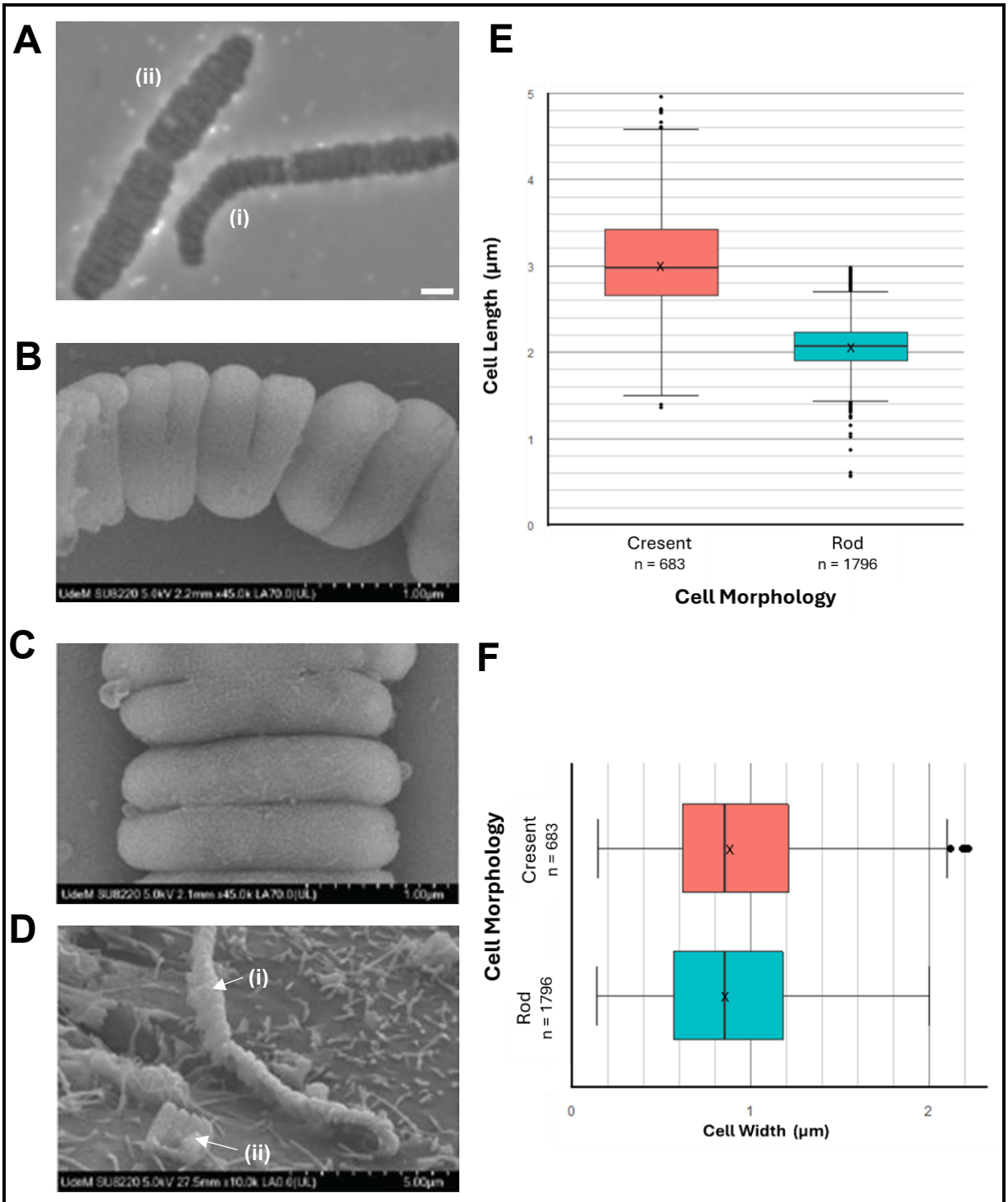

Figure 8: Rod-shaped & Crescent-shaped *C. kuhniae*. (A) Phase contrast image of two morphotypes of *C. kuhniae,* (i) and (ii). Scale bar is 2 µm. Scanning electron micrographs of **(B)** rod-shaped *C. kuhniae*, **(C)** crescent-shaped *C. kuhniae* and **(D)** *C. kuhniae* attached to human endometrial adenocarcinoma (i = rod-shaped, ii = crescent-shaped). Box Plots Illustrating **(E)** length & **(F)** width of crescent-shaped (pink) and rod-shaped *C. kuhniae* (blue)**.** Black points are outliers that fall outside Q1-1.5*IQR and Q3+1.5*IQR. Median is represented by a black line, mean is represented by X. (Images B-D are courtesy of Veyrier Lab, INRS Laval, Canada).

C. kuhniae Exhibits Bistable Ploidy Based on *ori* DNA FISH

DNA FISH was performed to determine the location of the *ori* in *C. kuhniae*. Probes were designed to specifically target the 8430 bp long *ter* region of *C. kuhniae* at 804,121 bp (figure 9 A).

Quantification revealed that only one focus was present in the majority of rod-shaped cells (82.35%, n=140), with two or more present in only 17.62% (n=30) of cells (figure 9 B). Conversely, 46.67% of crescent-shaped cells contained 2 foci (n=98), with 31.9% containing three or more (n= 67), and only 21.43% (n=45) containing a single focus (figure 9 B). These results indicate that the two morphotypes of *C. kuhniae* likely have different ploidy; rod-shaped are predominantly monoploid, whereas crescent-shaped cells are predominantly diploid.

Population level analysis revealed that, in rod-shaped cells with only one focus, the *ori* primarily localised to the bottom third of the long axis (0 – 0.3; see foci distribution over the cell length flanking panel D of figure 9), forming a cluster at the centre of the short axis (see foci distribution along the normalised cell width overlying panel D of figure 9). Population-level analysis of rod-shaped cells containing two or more foci, revealed that the *ori* primarily remained in the bottom third of the long axis but spread across the short axis, with two clusters situated side-by-side (see bimodal distribution of foci along the normalised cell width overlying figure 9 E).

Irrespective of the number of foci, population level analysis of crescent-shaped cells displayed two cluster of foci, one found in the top third of the cell and one found in the bottom third (see bimodal distributions of foci along the normalized cell length flanking panel G and H of figure 9). Foci were similarly spread across the short axis (see distributions of foci along the normalized cell width overlying panels G and H of Figure 9 G).

Altogether, *ori* DNA FISH reveals that *C. kuhniae* exhibits bistable ploidy. Rod-shaped cells are predominantly monoploid with the *ori* located in a single pole (figure 9 C), whereas crescent-shaped cells are mostly diploid with an *ori* per pole (figure 9 F). The formation of adjacent clusters spread across the short axis in rod-shaped cells suggests that chromosome segregation occurs laterally.

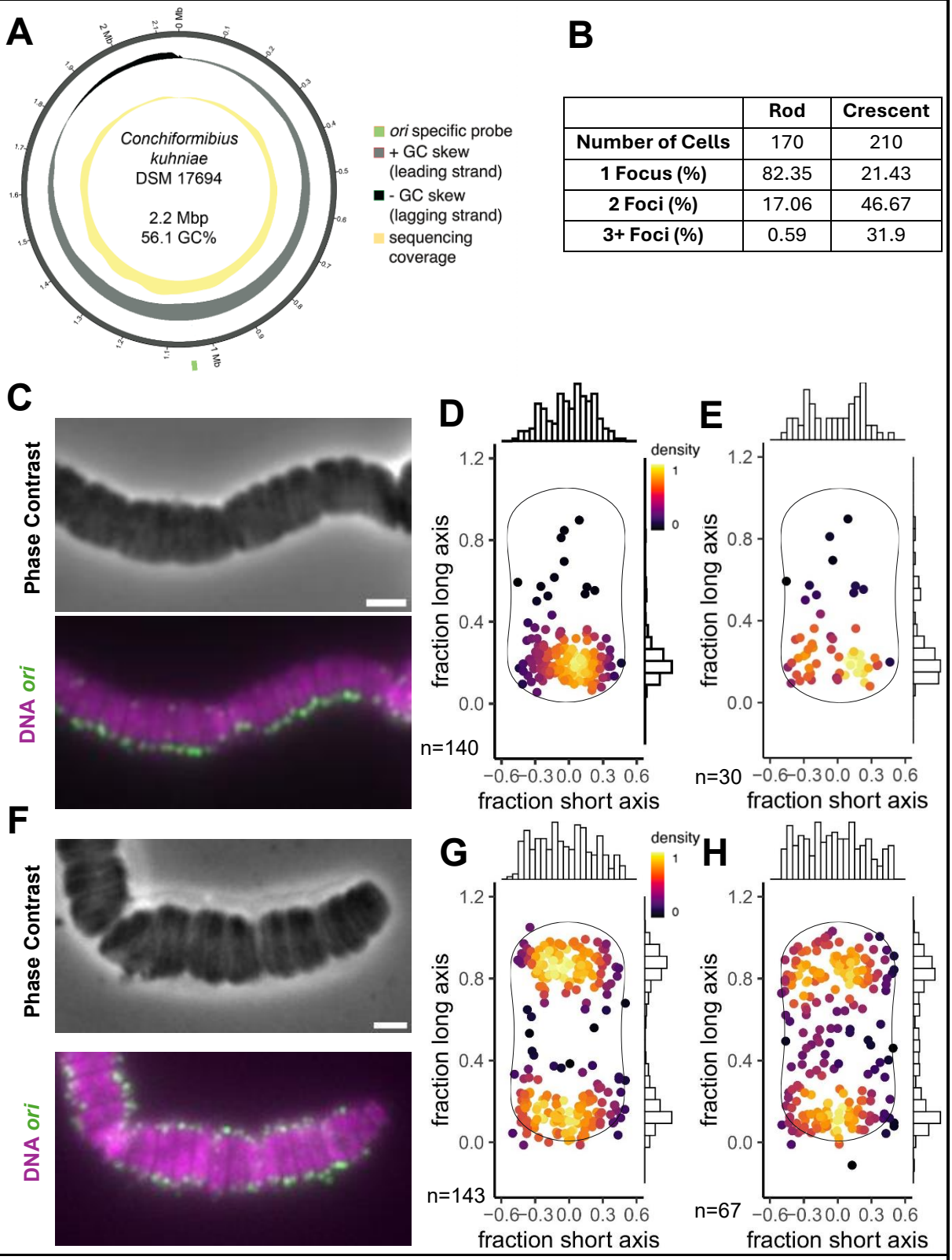

	Rod	Crescent
Number of Cells	170	210
1 Focus (%)	82.35	21.43
2 Foci (%)	17.06	46.67
3+ Foci (%)	0.59	31.9

Figure 9: DNA FISH Targeting the *ori* of *C. kuhniae*. **(A)** GC Skew map of *C. kuhniae* genome with *ori* probe marked. **(B)** Total number of cells & percentage containing 1, 2 & 3+ foci. Representative images of *ori* probe in **(C)** rod-shaped and **(F)** crescent-shaped cells. Upper panels are phase contrast images. Lower panels are overlay of the DNA (Hoechst 33342) signal (magenta) and the DNA FISH signal (green). Scale bar is 2 µm. Heat maps representing the location of *ori* probe in rod-shaped cells with **(D)** 1 focus and **(E)** 2 or more foci. Heat maps representing the location of *ori* probe in crescent-shaped cells with **(G)** 1-2 foci and **(H)** 3 or more foci. Each focus is mapped based on its relative position along the normalised length and width of the corresponding cell.

C. kuhniae Exhibits Bistable Ploidy Based on *ter* DNA FISH

DNA FISH was performed to localise the *ter* of *C. kuhniae* using specific probes targeting the 8430 bp long *ter* region of *C. kuhniae* beginning at 804,121 bp (figure 10 A).

The number of *ter* foci per cell varied between rod-shaped and crescent-shaped cells. Rod-shaped cells predominantly contained only one focus (87%, n= 1012), with only 12.6% of cells containing two or more foci (n = 151) (figure 10 B). These results indicate that rod-shaped *C. kuhniae* is likely monoploid. In cells containing one focus, the *ter* primarily localised to the upper third of the long axis, clustering at the centre of the short axis (figure 10 D). When two foci were present, *ter* foci were more dispersed, but a cluster was observable in the upper third of the long axis (figure 10 E). This cluster was spread laterally across the short axis, contrasting the more concentrated localisation observed in cells containing only a single focus (figure 10 D & E).

The majority of crescent-shaped cells, 64% (n= 367), contained only one *ter* focus, with multiple foci present in 36% of cells (n = 200) (figure 10 B). Despite the prevalence of cells with a single focus, the ratio to cells with single to multiple foci was significantly lower (1.8:1) than in the rod-shaped cells (6.7:1). This indicates that crescent-shaped cells are likely diploid. The *ter* primarily localised to the central third of the long axis irrespective of the number of foci present in the cell (figure 10 G & H). When looking at the foci distributions, a plateau of foci was visible at width position 0.3 – 0.3 in cells with 2 foci (figure 10 G) but the plateau flattened in cells with three or more foci (figure 10 H).

DNA FISH experiments targeting the *ter* region indicate that rod-shaped and crescent-shaped cells are primarily monoploid and diploid, respectively. In rod-shaped cells, the *ter* signal predominantly localises to one of the cell poles (figure 10 C), whereas in crescent-shaped cells, it is typically found at midcell (figure 10 F). These findings further support lateral chromosome segregation: in cells containing multiple *ter* foci (two or more in rods, and three or more in crescents), the foci form laterally spread clusters across the short axis in both morphotypes.

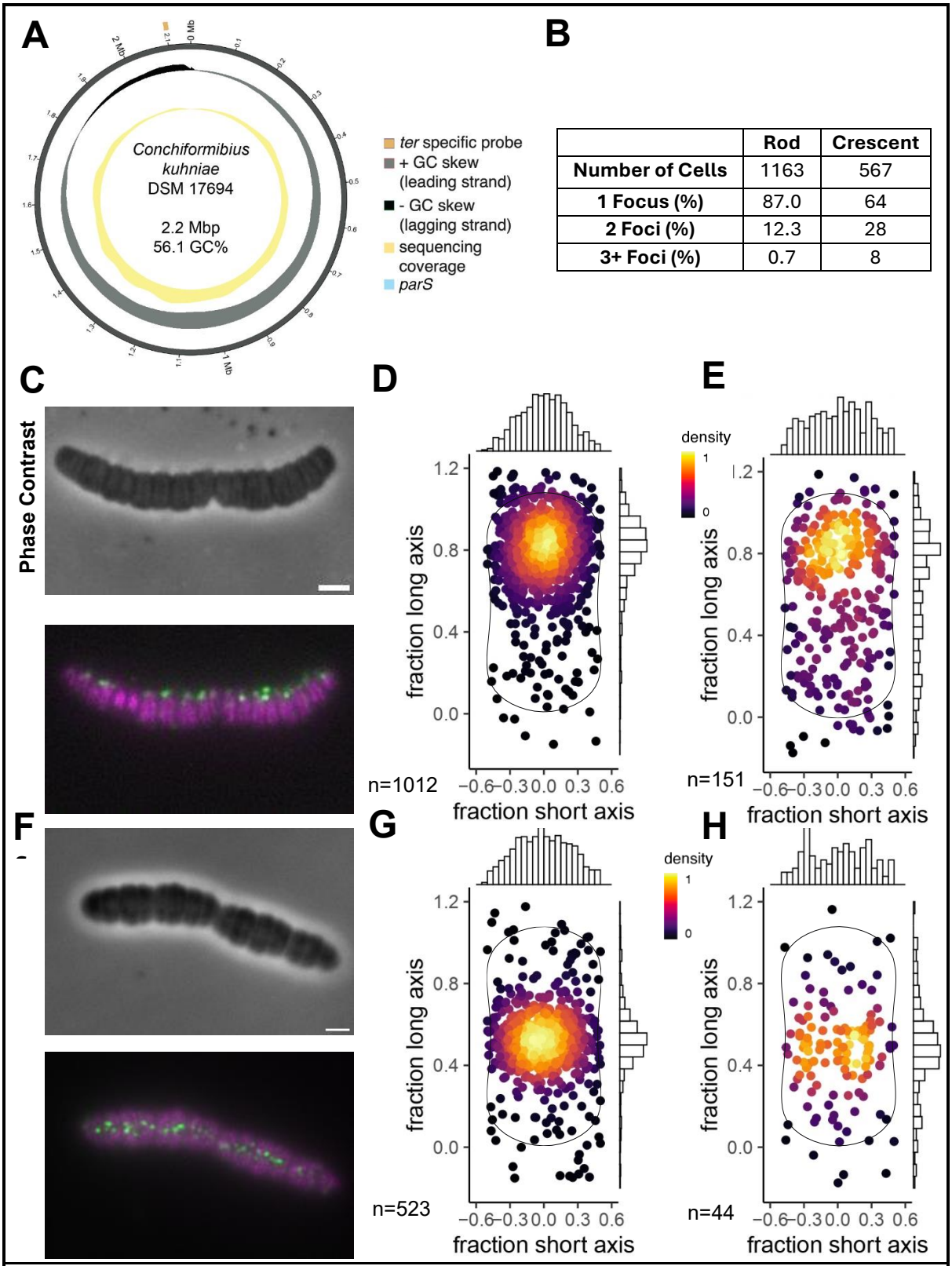

	Rod	Crescent
Number of Cells	1163	567
1 Focus (%)	87.0	64
2 Foci (%)	12.3	28
3+ Foci (%)	0.7	8

Figure 10: DNA FISH Targeting the *ter* of *C. kuhniae*. **(A)** GC Skew map of *C. kuhniae* genome with *ter* probe marked. **(B)** Total number of cells & percentage containing 1, 2 & 3+ foci. Representative images of *ter* probe in **(C)** rod-shaped and **(F)** crescent-shaped cells. Upper panels are phase contrast images. Lower panels are overlay of the DNA (Hoechst 33342) signal (magenta) and the DNA FISH signal (green). Scale bar is 2 µm. Heat maps representing the location of *ter* probe in rod-shaped cells with **(D)** 1 focus and **(E)** 2 or more foci. Heat maps representing the location of *ter* probe in crescent-shaped cells with **(G)** 1-2 foci and **(H)** 3 or more foci. Each focus is mapped based on its relative position along the normalised length and width of the corresponding cell.

Predominance of Rod-shaped Monoploid *C. kuhniae* in Stationary Phase

Experiments on *C. kuhniae* cultures sampled during the exponential phase revealed two morphotypes: ~2µm-long rod-shaped monoploid cells and ~3µm long crescent-shaped diploid cells. However, it was unclear whether the two cell types persisted throughout the entire growth cycle.

To investigate the abundance of these morphotypes across different growth phases, *C. kuhniae* was inoculated into liquid GCB media and the growth was monitored periodically by measuring the OD_{600}. Samples were collected and fixed at multiple points corresponding to the lag, log (exponential), and stationary phases of growth. DNA FISH targeting the origin of replication (*ori*) was performed on each sample. This enabled visual distinction between the two morphotypes, using characteristic *ori* localisation to one or both cell poles (rod-shaped monoploid and crescent-shaped diploid respectively).

The relative abundance of monoploid (rod-shaped) filaments was quantified and compared to the diploid (crescent-shaped) filaments. In samples taken lag phase both cell types were present in nearly equal numbers, with diploid filaments occurring at only slightly higher frequencies (figure 11). This ratio remained stable during log (exponential) phase (figure 11).

However, as the cultures entered stationary phase, the proportion of monoploid filaments increased significantly, becoming the dominant form (figure 11). They accounted for approximately 70% of all observed filaments, while the frequency of diploid filaments declined by more than 20% (figure 11). This transition suggests a growth phase-dependent regulation of ploidy state and morphology. Of note, no biological replicates were performed.

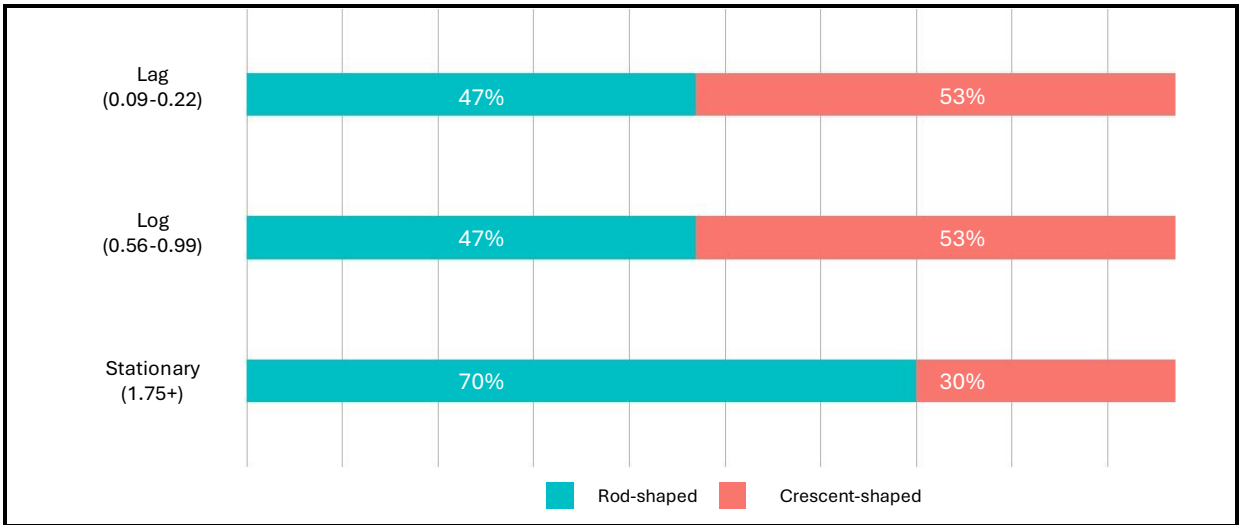

Figure 11: Proportion of Monoploid & Diploid *C. kuhniae* Filaments at Different Growth Stages. The OD_{600} range for each phase of growth is displayed on the right. Data from a single experiment.

Discussion

The *right* & *left* Chromosomal Arms of *A. filiformis* are Stably localised to Midcell

Previous experiments revealed that the monoploid *A. filiformis* chromosome adopts a stable longitudinal *ori-ter* configuration, with the *ori* at the host-attached pole and the *ter* at the free pole (Viehboeck et al., 2024). Stable longitudinal configuration is believed to be maintained through longitudinal septation and lateral segregation of the sister (newly replicated) chromosomes, likely mediated by the ParABS system.

Diploid *S. muelleri* and *C. steedae* are closely related to *A. filiformis*, sharing a similarly stable configuration and undergoing lateral segregation of their chromosomes (Viehboeck et al., 2024). Despite these similarities, chromosome conformation capture coupled to high-throughput sequencing (3C-seq) of *A. filiformis* suggested that interarm contacts occur at a significantly lower frequency than in *S. muelleri* and *C. steedae* (displayed by weaker secondary diagonal in 3C-seq-based genetic contact maps (Viehboeck et al., 2024). This led to the hypothesis that, in contrast to *ori* and *ter*, the chromosomal arms in *A. filiformis* may be more dynamic, i.e., change their localisation pattern throughout the cell cycle. This free movement may consequently reduce the frequency of interarm contacts.

To test this hypothesis, DNA FISH was used to localise the centre of the *left* (probe L) and *right* (probe R) chromosomal arms. The presence of only one fluorescence focus in the majority of cells was consistent with previous observations pertaining the *ori* and *ter,* confirming *A. filiformis* is monoploid (Viehboeck et al., 2024). The small proportion of cells containing two L or R foci likely reflects cells post chromosome replication, but before septation is complete. In cells bearing a single focus, this was mostly localised at midcell (defined as the centre of the long axis and the centre of the short axis). In cells bearing two foci, these still occupied the central third of the long axis but foci were more spread along the short axis. Notably, irrespective of the number of foci/cells detected, the R foci were more dispersed along the long axis. The broader distribution of R probe foci along the long axis suggests greater positional flexibility of the right arm, indicating it may be more dynamic than the left (figure 12).

Stable localisation of the *ori* to the proximal pole is believed to be mediated by binding of the ParB protein to seven *parS* sites situated approximately 100 Kb left of the *ori* (figure 5 A), and to the binding of this ParB-*parS* complex to a yet to be identified membrane anchor (Viehboeck et al., 2024). This was supported by immunostaining showing localization of the ParB protein at the proximal pole of *A. filiformis* (Viehboeck et al., 2024) as well as by CHIP-seq (data not shown). The fact that all seven *parS* are located to the left of the *ori*, which is apparently anchored to the pole, could explain the higher positional stability of left arm relative to right arm observed by DNA FISH.

What could anchor *A. filiformis* ParB to the membrane? Intriguingly, like ParB, MreB localised at the proximal pole (Krause, unpublished) suggesting that this cytoskeletal protein may be essential to anchor the ParBS complex to the host-attached pole.

What could explain the relatively low frequence in lateral contacts observed by 3C-seq? Despite the slightly higher dispersion of R along the long axis, L and R were mostly at midcell and segregated laterally (figure12). Therefore, the low frequency of inter-arm DNA contacts cannot be explained by unrestricted movement of the arms. SMC-mediated (structural maintenance of chromosomes) “handcuffing” is central to the formation of interarm contacts (Wilhelm et al., 2015). In species such as *Bacillus subtilis*, multiple *parS* sites flank the *ori* (Livny et al., 2007). ParB binds to these *parS* sites and recruits SMC complexes (Wilhelm et al., 2015). SMC, typically functioning within a condensin-like SMC–ScpA–ScpB complex, initiates bidirectional loop extrusion from the origin toward the terminus (Wilhelm et al., 2015). These loops stably align the *left* and *right* chromosomal arms, drawing them together and facilitating the formation of interarm contacts (Tran et al., 2017). Despite the presence of genes encoding the condensin complex SMC–ScpAB and ParABS system (Viehboeck et al., 2024), interarm contacts occur at low frequencies in *A. filiformis*. This could reflect an altered or absent SMC-mediated loop extrusion mechanism, caused by inefficient loading, rapid dissociation from DNA, or functional divergence of the SMC complex (Tran et al., 2017; Wilhelm et al., 2015). Differently phrased, the chromosomal arms of *A. filiformis* might be stably positioned but not handcuffed by SMC, resulting in a reduced frequency of interarm contacts.

While the differences in foci distribution in the left and right arms may indicate variation in chromosomal dynamics and stability, pointing to an underlying biological mechanism, technical factors must also be considered. Although we detected 81 cells containing 2 R foci, we detected only 17 cells containing 2 L foci. The lower number of cells containing two L foci may reflect differences in the probes ability to penetrate the cell and hybridise to the target region. Indeed, fluorescence foci were detected outside of the cell in the case of the R probe but none were detected outside in the case of the L probe. Both biological and technical explanation must therefore be considered when interpreting DNA FISH results. Nevertheless, these results demonstrate that lower frequency of inter-arm DNA contacts observed in *A. filiformis* (compared to *S. muelleri* and *C. steedae*) is likely not attributable to instability in the *left* and *right* chromosomal arms. Further experiments are therefore required to identify the mechanism reducing interactions between the chromosomal arms.

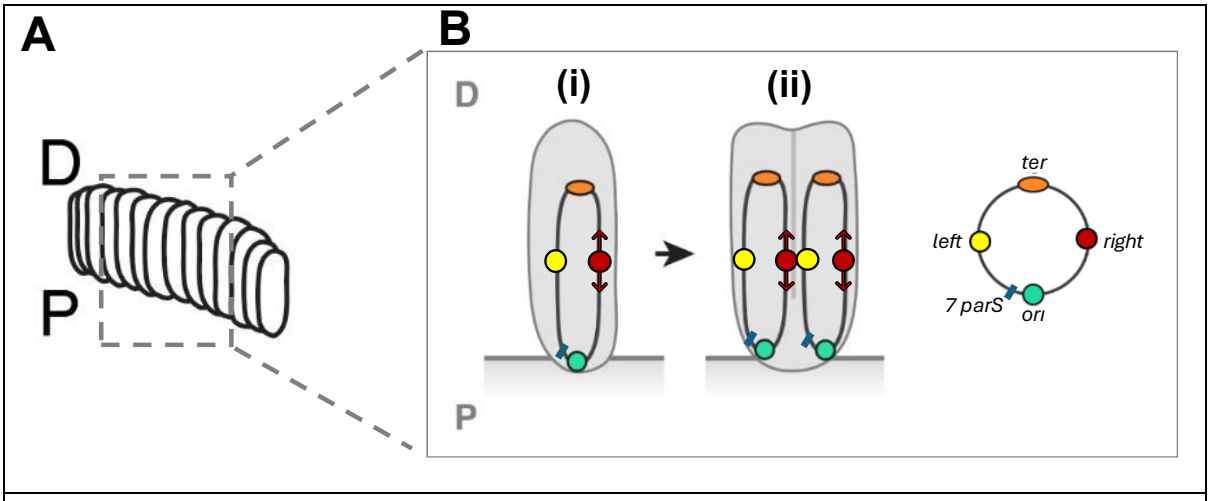

Figure 12: Filament Sketch & Proposed Chromosome Configuration of *A. filiformis*. (A) Sketch *of A. filiformis* filament. **(B)** Proposed chromosome configuration in (i) nondividing and (ii) dividing cells. P: Proximal, host attached pole. D: Distal, free pole. *ori* (green), *ter* (orange), seven *parS* sites (blue) and centre of *left* and *right* arms (yellow & red, respectively). Red arrows illustrate the observed higher dynamicity of the R arm with respect to the L arm. (Adapted from Viehboeck et al., 2024)

A 5X-*parS* Cluster Situated 206,519 bp Away from *ori* (Rather Than Two *ori*-Adjoining *parS* Sites) May Mediate the Stable Chromosome Configuration & Lateral Chromosome Segregation in *S. muelleri*

DNA FISH and 3D structured illumination microscopy (3D-SIM) experiments on the diploid *S. muelleri* revealed that, although the *ter* was stably localised at midcell and the *ori* was sub-polar (supplemental figure 1) (Viehboeck et al., 2024). In contrast, in the related monoploid *A. filiformis* and diploid *C. steedae ori* was invariably polar and *ter* was either polar or at midcell resulting in an *ori-ter* and *ori-ter-ter-ori* configuration, respectively (Viehboeck et al., 2024).

S. muelleri chromosome bears a total of 10 *parS* sites, three are positioned near the *ori* (proximal) and two near the *ter* (distal). Additionally, a cluster of five proximal *parS* sites (5X-*parS*) is located approximately 206,519 bp on one side of the *ori*. The 5X-*parS* cluster was specifically targeted using DNA FISH. The majority of cells contained two *5X-parS foci* supporting diploidy. A smaller proportion of cells contained three or more foci, likely representing cells undergoing replication but not having completed septation yet. Population analysis found that *parS* foci primarily localised at the cell poles irrespective of the number of foci present. In conclusion, the 5X-*parS* cluster of each of the two chromosomes was polar throughout the cell cycle and segregated laterally. This new chromosome configuration will be referred to as *5XparS – ori – ter – ter – ori – 5XparS* (figure 13).

This stable chromosome configuration diverges from that seen in the related *A. filiformis* and diploid *C. steedae* and may be unique. The stable polar localisation of the 5X-*parS* cluster is likely mediated by the binding of ParB, forming a ParB-5X*parS* complex that is anchored to the pole by a yet unknown membrane protein. In other

organisms that configure their chromosomes longitudinally (e.g. *C. crescentus* or *V. cholerae*), and possibly in *A. filiformis* (see above), ParB accumulation at the pole is dependent on the actin homologue MreB (Toro et al., 2008). The polar anchoring of ParB relies on scaffold proteins like PopZ and HubP, which are absent from *Neisseriaceae* species (Bowman et al., 2008). The polar anchoring of ParB relies on scaffold proteins like PopZ and HubP, which are absent from *Neisseriaceae* species (Bowman et al., 2008). *S. muelleri,* ParB is not restricted to the poles but is distributed throughout the cell. This, combined with the presence of proximal and distal *parS* sites that can be bound by purified ParB protein (Krause, unpublished), suggests that ParB complexes at *ori* and at *ter* may play a role in chromosome configuration and segregation.

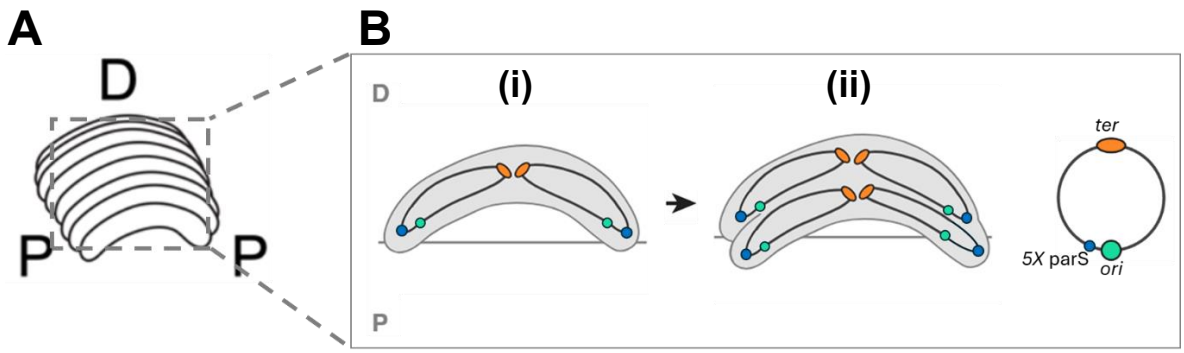

Figure 13: Filament Sketch & Proposed Chromosome Configuration of *S. muelleri*. (A) Filament sketch of crescent-shaped *S. muelleri*. **(B)** Proposed chromosome configuration in (i) nondividing and (ii) dividing cells. P: Proximal, host attached pole. D: Distal, free, unattached side. *ori* (green), *ter* (orange) and 5X-*parS* (blue). (Adapted from (Viehboeck et al., 2024)

Nucleoid Contraction in Translationally Halted *S. muelleri & C. steedae* suggests coupling of transcription and translation at the inner membrane

In bacteria with low nucleocytoplasmic ratio, the nucleoid normally occupies midcell with mature ribosomes pushed to the cell periphery, located between the chromosome and the inner membrane (Gray et al., 2019). It is widely believed that the coupling of transcription and translation for inner membrane proteins anchors the chromosome to the cell envelope. Chloramphenicol inhibits peptidyl transferase activity of the bacterial ribosome, preventing protein chain elongation and consequently halting protein synthesis (Wolfe & Hahn, 1965). When chloramphenicol treatment is used to block translation in organisms with a low nucleocytoplasmic ratio such as *E. coli* and *B. subtilis*, the nucleoid remains localised to the centre of the cell but contracts (Roggiani & Goulian, 2015). The collapse of the nucleoid is attributed to loss of membrane tethering at loci encoding membrane proteins, which are no longer anchored to the cell envelope once translation is halted (Roggiani & Goulian, 2015).

In multicellular *Neisseriaceae S. muelleri* and *C. steedae,* following chloramphenicol treatment, a marked reduction in DNA signal was detected in the central third of the cell. In other words, two nucleoids were discernible in translationally halted *S. muelleri* and *C. steedae* suggesting diploidy. This is consistent with *ori*, *ter* and 5X-*parS* cluster DNA FISH (this work and (Viehboeck et al., 2024). More generally, chloramphenicol-

induced nucleoid compaction suggests that, like in model rods, mature ribosomes are excluded from the nucleoids and can be involve in transertion (transcription-translation coupling at the membrane).

Unexpectedly, translationally halted *C. steedae* also displayed significant morphological defects. This response to translational arrest indicates that in this species, transcription-translation coupling at the membrane (transertion) may not be uniformly distributed along the chromosome. The uneven distribution of transertion sites may reflect specialised genomic domains or differing local transcriptional activity along the filament. Collectively, these experiments indicate close interdependence between chromosome organisation and cell architecture in multicellular *Neisseriaceae*.

Phenotypic Heterogeneity in *C. kuhniae*

C. kuhniae displayed striking phenotypic heterogeneity within a single population, displaying two distinct cell morphologies: ~2 µm rod-shaped cells and ~3 µm crescent-shaped cells. Initial observations of this dimorphism raised concerns of contamination, 16S rRNA gene sequencing detected the presence of only one strain of *C. kuhniae* (Krause, unpublished, Data not shown). FISH probes specifically designed to target the *ori* and *ter* of *C. kuhniae* penetrated and bound the DNA of both cell types, further supporting the presence of only a single strain of *C. kuhniae*.

DNA FISH experiments targeting the *ori* and *ter* regions of *C. kuhniae* also revealed distinct ploidy states within the same population. The majority of rod-shaped cells contained only a single *ori* or *ter* focus, indicating they are monoploid. Both *ori* and *ter* were polar. Although experimental limitations prevent the visualisation of more than one genetic locus per cell, based on already known chromosome configurations, we assume that, within one cell, *ori* and *ter* are located at the opposite poles, so called longitudinal (*ori-ter*) configuration.

Experimental limitations prevent the visualisation of more than one genetic locus per cell. Based on established chromosome configurations, we assume that, within one cell, *ori* and *ter* are located at the opposite poles, so called longitudinal (*ori-ter*) configuration. A subset of rod-shaped cells possessed two or more foci. Population analyses found that the majority of foci in these cells remained polar but spread across the short axis of the cell, indicative of lateral chromosome segregation. This consistent polar localisation across different stages of the cell cycle suggests that the longitudinal chromosome configuration (*ori–ter*) is stable (figure 14 A-C). This organisation is reminiscent of the stable longitudinal chromosome configuration and lateral segregation in the monoploid oral symbiont *A. filiformis* ((Viehboeck et al., 2024) and this work).

Crescent-shaped cells are likely diploid, predominantly containing two *ori* foci, one at each pole, a pattern that remains consistent in cells with one, two, or more foci.

The *ter* predominantly localised to the central third of the long axis irrespective of the number of foci in the cell indicating the *ter* localises to midcell and spread across the short axis. In contrast to the *ori*, only one *ter* foci was present in the majority of crescent-shaped cells. A similarly seemingly paradoxical pattern was noted in the related *S. muelleri*, with the majority of cells containing two *ori* foci located sub-polarly at either end of the cell and a single, centrally localised *ter* focus ((Viehboeck et al., 2024), Krause, unpublished). Upon closer inspection, cells with a single *ter* focus tended to have larger foci than those with multiple. This suggests that unresolved, closely spaced *ter* may appear as a single focus due to limitations in optical resolution. Similar experiments conducted on the larger *C. steedae* showed that the *ter* region also localised to midcell. Unlike in *S. muelleri* and *C. kuhniae*, however, the majority of *C. steedae* cells contained two or more foci, as expected in a diploid (Viehboeck et al., 2024). The ability to distinguish multiple foci in the larger *C. steedae* supports the idea that the true number of *ter* foci in *S. muelleri* and *C. kuhniae* is underestimated due to overlapping fluorescent signals. This may be due simply to close spatial proximity, or it may reflect a biological mechanism in which sister *ter* remain physically tethered following replication (Kleckner et al., 2014; Wang & Rudner, 2014).

Regardless of the underlying mechanism, DNA FISH targeting the *ter* indicates that crescent-shaped *C. kuhniae* cells are likely diploid, with *ter* consistently localised at midcell and exhibiting lateral chromosome segregation. Combined with *ori* localisation data, these findings suggest that crescent-shaped *C. kuhniae* also maintain a stable *ori–ter–ter–ori* configuration, similar to the related species *C. steedae* (figure 14 D & E).

In rapidly dividing cells, replication can be re-initiated before the previous cycle is completed, a phenomenon known as multifork replication (Youngren et al., 2014). As a result, daughter cells may inherit chromosomes that are already partially replicated and contain multiple *ori* (Youngren et al., 2014). This could be an alternatives explanation for the high number of *ori* foci relative to the *ter* observed in crescent-shaped C. *kuhniae* cells. Marker frequency analysis conducted on *A. filiformis*, *C. steedae* and *S. muelleri* found that compared to *E. coli*, no significant change in *ori-ter* ratio occurred (Viehboeck et al., 2024). This indicates that these related oral cavity symbionts do not undergo multifork replication and that *C. steedae* and *S. muelleri* are diploid. These results, coupled with the localisation of the *ori* to opposite extremes of the cell, make multifork replication unlikely. However, additional experiments would be required to completely discount it.

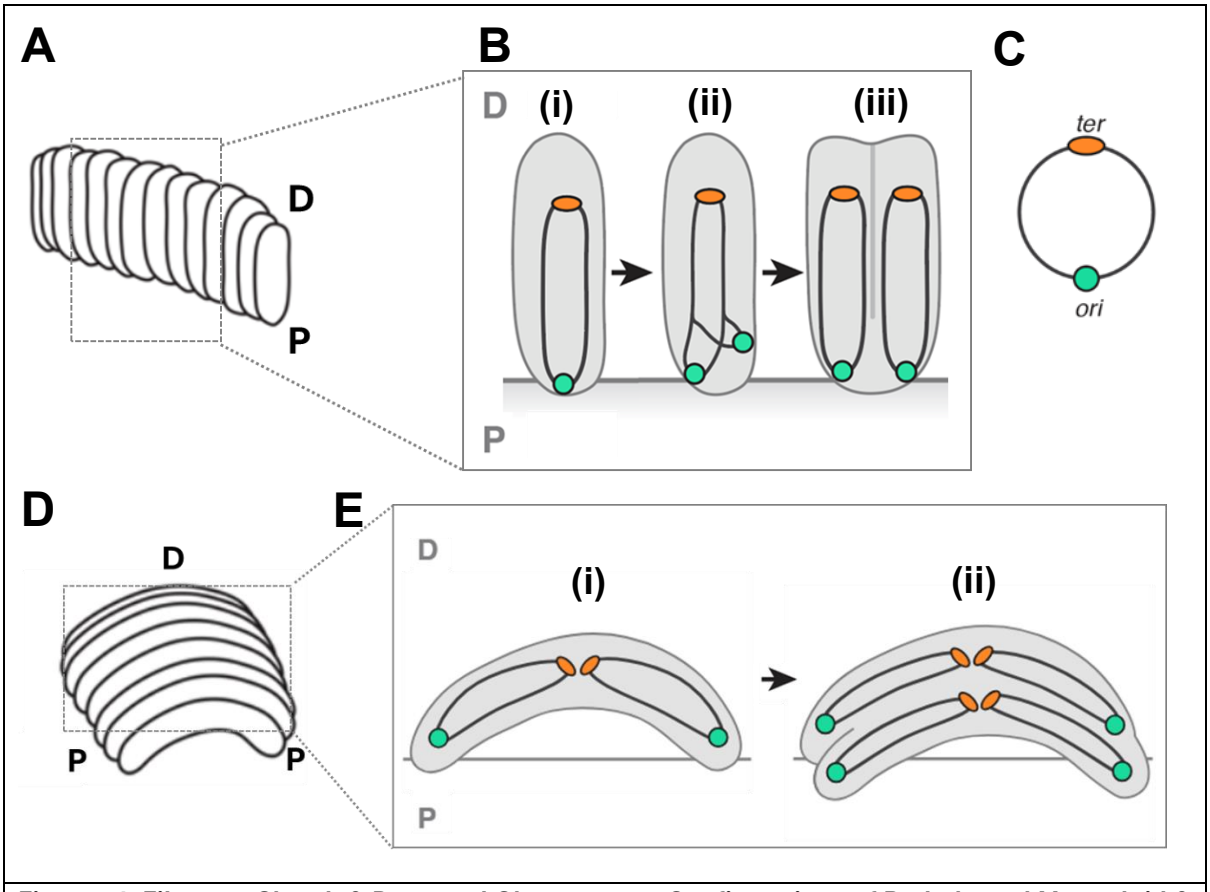

Figure 14: Filament Sketch & Proposed Chromosome Configurations of Rod-shaped Monoploid & Crescent-shaped Diploid *C. kuhniae*. (A) Filament sketch of rod-shaped *C. kuhniae* **(B)** Proposed chromosome configuration in (i) nondividing and (ii) early dividing (showing lateral segregation) and (iii) late dividing monoploid, rod-shaped *C. kuhniae*. **(C)** Chromosome map for both morphotypes. **(D)** Filament sketch of crescent-shaped C. *kuhniae*. **(E)** Proposed map of the chromosome configuration in (i) nondividing and (ii) dividing crescent-shaped *C. kuhniae*. *ori* (green) and *ter* (orange). P: Proximal (host-attached) pole, D: Distal (free / unattached) pole / side. (Viehboeck et al., 2024).

Stationary Phase Enrichment of Rod-Shaped Monoploid *C. kuhniae*: A Trade-Off Between Adhesion and Survival?

We observed similar ratios of rod-shaped/crescent-shaped *C. kuhniae* cells in lag and log (exponential) phase. As cultures entered stationary phase the abundance of rod-shaped filaments increased significantly making up approximately 70% of the population.

The existence of distinct ploidy states within the same species is not unique to *C. kuhniae* (Soppa, 2014). Variations in ploidy across bacterial growth stages are well-documented and often serve as a response to changing physiological demands (Pecoraro et al., 2011). This genetic flexibility enables rapid adaptation and increased resilience to environmental stresses (Soppa, 2014; Vega-Cabrera et al., 2024). Ploidy is typically low during the lag phase, increases during exponential phase, and declines as cells enter stationary phase (Maldonado et al., 1994; Riaz et al., 2021). During exponential growth, increased ploidy supports rapid replication, gene expression, and genome maintenance, while in stationary phase, reduced ploidy aids in resource

conservation and stress resistance (Pecoraro et al., 2011). For example, in *Deinococcus radiodurans,* known for its extreme radiation resistance, the number of genome copies depends on the growth conditions (Cox & Battista, 2005). However, in a synchronised population of *D. radiodurans* at the same growth phase (e.g., exponential phase), the average ploidy level is fairly consistent across cells, with natural variation between individuals. Cells in lag phase usually contain 4-6 chromosomes, rising to 8-10 and peaking at 16 in exponential phase before declining in stationary phase to ~4 in stationary phase (Hansen, 1978; Makarova et al., 2001; Sale, 2007). In contrast, when grown in complex media, *Azotobacter vinelandii* exhibits continued ploidy increase into stationary phase. Beginning with only four chromosome copies in lag phase but increasing up to ~80 copies in stationary phase. However, in a defined synthetic media, *A. vinelandii* maintains a maximum of four chromosome copies in lag and exponential phase and appears to revert to a monoploid state in stationary phase (Maldonado et al., 1994; Soppa, 2014). This highlights that ploidy variation across growth phases can also be influenced by the external environment such as nutrient availability.

If increased ploidy in *C. kuhniae* were a stress response or a mechanism to maximise proliferation, diploid cells should be more abundant in exponential phase. Instead, crescent-shaped diploid and rod-shaped monoploid cells are equally represented during lag and exponential phases, with monoploid rod-shaped cells becoming dominant in stationary phase. Although quantification along the growth phase must be repeated, if confirmed, the higher abundance of monoploid cells in stationary phase may represent a survival strategy under nutrient-limited conditions (Riaz et al., 2021). During this phase, metabolic efficiency becomes critical, and cells shift from active growth to maintenance and stress tolerance. Reduced ploidy allows cells to conserve energy and resources by minimising the demands of DNA replication, transcription, and protein synthesis (Riaz et al., 2021). Results presented above demonstrate that both rod-shaped monoploid and crescent-shaped diploid cells are actively dividing during exponential growth. However, under nutrient-limited conditions, replication in diploid cells may slow due to their greater resource demands. In contrast, monoploid cells, with a lower metabolic burden, may continue proliferating more efficiently, leading to their increased prevalence during the stationary phase.

To sum up, if it is known that environmental conditions (e.g., nutrient availability) may affect ploidy, *C. kuhniae* is still remarkable because, two morphs co-exist concomitantly irrespective of the growth stage. An environmental condition that results in a monomorphic population, if existing, has not been discovered yet.

What could be the implication of *C. kuhniae* dimorphism? Previous studies on the related oral symbiont, *A. filiformis, S. muelleri* and *C. steedae* have revealed the presence of fimbriae, thin, filamentous appendages that play a critical role in colonisation by mediating attachment to host surfaces (Hedlund & Tønjum, 2015; G. E.

Kaiser & Starzyk, 1973; Nyby et al., 1977); Krause unpublished). In the rod-shaped *A. filiformis*, fimbriae are localised exclusively to one cell pole, which also contains the *ori* suggesting a coordinated spatial organisation of replication and host-attachment machinery. The crescent-shaped, S. *muelleri*, *C. steedae* and *C. kuhniae*, are fimbriated along the concave ventral surface, which they use to attach to the host surface. Crescent-shaped cells have a larger surface area in contact with the host, compared to rod-shaped cells (supplemental figure 3). This may enhance their adherence and promote more stable host attachment. Crescent-shaped *C. kuhniae* (figure 15 A) therefore likely adhere more strongly to the oral mucosa than their rod-shaped counterparts (figure 15 B). In this context, transitioning from crescent to rod could be advantageous upon entering stationary phase, as detachment may help the cells to detach from a nutrient-poor substrate and re-attach to a different (nutrient-rich) substate.

This dynamic is reminiscent of the dimorphic life cycle of *Caulobacter crescentus*, in which a sessile, stalked cell remains firmly attached to a surface and undergoes asymmetric division to produce a motile swarmer cell (Govers & Jacobs-Wagner, 2020). The swarmer, while capable of chemotactic dispersal, cannot replicate until it undergoes terminal differentiation into a stalked cell and reattaches to a surface (Woldemeskel & Goley, 2017). Such life-cycle strategies are thought to optimise colonisation while ensuring propagation under fluctuating environmental conditions (Govers & Jacobs-Wagner, 2020; Rampelotto & Woldringh, 2024; Walls & Rosenthal, 2024). Unlike *C. crescentus*, there is currently no evidence that the crescent-shaped diploid and rod-shaped monoploid forms of *C. kuhniae* represent sequential stages in a dimorphic cycle. No observations thus far have suggested that that crescent-shaped diploids can transition into rod-shaped monoploids or vice versa. DNA FISH analysis indicates that both morphotypes are capable of chromosome segregation (and therefore of cell division), implying that they may represent stable and coexisting forms rather than transient developmental stages.

It should be noted that, due to technical difficulties encountered during bacterial cultivation in liquid medium, replicates are lacking. The data presented in Figure 11 is therefore based on a single experiment. While these findings offer intriguing preliminary evidence for a shift toward rod-shaped monoploidy during stationary phase, the lack of replication limits the strength of any conclusions that can be drawn. Previous experiments examining only exponential-phase populations typically observed nearly equal proportions of both morphotypes, with the diploid form generally present at slightly higher frequencies, consistent with the results shown in Figure 11 (Supplemental figure 4). Additional biological replicates will be necessary to validate these observations and to determine whether the apparent enrichment of rod-shaped monoploid cells in stationary phase reflects specific changes in growth rate, survival strategy, or environmental adaptation.

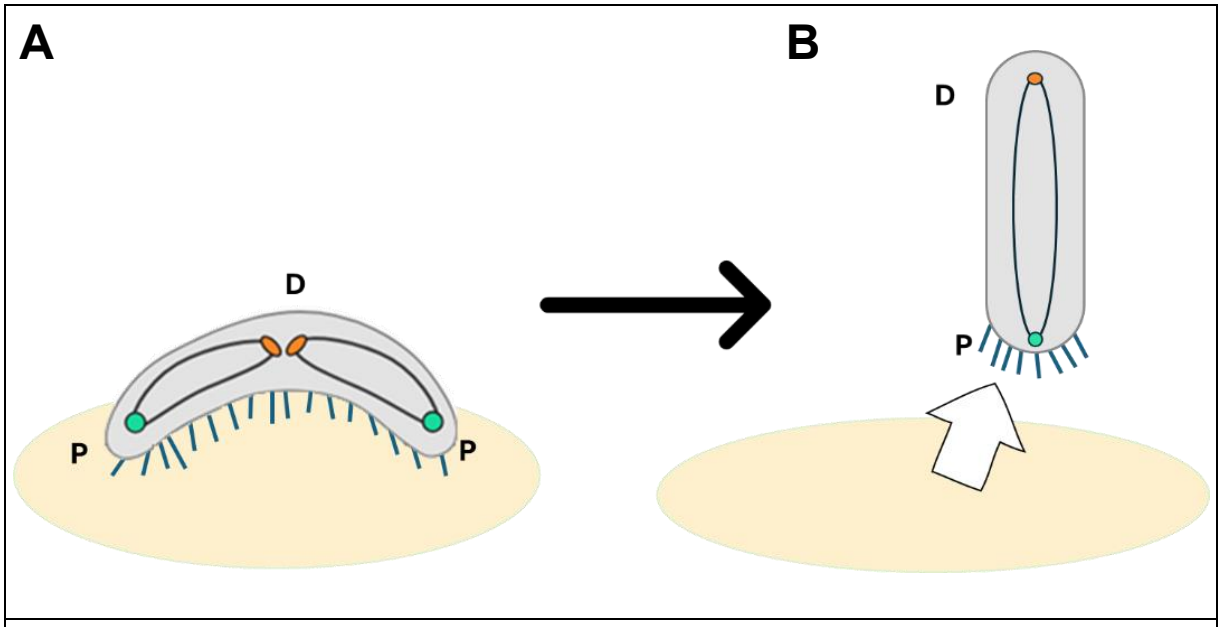

Figure 15: Proposed Differences in Colonisation Competence in Crescent-shaped & Rod-shaped *C. kuhniae*. (A) Crescent-shaped diploid cells with fimbriae attaching to host surface (cream). **(B)** Rod-shaped monoploid cells detaching from host surface. *ori* (green) and *ter* (orange). Fimbriae represented by navy lines. P: Proximal (host-attached) pole, D: Distal (free / unattached) pole / side. (Viehboeck et al., 2024).

Conclusion and Future Directions

In previous decades, research into bacterial cell biology has primarily focused on model, rod-shaped organisms such as *Escherichia coli* and *Bacillus subtilis* that may be facultatively associated with multicellular eukaryotes. While recent years have seen growing interest in the unique cell biology of obligate host-associated bacteria, this attention has largely centred on pathogens. Despite the crucial roles that microbial symbionts play in ecosystem stability and host health, the fundamental biology of mutualistic symbionts remains comparatively understudied.

This master's thesis builds on previous work showing stable chromosome configuration and lateral segregation in multicellular oral symbionts of the *Neisseriaceae* family (Viehboeck et al., 2024). It addresses key questions in *A. filiformis* and *S. muelleri* and presents the first known report of bistable ploidy in a bacterium, *C. kuhniae*. Results thus far suggest that the ParBS complex, plays a central role in stable chromosome configuration and lateral segregation but the putative membrane anchor awaits identification, and the role of ParA remains unclear. Genetic tractability of *C. kuhniae* presents a new and exciting opportunity to dissect these processes in detail. Potential experimental directions outlined below aim to further characterise the molecular the molecular mechanisms of chromosome configuration and segregation in multicellular *Neisseriaceae*. In parallel, the discovery of bistable ploidy in *C. kuhniae* opens up new lines of inquiry into how ploidy variation influences bacterial fitness and host colonisation.

Defective SMC handcuffing May Underlie Reduced Inter-Arm Contacts in *A. filiformis*

Despite the presence of genes encoding for the condensin complex SMC–ScpAB and ParABS system, interarm contacts occurred at low frequencies in *A. filiformis* (Viehboeck et al., 2024). This may be due to the absence of an SMC-based, *ori-ter*–oriented loop extrusion mechanism. To directly test this, the loop extrusion activity of *A. filiformis* SMC can be reconstituted in vitro and visualised using single-molecule DNA curtain assays combined with total internal reflection fluorescence (TIRF) microscopy (Collins et al., 2014; Ganji et al., 2018). In this setup, recombinant *A. filiformis* SMC complexes and ParB proteins are introduced to surface-tethered DNA substrates containing *parS* sites. This allows real-time observation of SMC recruitment by ParB to *ori*-proximal regions and direct assessment of ATP-dependent loop extrusion. Crucially, this assay can also be used to determine whether loop extrusion occurs bidirectionally, symmetrically, and at rates consistent with known SMC complexes from other bacteria (Ganji et al., 2018). Failure to observe robust loop extrusion, or abnormal dynamics, would support the hypothesis, that the reduced frequency of inter-arm contact

frequency in vivo is caused by SMC not handcuffing the DNA but mediating chromosome segregation through a yet unknown mechanism.

This in vitro reconstitution assay can be complemented with additional experiments on SMC DNA binding and localisation. Electrophoretic mobility shift assays (EMSAs) or other SMC loading assays can be used to evaluate ParB-dependent recruitment of SMC to *parS*-containing DNA (Sullivan et al., 2009). Weak or absent SMC binding in these assays would indicate deficient loading and likely absence of loop extrusion. Additionally, CHIP-seq and immunostaining with an anti-SMC antibody can be employed to show DNA binding in vivo and to determine SMC subcellular localisation in fixed *A. filiformis* cells (Viehboeck et al., 2024).

Anchoring of Polar *S. muelleri* 5X-*parS* Cluster

To uncover the mechanism anchoring the 5X-*parS* cluster at the cell poles in *S. muelleri* and its role in driving chromosome segregation, a combination of biochemical and cell imaging methods can be employed.

In several bacteria, MreB plays a key role in positioning chromosome segregation machinery, including ParB-*parS* complexes (Toro et al., 2008). To determine whether this cytoskeletal protein is involved in maintaining the polar localisation of the 5X-*parS* cluster in *S. muelleri*, DNA FISH targeting the 5X-*parS* cluster could be applied to cells treated with the MreB-depolymerizing drug A22. If inhibition of MreB disrupts the polar localisation of the 5X-*parS* cluster, it would suggest that this actin homologue is important for anchoring the ParB–*parS* complex to the poles.

To identify putative membrane-associated proteins that may serve as anchors for the ParB–5X-*parS* complex at the poles, co-immunoprecipitation (co-IP) using anti-ParB antibodies could be carried out (Lin & Lai, 2017). The co-precipitating proteins would then be identified using mass spectrometry analysis (Lin & Lai, 2017). Super-resolution microscopy techniques, such as structured illumination microscopy (SIM), can then be used to examine the co-localisation of ParB and the 5*parS* cluster with membrane or polar markers, including any candidate proteins identified through co-IP. This integrated strategy will help map how ParB–5X-*parS* complexes are positioned relative to potential anchoring proteins at the cell poles.

Role of Transertion in Chromosome Organisation in Multicellular *Neisseriaceae*

Nucleoid contraction in translationally halted *S. muelleri* and *C. steedae indicates that t*ransertion (transcription-translation coupling at the inner membrane) likely occurs and plays an important role in chromosome organisation. To provide additional evidence several experimental techniques could be employed.

Direct visual evidence of transertion can be obtained by visualising DNA–inner membrane contacts using high-resolution imaging techniques such as structured

illumination microscopy (SIM) (Spahn et al., 2025). Control (untreated) and chloramphenicol-treated *S. muelleri* and *C. steedae cells* are fixed and simultaneously stained with DNA dyes (e.g., Hoechst or DAPI) and membrane stains (e.g., FM4-64 or DiOC60). Quantitative imaging revealing an increased separation between DNA and the membrane in chloramphenicol-treated cells would support transertion-mediated tethering (Spahn et al., 2025).

A ribosome–membrane co-fractionation assay can be performed to biochemically assess the physical association between ribosomes and the inner membrane. Cell lysates are fractionated by sucrose gradient ultracentrifugation to separate membrane-bound components from soluble cytoplasmic material (Herskovits & Bibi, 2000). Collected fractions can then be probed by Western blotting for conserved ribosomal proteins (e.g., RplL, RpsA) and inner membrane markers (e.g., SecY) (Herskovits & Bibi, 2000). A reduction in ribosome co-sedimentation with membrane fractions in chloramphenicol-treated cells compared to untreated controls would provide strong biochemical evidence supporting transertion occurs. This approach enables detailed tracking of ribosome distribution across gradient fractions and allows direct comparison of membrane association under active versus translation-inhibited conditions.

Finally, subcellular fractionation combined with RNA sequencing would be a complementary approach to investigate transertion by profiling the localisation of mRNAs within bacterial cells (Kannaiah et al., 2019). This method enables genome-wide analysis of transcript distribution, by separating membrane-associated fractions from cytosolic components. Enrichment of mRNAs encoding inner membrane proteins in membrane fractions under normal conditions, and their depletion following chloramphenicol treatment, would indicate that mRNA membrane association depends on active translation (Kannaiah et al., 2019). This would further support the role of transertion in organising the chromosome through co-translational tethering to the inner membrane.

C. kuhniae: A New Genetic Tool to Explore the Mechanism Mediating Stable Chromosome Configuration & Lateral Chromosome Segregation in Multicellular *Neisseriaceae*

The ParABS System

We hypothesis that the ParABS chromosome segregation system mediates the stable longitudinal chromosome configuration and lateral segregation in A. *filiformis, S. muelleri* and *C. steedae*. However, the lack of tools for targeted genetic manipulation in these species has hindered in-depth functional analysis. The recently achieved genetic tractability of *C. kuhniae* provides a valuable opportunity to develop and apply new experimental approaches to investigate the role of ParABS in multicellular

Neisseriaceae. This will be achieved by a combination of genetic manipulation, live-cell imaging, and biochemical characterisation.

Preliminary work in *C. kuhniae* has already successfully produced *parB* deletion mutants, resulting in cells with significantly altered morphology and DNA localisation (supplemental figure 2 A, B, F & G, supplemental figure 3 B). This suggests that *C. kuhniae* ParB is required for tethering the *parS* sites to the poles, and for cell shape maintenance. To further investigate the role of ParABS in chromosome organisation, *parA* deletion mutants will also be generated and DNA FISH experiments targeting the *ori* and *ter* will be carried out on both mutants to identify any variations in chromosome orientation and segregation (Viehboeck et al., 2024) This will be compared to the *ori* and *ter* localisation in wild type *C. kuhniae (presented above)*. Chromosome conformation capture (Hi-C) will be applied to evaluate the global impact of *parA* and *parB* deletions on chromosome architecture (Viehboeck et al., 2024).

To complement these mutant analyses and directly visualise the segregation machinery in live cells, *C. kuhniae* strains expressing fluorescently tagged ParA and ParB will be constructed. While ParB localisation is expected to reflect previous immunostaining results, real-time imaging of ParA will provide critical insight into how this Walker-type ATPase contributes to the lateral segregation of chromosomes across the cell body.

Recombinant *C. kuhniae* ParA, ParB and FLAG-tagged ParB will be produced to enable biochemical characterisation of the chromosome segregation machinery. His-tagged proteins will be expressed using a pET16B-based system and purified via nickel affinity chromatography. The binding affinity of purified ParB to predicted *parS* sites will be assessed electrophoretic mobility shift assays (EMSAs) (Viehboeck et al., 2024; Weber et al., 2019). To identify potential interacting partners responsible for anchoring ParB at the cell poles, FLAG-tagged ParB will be used in co-immunoprecipitation experiments (Kawalek Adam et al., 2023). Direct protein–protein interactions between ParA and ParB will be evaluated both in vitro and in a bacterial two-hybrid (BACTH) system (Donovan et al., 2012; Kawalek Adam et al., 2023). By testing ParA binding to truncated ParB variants, BACTH assays will further enable the mapping of ParA–ParB interaction domains. Nucleotide-binding assays using radiolabelled nucleotides will be performed to determine whether *C. kuhniae* ParB functions as a CTPase.

Finally, Chromatin immunoprecipitation followed by high-throughput sequencing (ChIP-seq) will then be carried out to validate the direct interaction between ParB and its target DNA sequences (*parS*) in (Anchimiuk et al., 2021). Using a specific anti-ParB antibody, a map of genome-wide distribution of ParB binding sites in *C. kuhniae* will be produced. These experiments will determine whether ParB is enriched at the predicted *parS* sites and whether its binding profile is altered in different morphotypes or growth phases.

The SMC Complex

Current evidence suggests that SMC complex is essential for chromosome segregation in multicellular *Neisseriaceae*, indeed, *C. kuhniae smc* deletion mutants displayed chromosome segregation and morphological defects (supplemental figure 2 C & D). We hypothesis that the SMC/ScpAB complexes are recruited to the DNA by ParB-*parS* and then mediate lateral chromosome segregation. To test this, similar experimental strategies as those employed for ParB will be used.

C. kuhniae smc deletion mutants will be subjected to DNA FISH using *ori-* and *ter-*specific probes to determine and compared to the wild type) (Viehboeck et al., 2024). Hi-C chromosome conformation capture will be employed to assess how *smc* deletions globally alter chromosome architecture. Differences in chromosomal contact maps of wild-type and *smc* deletion mutants of both planktonic and surface attached *C. kuhniae* will help determine if environmental context influences the role of SMC in shaping 3D genome structure. Hi-C contact maps will be combined with transcriptomic data generated from wild-type and *smc* mutant strains to explore potential correlations between genome organisation and gene expression. Finally, to directly identify the genomic regions bound by the SMC complex, ChIP-seq will be performed using a custom antibody raised against recombinant *C. kuhniae* SMC. This will allow in vivo mapping of SMC-associated loci and help determine whether these coincide with predicted chromosomal loops or boundaries identified in the Hi-C data.

The Role of Bistable Ploidy in the Survival & Host Colonisation of *C. kuhniae*

The exact cause of bistable ploidy in *C. kuhniae* remains unclear. However, the higher prevalence of rod-shaped monoploid cells suggests it may be an adaptive strategy for enhancing survival under nutrient-depleted conditions. Furthermore, differences in fimbrial positioning between the two morphotypes may correlate with varying abilities to colonise host surfaces. To uncover the underlying mechanisms and ecological significance of bistable ploidy will require a combination of genetic, microscopic, and functional assays.

To identify transcription factors or stress response proteins unique to each morphotype, comparative transcriptomic analysis will be carried out. Rod-shaped monoploid and crescent-shaped diploid cells from both exponential and stationary phases will be isolated using fluorescence-activated cell sorting (FACS), based on differences in morphology and DNA content (Shapiro, 2005). RNA will then be extracted from each population, subjected to sequencing to capture their gene expression profiles and then the transcriptomes across cell types and growth phases will be

compared (Viehboeck et al., 2024). This comparative analysis will then be used to guide the design of targeted genetic manipulations aimed at creating stable strains of both rod-shaped monoploid and crescent-shaped diploid *C. kuhniae*.

Obtaining these monoploid or diploid only *C. kuhniae* stains will enable direct investigation into how specific genes influence cell shape, stress response, and survival. These engineered strains will enable us to directly test the functional roles of specific genes in shaping cell morphology, stress resilience, and survival strategies. They will also provide a system to compare the response of each morphotype to environmental stress or their ability to adhere to and colonise host surfaces. The colonisation competence of rod-shaped and crescent-shaped *C. kuhniae* will be evaluated by first incubation with human epithelial cell lines OKF6/TERT-2 or NOK-SI (Cuadra et al., 2023). This is followed by washing to remove non-adhered *C. kuhniae* with human cell-attached *C. kuhniae* remaining. The number of attached *C. kuhniae* can then be quantified through various methods, including performing flow cytometry or colony-forming unit (CFU) assays on epithelial cell lysis. Additionally, fluorescence microscopy can be employed to visualise fluorescently labelled *C. kuhniae* strains, or alternatively, cells can be stained with a vital dye such as Syto9 directly on the slide.

References

Anchimiuk, A., Lioy, V. S., Bock, F. P., Minnen, A., Boccard, F., & Gruber, S. (2021). A low Smc flux avoids collisions and facilitates chromosome organization in Bacillus subtilis. *eLife*, *10*, e65467. https://doi.org/10.7554/eLife.65467

Angert, E. R. (2005, March). Alternatives to binary fission in bacteria. In *Nature Reviews Microbiology* (Vol. 3, Issue 3, pp. 214–224). https://doi.org/10.1038/nrmicro1096

Arweiler, N. B., & Netuschil, L. (2016). The Oral Microbiota. In A. Schwiertz (Ed.), *Microbiota of the Human Body: Implications in Health and Disease* (pp. 45–60). Springer International Publishing. https://doi.org/10.1007/978-3-319-31248-4_4

Barrero-Canosa, J., Moraru, C., Zeugner, L., Fuchs, B. M., & Amann, R. (2017). Direct-geneFISH: a simplified protocol for the simultaneous detection and quantification of genes and rRNA in microorganisms. *Environmental Microbiology*, *19*(1), 70–82. https://doi.org/10.1111/1462-2920.13432

Baumann, P., & Baumann, L. (1998). *Buchnera-aphidicola-The-endosymbiont-of-aphids*.

Bonner, J. T. (1998). The origins of multicellularity. *Integrative Biology: Issues, News, and Reviews*, *1*(1), 27–36. https://doi.org/10.1002/(SICI)1520-6602(1998)1:1<27::AID-INBI4>3.0.CO;2-6

Bowman, G. R., Comolli, L. R., Zhu, J., Eckart, M., Koenig, M., Downing, K. H., Moerner, W. E., Earnest, T., & Shapiro, L. (2008). *A Polymeric Protein Anchors the Chromosomal Origin/ParB Complex at a Bacterial Cell Pole*. https://doi.org/10.1016/j.cell.2008.07.015

Bright, M., & Bulgheresi, S. (2010, March). A complex journey: Transmission of microbial symbionts. In *Nature Reviews Microbiology* (Vol. 8, Issue 3, pp. 218–230). https://doi.org/10.1038/nrmicro2262

Chiu, L., Bazin, T., Truchetet, M. E., Schaeverbeke, T., Delhaes, L., & Pradeu, T. (2017, December). Protective microbiota: From localized to long-reaching co-immunity. In *Frontiers in Immunology* (Vol. 8, Issue DEC). Frontiers Media S.A. https://doi.org/10.3389/fimmu.2017.01678

Collins, B. E., Ye, L. F., Duzdevich, D., & Greene, E. C. (2014). DNA curtains: Novel tools for imaging protein–nucleic acid interactions at the single-molecule level. *Methods in Cell Biology*, *123*, 217–234. https://doi.org/10.1016/B978-0-12-420138-5.00012-4

Cox, M. M., & Battista, J. R. (2005). Deinococcus radiodurans—The consummate survivor. *Nature Reviews Microbiology*, *3*(11), 882–892. https://doi.org/10.1038/NRMICRO1264;KWRD=LIFE+SCIENCES

Cuadra, G. A., Shamim, A., Shah, R., Morgan, J., & Palazzolo, D. L. (2023). Comparison of Culture Media for In Vitro Expansion of Oral Epithelial Keratinocytes. *Applied Biosciences*, *2*(2), 308–327. https://doi.org/10.3390/applbiosci2020021

Deo, P. N., & Deshmukh, R. (2019, January). Oral microbiome: Unveiling the fundamentals. In *Journal of Oral and Maxillofacial Pathology* (Vol. 23, Issue 1, pp. 122–128). Wolters Kluwer Medknow Publications. https://doi.org/10.4103/jomfp.JOMFP_304_18

Dethlefsen, L., McFall-Ngai, M., & Relman, D. A. (2007). An ecological and evolutionary perspective on human–microbe mutualism and disease. *Nature 2007 449:7164*, *449*(7164), 811–818. https://doi.org/10.1038/nature06245

Dewar, J. M., & Walter, J. C. (2017). Mechanisms of DNA replication termination. *Nature Reviews. Molecular Cell Biology*, *18*(8), 507. https://doi.org/10.1038/NRM.2017.42

Dewhirst, F. E., Chen, T., Izard, J., Paster, B. J., Tanner, A. C. R., Yu, W. H., Lakshmanan, A., & Wade, W. G. (2010). The human oral microbiome. *Journal of Bacteriology*, *192*(19), 5002–5017. https://doi.org/10.1128/JB.00542-10

Dillon, S. C., & Dorman, C. J. (2010). Bacterial nucleoid-associated proteins, nucleoid structure and gene expression. *Nature Reviews Microbiology 2010 8:3*, *8*(3), 185–195. https://doi.org/10.1038/nrmicro2261

Donovan, C., Sieger, B., Krämer, R., & Bramkamp, M. (2012). A synthetic Escherichia coli system identifies a conserved origin tethering factor in Actinobacteria. *Molecular Microbiology*, *84*(1), 105–116. https://doi.org/10.1111/J.1365-2958.2012.08011.X

Douglas, A. E. (2009). *Endosymbionts and intracellular parasites*.

Dudek, N. K., Galaz-Montoya, J. G., Shi, H., Mayer, M., Danita, C., Celis, A. I., Viehboeck, T., Wu, G.-H., Behr, B., Bulgheresi, S., Huang, K. C., Chiu, W., & Relman, D. A. (2023). *Previously uncharacterized rectangular bacterial structures in the dolphin mouth*. https://doi.org/10.1038/s41467-023-37638-y

Duggin, I. G., & Bell, S. D. (2009). Termination Structures in the Escherichia coli Chromosome Replication Fork Trap. *Journal of Molecular Biology*, *387*(3), 532–539. https://doi.org/10.1016/J.JMB.2009.02.027

Duggin, I. G., Wake, R. G., Bell, S. D., & Hill, T. M. (2008). The replication fork trap and termination of chromosome replication. *Molecular Microbiology*, *70*(6), 1323–1333. https://doi.org/10.1111/J.1365-2958.2008.06500.X;JOURNAL:JOURNAL:13652958;WGROUP:STRING:PUBLICATION

Egan, A., & Vollmer, W. (2013). The physiology of bacterial cell division. *Annals of the New York Academy of Sciences*, *1277*(1), 8–28. https://doi.org/10.1111/j.1749-6632.2012.06818.x

Egan, S., Fukatsu, T., & Francino, M. P. (2020). Opportunities and Challenges to Microbial Symbiosis Research in the Microbiome Era. *Frontiers in Microbiology*, *11*, 1150. https://doi.org/10.3389/FMICB.2020.01150

Farkas, A., Maróti, G., Dürgo, H., Györgypál, Z., Lima, R. M., Medzihradszky, K. F., Kereszt, A., Mergaert, P., & Kondorosi, É. (2014). Medicago truncatula symbiotic peptide NCR247 contributes to bacteroid differentiation through multiple mechanisms. *Proceedings of the National Academy of Sciences of the United States of America*, *111*(14), 5183–5188. https://doi.org/10.1073/PNAS.1404169111/-/DCSUPPLEMENTAL

Ferreira-Halder, C. V., Faria, A. V. de S., & Andrade, S. S. (2017, December). Action and function of Faecalibacterium prausnitzii in health and disease. In *Best Practice and Research: Clinical Gastroenterology* (Vol. 31, Issue 6, pp. 643–648). Bailliere Tindall Ltd. https://doi.org/10.1016/j.bpg.2017.09.011

Frank, S. A. (1997). Models of Symbiosis. *The American Naturalist*, *150*(S1), S80–S99. https://doi.org/10.1086/286051

Galperin, M. Y. (2007). Linear chromosomes in bacteria: No straight edge advantage? *Environmental Microbiology*, *9*(6), 1357–1362. https://doi.org/10.1111/J.1462-2920.2007.01328.X

Ganji, M., Shaltiel, I. A., Bisht, S., Kim, E., Kalichava, A., Haering, C. H., & Dekker, C. (2018). Real-time imaging of DNA loop extrusion by condensin. *Science*, *360*(6384), 102–105. https://doi.org/10.1126/SCIENCE.AAR7831/SUPPL_FILE/AAR7831S9.MP4

Genco, R. J., Grossi, S. G., Ho, A., Nishimura, F., & Murayama, Y. (2005). A Proposed Model Linking Inflammation to Obesity, Diabetes, and Periodontal Infections. *Journal of Periodontology*, *76*(11S), 2075–2084. https://doi.org/10.1902/JOP.2005.76.11-S.2075;WEBSITE:WEBSITE:AAP

Glatthardt, T., Lima, R. D., Mattos, R. M. de, & Ferreira, R. B. R. (2024, January). Microbe Interactions within the Skin Microbiome. In *Antibiotics* (Vol. 13, Issue 1). Multidisciplinary Digital Publishing Institute (MDPI). https://doi.org/10.3390/antibiotics13010049

Govers, S. K., & Jacobs-Wagner, C. (2020). Caulobacter crescentus: Model system extraordinaire. *Current Biology*, *30*(19), R1151–R1158. https://doi.org/10.1016/j.cub.2020.07.033

Han, Y. W., & Wang, X. (2013). Mobile Microbiome: Oral Bacteria in Extra-oral Infections and Inflammation. *Journal of Dental Research*, *92*(6), 485. https://doi.org/10.1177/0022034513487559

Hansen, M. T. (1978). Multiplicity of genome equivalents in the radiation-resistant bacterium Micrococcus radiodurans. *Journal of Bacteriology*, *134*(1), 71. https://doi.org/10.1128/JB.134.1.71-75.1978

Harju, J., & Broedersz, C. P. (2024). Physical models of bacterial chromosomes. *Molecular Microbiology*, *123*(2), 143–153. https://doi.org/10.1111/MMI.15257;JOURNAL:JOURNAL:13652958;WGROUP:STRING:PUBLICATION

Hedlund, B. P., & Kuhn, D. A. (2006). The Genera Simonsiella and Alysiella. *The Prokaryotes*, 828–839. https://doi.org/10.1007/0-387-30745-1_38

Hedlund, B. P., & Tønjum, T. (2015). Simonsiella. In *Bergey's Manual of Systematics of Archaea and Bacteria* (pp. 1–12). Wiley. https://doi.org/10.1002/9781118960608.gbm00983

Heinzelmann, R., Dutech, C., Tsykun, T., Labbé, F., Soularue, J. P., & Prospero, S. (2019, January). Latest advances and future perspectives in Armillaria research. In *Canadian Journal of Plant Pathology* (Vol. 41, Issue 1, pp. 1–23). Taylor and Francis Inc. https://doi.org/10.1080/07060661.2018.1558284

Herskovits, A. A., & Bibi, E. (2000). Association of Escherichia coli ribosomes with the inner membrane requires the signal recognition particle receptor but is independent of the signal recognition particle. *Proceedings of the National Academy of Sciences of the United States of America*, *97*(9), 4621. https://doi.org/10.1073/PNAS.080077197

Hollister, E. B., Gao, C., & Versalovic, J. (2014). Compositional and Functional Features of the Gastrointestinal Microbiome and Their Effects on Human Health. *Gastroenterology*, *146*(6), 1449. https://doi.org/10.1053/J.GASTRO.2014.01.052

Jalal, A. S. B., & Le, T. B. K. (2020, June). Bacterial chromosome segregation by the ParABS system. In *Open Biology* (Vol. 10, Issue 6). Royal Society Publishing. https://doi.org/10.1098/rsob.200097

Joshipura, K. J., Hung, H. C., Rimm, E. B., Willett, W. C., & Ascherio, A. (2003). Periodontal disease, tooth loss, and incidence of ischemic stroke. *Stroke*, *34*(1), 47–52. https://doi.org/10.1161/01.STR.0000052974.79428.0C

Joshipura, K. J., Rimm, E. B., Douglass, C. W., Trichopoulos, D., Ascherio, A., & Willett, W. C. (1996). Poor oral health and coronary heart disease. *Journal of Dental Research*, *75*(9), 1631–1636. https://doi.org/10.1177/00220345960750090301;JOURNAL:JOURNAL:JDRB;REQUESTEDJOURNAL:JOURNAL:JDRB;PAGE:STRING:ARTICLE/CHAPTER

Joyeux, M. (2015). Compaction of bacterial genomic DNA: Clarifying the concepts. *Journal of Physics: Condensed Matter*, *27*(38), 383001. https://doi.org/10.1088/0953-8984/27/38/383001

Kaiser, D. (2001). Building a multicellular organism. *Annual Review of Genetics*, *35*(1), 103–123.

Kaiser, G. E., & Starzyk, M. J. (1973). Ultrastructure and cell division of an oral bacterium resembling Alysiella filiformis. *Canadian Journal of Microbiology*, *19*(3), 325–327. https://doi.org/10.1139/m73-054

Kaltenpoth, M., Flórez, L. V., Vigneron, A., Dirksen, P., & Engl, T. (2025). Origin and function of beneficial bacterial symbioses in insects. *Nature Reviews Microbiology 2025*, 1–17. https://doi.org/10.1038/s41579-025-01164-z

Kannaiah, S., Livny, J., & Amster-Choder, O. (2019). Spatiotemporal Organization of the E. coli Transcriptome: Translation Independence and Engagement in Regulation. *Molecular Cell*, *76*(4), 574-589.e7. https://doi.org/10.1016/J.MOLCEL.2019.08.013/ASSET/F7870A46-FB61-46B2-A72E-A37E0D7D3E26/MAIN.ASSETS/GR7.JPG

Kawalek Adam, Glabski Krzysztof, Bartosik Aneta Agnieszka, Wozniak Dominika, Kusiak Magdalena, Gawor Jan, Zuchniewicz Karolina, & Jagura-Burdzy Grazyna. (2023). Diverse Partners of the Partitioning ParB Protein in Pseudomonas aeruginosa. *Microbiology Spectrum*, *11*(1), e04289-22. https://doi.org/10.1128/spectrum.04289-22

Kisner, J. R., & Kuwada, N. J. (2020). Nucleoid-mediated positioning and transport in bacteria. *Current Genetics*, *66*(2), 279–291. https://doi.org/10.1007/S00294-019-01041-2/FIGURES/2

Kleckner, N., Fisher, J. K., Stouf, M., White, M. A., Bates, D., & Witz, G. (2014). The bacterial nucleoid: Nature, dynamics and sister segregation. *Current Opinion in Microbiology*, *22*, 127–137. https://doi.org/10.1016/J.MIB.2014.10.001

Kondorosi, E., Mergaert, P., & Kereszt, A. (2013). A Paradigm for endosymbiotic life: Cell differentiation of rhizobium bacteria provoked by host plant factors. *Annual Review of Microbiology*, *67*(Volume 67, 2013), 611–628. https://doi.org/10.1146/ANNUREV-MICRO-092412-155630/CITE/REFWORKS

Konieczny, I., & Helinski, D. R. (1997). Helicase Delivery and Activation by DnaA and TrfA Proteins during the Initiation of Replication of the Broad Host Range Plasmid RK2*. *THE JOURNAL OF BIOLOGICAL CHEMISTRY*, *272*(52), 33312–33318. https://doi.org/10.1074/jbc.272.52.33312

Kundu, P., Blacher, E., Elinav, E., & Pettersson, S. (2017, December). Our Gut Microbiome: The Evolving Inner Self. In *Cell* (Vol. 171, Issue 7, pp. 1481–1493). Cell Press. https://doi.org/10.1016/j.cell.2017.11.024

Leisch, N., Verheul, J., Heindl, N. R., Gruber-Vodicka, H. R., Pende, N., Blaauwen, T. D., & Bulgheresi, S. (2012). Growth in width and FtsZ ring longitudinal positioning in a gammaproteobacterial symbiont. *Current Biology*, *22*(19), R831–R832. https://doi.org/10.1016/J.CUB.2012.08.033

Li, X., Kolltveit, K. M., Tronstad, L., & Olsen, I. (2000). Systemic Diseases Caused by Oral Infection. *Clinical Microbiology Reviews*, *13*(4), 547. https://doi.org/10.1128/CMR.13.4.547-558.2000

Lin, J.-S., & Lai, E.-M. (2017). Protein–Protein Interactions: Co-Immunoprecipitation. In L. Journet & E. Cascales (Eds.), *Bacterial Protein Secretion Systems: Methods and Protocols* (pp. 211–219). Springer. https://doi.org/10.1007/978-1-4939-7033-9_17

Livny, J., Yamaichi, Y., & Waldor, M. K. (2007). Distribution of Centromere-Like parS Sites in Bacteria: Insights from Comparative Genomics. *Journal of Bacteriology*, *189*(23), 8693. https://doi.org/10.1128/JB.01239-07

Lloyd-Price, J., Abu-Ali, G., & Huttenhower, C. (2016, April). The healthy human microbiome. In *Genome Medicine* (Vol. 8, Issue 1). BioMed Central Ltd. https://doi.org/10.1186/s13073-016-0307-y

Lu, M., Xuan, S., & Wang, Z. (2019, March). Oral microbiota: A new view of body health. In *Food Science and Human Wellness* (Vol. 8, Issue 1, pp. 8–15). Elsevier B.V. https://doi.org/10.1016/j.fshw.2018.12.001

Lyons, N. A., & Kolter, R. (2015). On the evolution of bacterial multicellularity. *Current Opinion in Microbiology*, *24*, 21–28. https://doi.org/10.1016/J.MIB.2014.12.007

Makarova, K. S., Aravind, L., Wolf, Y. I., Tatusov, R. L., Minton, K. W., Koonin, E. V., & Daly, M. J. (2001). Genome of the extremely radiation-resistant bacterium Deinococcus radiodurans viewed from the perspective of comparative genomics. *Microbiology and Molecular Biology Reviews : MMBR*, *65*(1), 44–79. https://doi.org/10.1128/MMBR.65.1.44-79.2001

Maldonado, R., Jimenez, J., & Casadesusl, J. (1994). Changes of Ploidy during the Azotobacter vinelandii Growth Cycle. In *JOURNAL OF BACTERIOLOGY* (Vol. 176, Issue 13, pp. 3911–3919).

Marsh, P. D. (2000). Role of the oral microflora in health. In *Microbial Ecology in Health and Disease* (Vol. 12, Issue 3, pp. 130–137). Taylor and Francis A.S. https://doi.org/10.1080/089106000750051800

Moran, N. A. (2006). Symbiosis. *Current Biology*, *16*(20), R866–R871. https://doi.org/10.1016/j.cub.2006.09.019

Moraru, C., & Barrero-Canosa, J. (2021). Linking Microbes to Their Genes at Single Cell Level with Direct-geneFISH. In *Fluorescence In Situ Hybridization (FISH) for Microbial Cells: Methods and Concepts, Methods in Molecular Biology*.

Neu, J., & Rushing, J. (2011, June). Cesarean Versus Vaginal Delivery: Long-term Infant Outcomes and the Hygiene Hypothesis. In *Clinics in Perinatology* (Vol. 38, Issue 2, pp. 321–331). https://doi.org/10.1016/j.clp.2011.03.008

Niki, H., & Hiraga, S. (1998). Polar localization of the replication origin and terminus in Escherichia coli nucleoids during chromosome partitioning. *Genes & Development*, *12*(7), 1036. https://doi.org/10.1101/GAD.12.7.1036

Niki, H., Yamaichi, Y., & Hiraga, S. (2000). Dynamic organization of chromosomal DNA in Escherichia coli. *Genes & Development*, *14*(2), 212. https://doi.org/10.1101/gad.14.2.212

Nyby, M. D., Gregory, D. A., Kuhn, D. A., & Pangborn, J. (1977). Incidence of Simonsiella in the oral cavity of dogs. *Journal of Clinical Microbiology*, *6*(1), 87–88. https://doi.org/10.1128/jcm.6.1.87-88.1977

Nyongesa, S., Weber, P. M., Bernet, È., Pulido, F., Nieves, C., Nieckarz, M., Delaby, M., Viehboeck, T., Krause, N., Rivera-Millot, A., Nakamura, A., Vischer, N. O. E., vanNieuwenhze, M., Brun, Y. V., Cava, F., Bulgheresi, S., & Veyrier, F. J. (2022). Evolution of longitudinal division in multicellular bacteria of the Neisseriaceae family. *Nature Communications*, *13*(1). https://doi.org/10.1038/s41467-022-32260-w

Ogunrinola, G. A., Oyewale, J. O., Oshamika, O. O., & Olasehinde, G. I. (2020). The Human Microbiome and Its Impacts on Health. *International Journal of Microbiology*, *2020*. https://doi.org/10.1155/2020/8045646

Ott, J. A., Gruber-Vodicka, H. R., Leisch, N., & Zimmermann, J. (2014). Phylogenetic confirmation of the genus Robbea (Nematoda: Desmodoridae, Stilbonematinae) with the description of three new species. *Systematics and Biodiversity*, *12*(4), 434. https://doi.org/10.1080/14772000.2014.941038

Oulhen, N., Schulz, B. J., & Carrier, T. J. (2016). English translation of Heinrich Anton de Bary's 1878 speech, 'Die Erscheinung der Symbiose' ('De la symbiose'). *Symbiosis*, *69*(3), 131–139. https://doi.org/10.1007/S13199-016-0409-8/FIGURES/2

Parmentier, E., & Michel, L. (2013). Boundary lines in symbiosis forms. *Symbiosis*, *60*(1), 1–5. https://doi.org/10.1007/s13199-013-0236-0

Patil, S., Rao, R., Amrutha, N., & Sanketh, D. (2013). Oral Microbial Flora in Health. *World Journal of Dentistry*, *4*. https://doi.org/10.5005/jp-journals-10015-1242

Pecoraro, V., Zerulla, K., Lange, C., & Soppa, J. (2011). Quantification of Ploidy in Proteobacteria Revealed the Existence of Monoploid, (Mero-)Oligoploid and Polyploid Species. *PLoS ONE*, *6*(1), e16392. https://doi.org/10.1371/JOURNAL.PONE.0016392

Pende, N., Wang, J., Weber, P. M., Verheul, J., Kuru, E., Rittmann, S. K. M. R., Leisch, N., VanNieuwenhze, M. S., Brun, Y. V., den Blaauwen, T., & Bulgheresi, S. (2018). Host-Polarized Cell Growth in Animal Symbionts. *Current Biology*, *28*(7), 1039-1051.e5. https://doi.org/10.1016/j.cub.2018.02.028

Penterman, J., Abo, R. P., Nisco, N. J. D., Arnold, M. F. F., Longhi, R., Zanda, M., & Walker, G. C. (2014). Host plant peptides elicit a transcriptional response to control the Sinorhizobium meliloti cell cycle during symbiosis. *Proceedings of the National Academy of Sciences of the United States of America*, *111*(9), 3561–3566. https://doi.org/10.1073/PNAS.1400450111/-/DCSUPPLEMENTAL

Perera, M., Al-Hebshi, N. N., Speicher, D. J., Perera, I., & Johnson, N. W. (2016). Emerging role of bacteria in oral carcinogenesis: A review with special reference to perio-pathogenic bacteria. In *Journal of Oral Microbiology* (Vol. 8, Issue 1). Co-Action Publishing. https://doi.org/10.3402/jom.v8.32762

Polz, M. F., Distel, D. L., Zarda, B., Amann, R., Felbeck, H., Ott, J. A., & Cavanaugh, C. M. (1994). Phylogenetic analysis of a highly specific association between ectosymbiotic, sulfur-oxidizing bacteria and a marine nematode. *Applied and Environmental Microbiology*, *60*(12), 4461–4467. https://doi.org/10.1128/aem.60.12.4461-4467.1994

Porter, N. T., Luis, A. S., & Martens, E. C. (2018, November). Bacteroides thetaiotaomicron. In *Trends in Microbiology* (Vol. 26, Issue 11, pp. 966–967). Elsevier Ltd. https://doi.org/10.1016/j.tim.2018.08.005

Rajasekaran, J. J., Krishnamurthy, H. K., Bosco, J., Jayaraman, V., Krishna, K., Wang, T., & Bei, K. (2024). Oral Microbiome: A Review of Its Impact on Oral and Systemic Health. *Microorganisms*, *12*(9), 1797. https://doi.org/10.3390/MICROORGANISMS12091797/S1

Ramond, E., Maclachlan, C., Clerc-Rosset, S., Knott, G. W., & Lemaitre, B. (2016). Cell division by longitudinal scission in the insect endosymbiont Spiroplasma poulsonii. *mBio*, *7*(4). https://doi.org/10.1128/MBIO.00881-16/ASSET/4DCE4F4E-7CF6-4BE8-AE62-934562A23463/ASSETS/GRAPHIC/MBO0041629160002.JPEG

Rampelotto, P. H., & Woldringh, C. L. (2024). Compaction and Segregation of DNA in Escherichia coli. *Life 2024, Vol. 14, Page 660*, *14*(6), 660. https://doi.org/10.3390/LIFE14060660

Reyes-Lamothe, R., & Sherratt, D. J. (2019). The bacterial cell cycle, chromosome inheritance and cell growth. *Nature Reviews Microbiology 2019 17:8*, *17*(8), 467–478. https://doi.org/10.1038/s41579-019-0212-7

Reyes-Lamothe, R., Wang, X., & Sherratt, D. (2008). Escherichia coli and its chromosome. *Trends in Microbiology*, *16*(5), 238–245. https://doi.org/10.1016/J.TIM.2008.02.003

Riaz, S., Xiao, M., Chen, P., Li, M., Cui, Y., & Darocha, M. (2021). The Genome Copy Number of the Thermophilic Cyanobacterium Thermosynechococcus elongatus E542 Is Controlled by Growth Phase and Nutrient Availability. *Applied and Environmental Microbiology*, *87*(9), e02993-20. https://doi.org/10.1128/AEM.02993-20

Rodríguez-Beltrán, J., DelaFuente, J., León-Sampedro, R., MacLean, R. C., & Millán, Á. S. (2021). Beyond horizontal gene transfer: The role of plasmids in bacterial evolution. *Nature Reviews Microbiology*, *19*(6), 347–359. https://doi.org/10.1038/S41579-020-00497-1;SUBJMETA=181,208,2482,325,326,631;KWRD=BACTERIAL+GENETICS,EVOLUTION,MICROBIAL+GENETICS

Roggiani, M., & Goulian, M. (2015). Chromosome-Membrane Interactions in Bacteria. *Annual Review of Genetics*, *49*, 115–129. https://doi.org/10.1146/annurev-genet-112414-054958

Rosenberg, E. (2024). Diversity of bacteria within the human gut and its contribution to the functional unity of holobionts. *Npj Biofilms and Microbiomes*, *10*(1), 1–5. https://doi.org/10.1038/S41522-024-00580-Y;SUBJMETA=326,631,692,700;KWRD=HEALTH+CARE,MICROBIOLOGY

Ruiz, L. M. R., Williams, C. L., & Tamayo, R. (2020). Enhancing bacterial survival through phenotypic heterogeneity. *PLOS Pathogens*, *16*(5), e1008439. https://doi.org/10.1371/JOURNAL.PPAT.1008439

Sale, J. E. (2007). Radiation Resistance: Resurrection by Recombination. *Current Biology*, *17*(1), R12–R14. https://doi.org/10.1016/j.cub.2006.11.037

Shapiro, H. M. (2005). *Practical Flow Cytometry*. Wiley. https://books.google.at/books?id=JhSyimPKuJwC

Shen, B. A., & Landick, R. (2019). Transcription of Bacterial Chromatin. *Journal of Molecular Biology*, *431*(20), 4040. https://doi.org/10.1016/J.JMB.2019.05.041

Shimizu, H., Miyamoto, J., Hisa, K., Ohue-Kitano, R., Takada, H., Yamano, M., Nishida, A., Sasahara, D., Masujima, Y., Watanabe, K., Nishikawa, S., Takahashi, S., Ikeda, T., Nakajima, Y., Yoshida, N., Matsuzaki, C., Kageyama, T., Hayashi, I., Matsuki, A., … Kimura, I. (2025). Sucrose-preferring gut microbes prevent host obesity by producing exopolysaccharides. *Nature Communications*, *16*(1), 1145. https://doi.org/10.1038/s41467-025-56470-0

Soppa, J. (2014). Polyploidy in Archaea and Bacteria: About Desiccation Resistance, Giant Cell Size, Long-Term Survival, Enforcement by a Eukaryotic Host and Additional Aspects. *Microbial Physiology*, *24*(5–6), 409–419. https://doi.org/10.1159/000368855

Soultanas, P. (2005). The Bacterial Helicase-Primase Interaction: A Common Structural/Functional Module. *Structure (London, England : 1993)*, *13*(6), 839. https://doi.org/10.1016/J.STR.2005.04.006

Spahn, C., Middlemiss, S., Gómez-de-Mariscal, E., Henriques, R., Bode, H. B., Holden, S., & Heilemann, M. (2025). The nucleoid of rapidly growing Escherichia coli localizes close to the inner membrane and is organized by transcription, translation, and cell geometry. *Nature Communications 2025 16:1*, *16*(1), 1–18. https://doi.org/10.1038/s41467-025-58723-4

Speck, C., & Messer, W. (2001). Mechanism of origin unwinding: Sequential binding of DnaA to double- and single-stranded DNA. *The EMBO Journal*, *20*(6), 1469. https://doi.org/10.1093/EMBOJ/20.6.1469

Steed, P. D. M. (1963). Simonsiellaceae farn.nov. With Characterization of Simonsiella crassa and Alysiella filif orrnis. In *T. gen. Microbiol* (Vol. 29, pp. 615–624).

Sullivan, N. L., Marquis, K. A., & Rudner, D. Z. (2009). Recruitment of SMC by ParB-parS Organizes the Origin Region and Promotes Efficient Chromosome Segregation. *Cell*, *137*(4), 697–707. https://doi.org/10.1016/J.CELL.2009.04.044

Toro, E., Hong, S.-H., Mcadams, H. H., & Shapiro, L. (2008). *Caulobacter requires a dedicated mechanism to initiate chromosome segregation*. www.pnas.org/cgi/content/full/

Tran, N. T., Laub, M. T., & Le, T. B. K. (2017). SMC Progressively Aligns Chromosomal Arms in Caulobacter crescentus but Is Antagonized by Convergent Transcription. *Cell Reports*, *20*(9), 2057. https://doi.org/10.1016/J.CELREP.2017.08.026

Vega-Cabrera, L., Skovgaard, O., & Toll-Riera, M. (2024, December). *Chromosomal plasticity can drive rapid adaptation in bacteria*. bioRxiv. https://doi.org/10.1101/2024.12.11.627208

Viehboeck, T., Weber, P. M., Krause, N., Varoquaux, N., Junier, I., Bulgheresi, S., & Lioy, V. S. (2024). *Stable chromosome configuration and loop-based polarization in animal symbionts 1*. https://doi.org/10.1101/2023.12.21.572873

Walls, A. W., & Rosenthal, A. Z. (2024). Bacterial phenotypic heterogeneity through the lens of single-cell RNA sequencing. *Transcription*, *15*(1–2), 48. https://doi.org/10.1080/21541264.2024.2334110

Wang, X., Brandão, H. B., Le, T. B. K., Laub, M. T., & Rudner, D. Z. (2017). Bacillus subtilis SMC complexes juxtapose chromosome arms as they travel from origin to terminus. *Science*, *355*(6324), 524–527. https://doi.org/10.1126/SCIENCE.AAI8982/SUPPL_FILE/WANG.SM.PDF

Wang, X., Llopis, P. M., & Rudner, D. Z. (2013). Organization and segregation of bacterial chromosomes. *Nature Reviews. Genetics*, *14*(3), 10.1038/nrg3375. https://doi.org/10.1038/NRG3375

Wang, X., & Rudner, D. Z. (2014, December). Spatial organization of bacterial chromosomes. In *Current Opinion in Microbiology* (Vol. 22, pp. 66–72). Elsevier Ltd. https://doi.org/10.1016/j.mib.2014.09.016

Weber, P. M., Moessel, F., Paredes, G. F., Viehboeck, T., Vischer, N. O. E., & Bulgheresi, S. (2019). A Bidimensional Segregation Mode Maintains Symbiont Chromosome Orientation toward Its Host. *Current Biology*, *29*(18), 3018-3028.e4. https://doi.org/10.1016/j.cub.2019.07.064

Weigel, W. A., & Dersch, P. (2018). Phenotypic heterogeneity: A bacterial virulence strategy. *Microbes and Infection*, *20*(9–10), 570–577. https://doi.org/10.1016/J.MICINF.2018.01.008

Wilhelm, L., Bürmann, F., Minnen, A., Shin, H. C., Toseland, C. P., Oh, B. H., & Gruber, S. (2015). SMC condensin entraps chromosomal DNA by an ATP hydrolysis dependent loading mechanism in Bacillus subtilis. *eLife*, *4*(MAY). https://doi.org/10.7554/ELIFE.06659

Woldemeskel, S. A., & Goley, E. D. (2017). Shapeshifting to Survive: Shape Determination and Regulation in Caulobacter crescentus. *Trends in Microbiology*, *25*(8), 673–687. https://doi.org/10.1016/J.TIM.2017.03.006/ASSET/B01FB62F-5F01-4806-BE56-DB8D29F0C2CE/MAIN.ASSETS/GR2.JPG

Workentine, M., & Surette, M. G. (2011). Complex Pseudomonas population structure in cystic fibrosis airway infections. *American Journal of Respiratory and Critical Care Medicine*, *183*(12), 1581–1583. https://doi.org/10.1164/RCCM.201105-0776ED;JOURNAL:JOURNAL:AJRCCM;WGROUP:STRING:DEFAULT

Yao, N. Y., & O'Donnell, M. (2009). Replisome structure and conformational dynamics underlie fork progression past obstacles. *Current Opinion in Cell Biology*, *21*(3), 336–343. https://doi.org/10.1016/J.CEB.2009.02.008

Youngren, B., Nielsen, H. J., Jun, S., & Austin, S. (2014). The multifork Escherichia coli chromosome is a self-duplicating and self-segregating thermodynamic ring polymer. *Genes and Development*, *28*(1), 71–84. https://doi.org/10.1101/GAD.231050.113,

Zachar, I., & Boza, G. (2020). Endosymbiosis before eukaryotes: Mitochondrial establishment in protoeukaryotes. *Cellular and Molecular Life Sciences*, *77*(18), 3503–3523. https://doi.org/10.1007/s00018-020-03462-6

Zhao, H., Chu, M., Huang, Z., Yang, X., Ran, S., Hu, B., Zhang, C., & Liang, J. (2017). Variations in oral microbiota associated with oral cancer. *Scientific Reports*, *7*(1). https://doi.org/10.1038/s41598-017-11779-9

Zheng, D., Liwinski, T., & Elinav, E. (2020, June). Interaction between microbiota and immunity in health and disease. In *Cell Research* (Vol. 30, Issue 6, pp. 492–506). Springer Nature. https://doi.org/10.1038/s41422-020-0332-7

Supplemental Figures

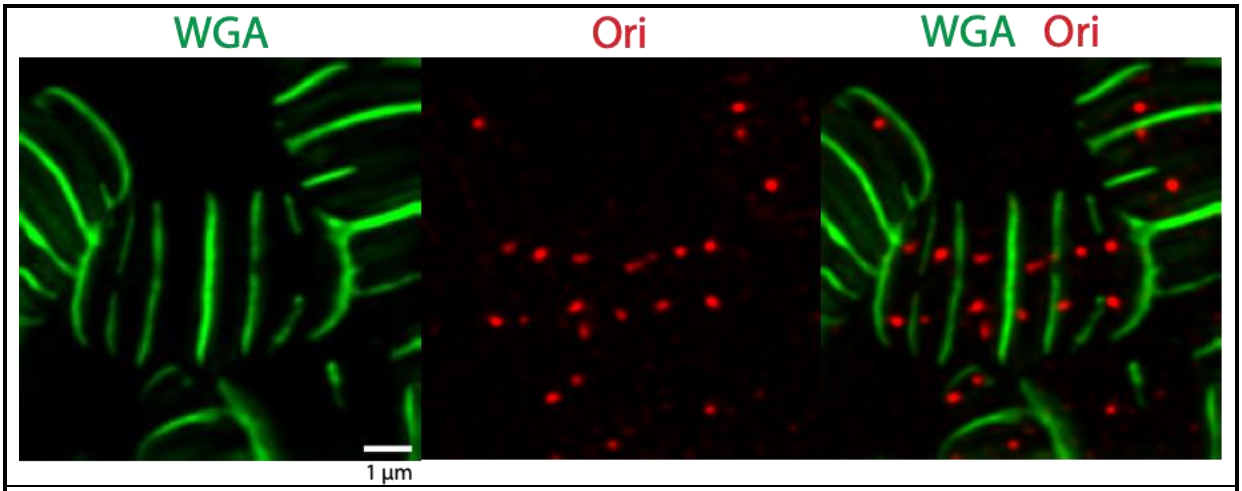

Supplemental Figure 1: Subpolar Localisation of *ori* in *S. muelleri*: Structured illumination microscopy (SIM) of *ori* (red) in *S. muelleri,* cell membrane stained with WGA (green). Scale bar is 1 µm. (Krause, unpublished).

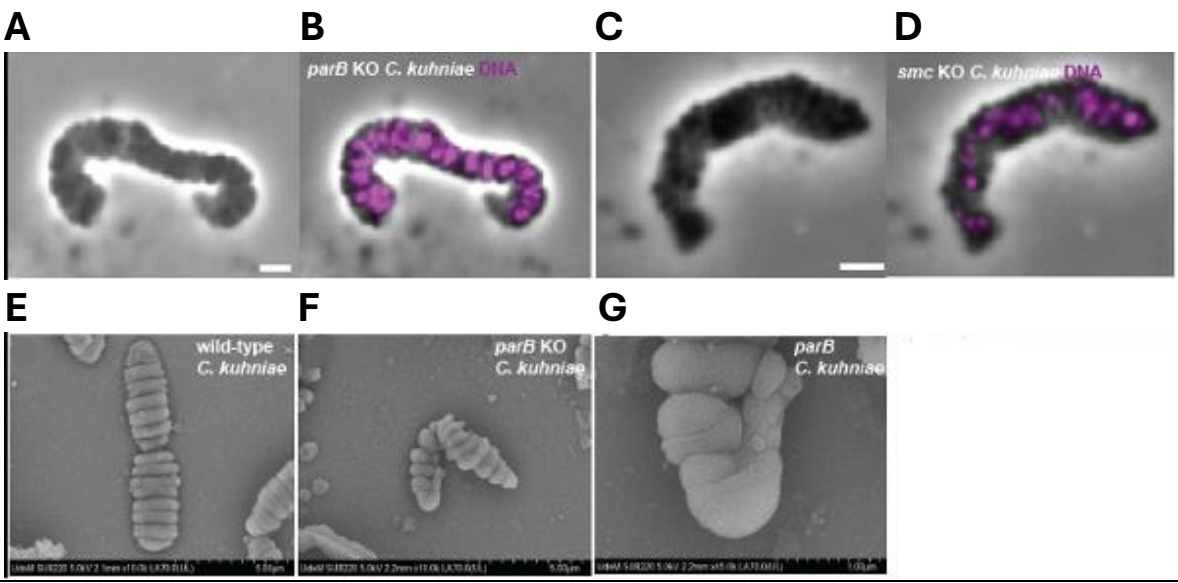

Supplemental Figure 2: DNA Localisation in Wild-type & *C. kuhniae* Deletion Mutants. (A-B) Top view of *C. kuhniae parB* deletion mutants or **(C-D)** *smc* deletion mutants stained with Hoechst to visualise the DNA (magenta). Abnormal cell morphology is evident in phase contrast panels. Scale bars are 2 µm. **(E-G)** Scanning electron micrograph of wild-type *C. kuhniae* **(E)** or *parB* deletion mutants **(F-G)**. ((A-D) Krause, unpublished, (E-G) Veyrier, unpublished).

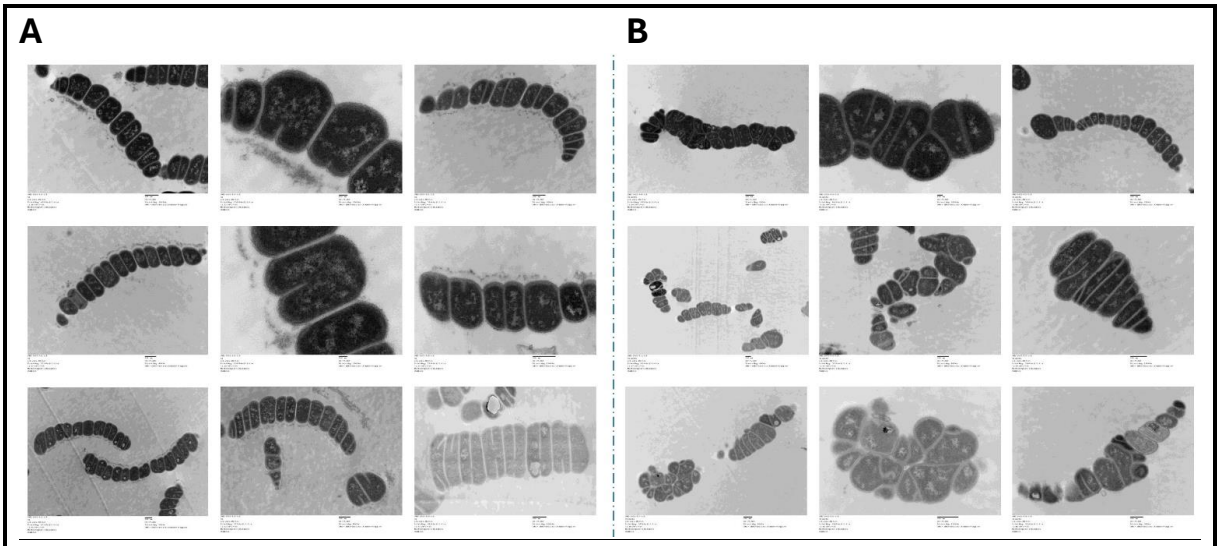

Supplemental Figure 3: Visualisation of Fimbria of *C. kuhniae*. Thin section electron microscopy images of **(A)** wild type *C. kuhniae* with fimbriae visible as fuzzy outline. **(B)** *parB* deletion mutants of *C. kuhniae* with disrupted morphology and no fuzzy outline visible. (Veyrier, unpublished).

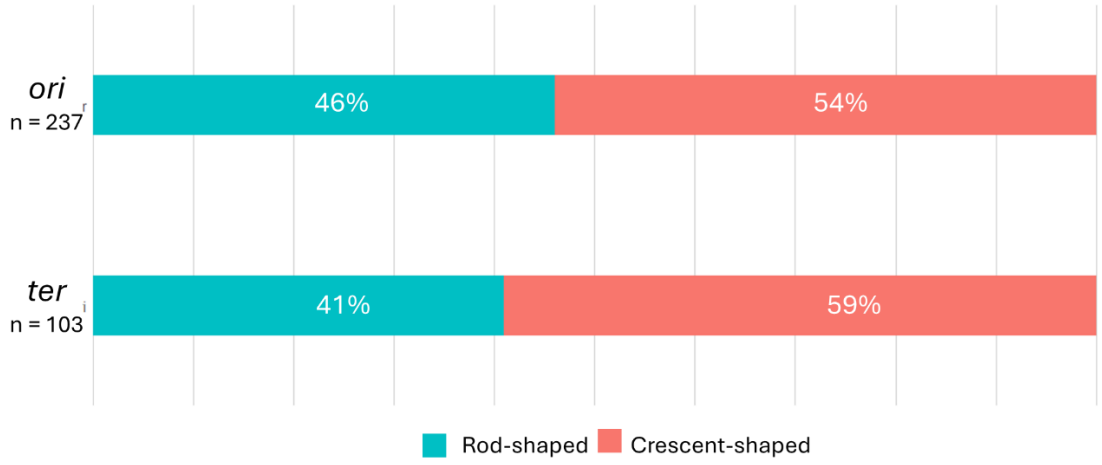

Supplemental Figure 4: Proportion of Rod-shaped & Crescent-shaped *C. kuhniae* Filaments. DNA FISH experiments targeting the *ori* or *ter* carried out on cells fixed during exponential growth from four independent cultures. (two for *ori* and *ter* respectively).

Supplemental Table 1: Morphometric Measurements of Rod-shaped & Crescent-shaped *C. kuhniae*.

		Crescent-shaped	Rod-shaped
Number of Cells		683	1796
Length (µm)	**Range**	1.352 – 4.958	0.553 – 2.971
	Median	2.974	2.0712
	Mean	3.048	2.069
	Standard Deviation	0.618	0.280
Width (µm)	**Range**	0.147 – 1.352	0.138 – 1.999
	Median	0.8602	0.85835
	Mean	0.937	0.903
	Standard Deviation	0.422	0.423